

The University Of Hull

Reinvestigating the relationships between the
Badenoch Group, Dalradian Supergroup and the
Grampian Shear Zone.

BEING A THESIS SUBMITTED FOR THE DEGREE OF
MASTER OF SCIENCE BY THESIS

IN THE UNIVERSITY OF HULL

BY LEWIS ALEXANDER EVASON BSC

05-2021

1. ABSTRACT

In situ monazite and titanite U-Pb LA-ICP-MS geochronology and combined petrological and microstructural analysis has revealed both Neoproterozoic and Ordovician deformation within the Grampian Shear Zone (GSZ), central Scotland. The Grampian Shear Zone has been posited to separate the Dalradian Supergroup from the Badenoch Group, representing either, a structural break, an orogenic unconformity or a shear zone that predominantly affects the top of the Glen Banchor Subgroup. New monazite U-Pb data gave Neoproterozoic ages which provide a youngest age of deformation/monazite growth within the GSZ at $824 \pm 2.73\text{Ma}$, with subsequent Neoproterozoic resetting of the monazite at $751.81 \pm 3.56\text{Ma}$ and a further resetting during the Early Ordovician/Late Cambrian at $485.85 \pm 2.63\text{Ma}$, from within sample RG1716. Monazite U-Pb data from sample RG1718 Ruthven Semipelite of the Corrieyairack Sub-Group (Grampian Group, of the Dalradian Supergroup) produced two distinct populations of monazite, one population of monazite growth associated with the Grampian Orogeny at $475.03 \pm 1.11\text{Ma}$, the other population from a detrital domain within the monazite produced lower intercept age of $475.51 \pm 2.84\text{Ma}$ and an upper intercept age of $3004.7 \pm 58\text{Ma}$, revealing that the Ruthven Semipelite shows a distinct lack of Neoproterozoic deformation. The titanite U-Pb data collected produced an age of $467.45 \pm 1.84\text{Ma}$ from Sample RG1703 a sheared garnet amphibolite from within the GSZ and $469 \pm 0.3\text{Ma}$ from sample RG1710 a Badenoch Group lithology. The titanites dated within the Garnet amphibolite are from a titanite population within the garnet cores and must date or predate the onset of garnet growth. These garnets subsequently developed large strain shadows indicating a reactivation of the GSZ after the garnet growth. Sample RG1710s titanite population contains rare rutile cores, biotite quartz intergrowth textures and, cordierite pseudomorphs indicating a higher grade mineralogy predating the titanites. This mineralogy may be related to eclogite deformation within the Badenoch Group which predates migmatization of the Dava Sub-Group.

2. ACKNOWLEDGEMENTS

For training on using the diamond rock cutting saw at the University of Hull, the cutting and polishing of thin sections, I would like to thank Mark Anderson. For assistance with metamorphic modelling using Theriak Domino and the calculation of FeO to Fe₂O₃, I would like to thank Kathryn Cutts. For guidance in LA-ICP-MS mapping and spot ablations and training for the use of the data reduction programme Lolite4, I would like to thank Kit Hardman. For assistance and training in thin section identification of phosphates, I would like to thank Jon Pownall. Rob Strachan for sharing his knowledge of the analysed and described lithologies. Martin Smith for sharing his knowledge of the analysed and described lithologies. I would like to thank Eddie Dempsey for sharing his knowledge of microstructural analysis, particularly the microstructural analysis of quartz. Anna Bird for supervision during the writing of the thesis and her assistance in keeping myself and my other supervisors at the University of Hull organised. My parents for their support during this master's program and the initial Covid-19 lockdown.

Contents

| | | |
|-----------|-------------------------------------------------------------------------------------------------------------|----|
| 1. | ABSTRACT | 2 |
| 2. | Acknowledgements | 3 |
| 1 | Introduction | 6 |
| 1.1 | Aims and objectives | 6 |
| 1.2 | Geology of Mainland Scotland | 8 |
| 1.3 | Grampian Terrane and Mainland Scotland | 10 |
| 1.3.1 | Tectonostratigraphy of the Grampian Terrane | 10 |
| 1.3.1.1 | Badenoch Group Stratigraphy | 11 |
| 1.3.1.2 | Grampian Group Stratigraphy | 12 |
| 1.3.1.2.1 | Appin Stratigraphy | 13 |
| 1.4 | Depositional Age and setting of Badenoch and Dalradian sediments | 14 |
| 1.5 | Badenoch Group metamorphism and geochronology | 16 |
| 1.5.1 | Eclogite Facies deformation | 16 |
| 1.5.2 | D1 Migmatization and Gneissose Deformation | 16 |
| 1.5.3 | D2 Shearing | 16 |
| 1.6 | Structural Deformation within the Grampian Terrane | 17 |
| 1.6.1 | Structural Deformation within the Badenoch Group | 17 |
| 1.6.2 | Structural Deformation within the Dalradian | 18 |
| 1.6.3 | Structural Deformation of the Geal Charm Osian steep Belt | 18 |
| 1.7 | Tectonic setting of deformation within the Grampian Terrane | 19 |
| 1.8 | Further Neoproterozoic deformation within the North Atlantic region outside of the Central Highland Terrane | 19 |
| 2 | Methodology | 24 |
| 2.1 | Sample Preparation | 24 |
| 2.1.1 | Sample collection | 24 |

| | | |
|---------|------------------------------------------------------|----|
| 2.1.2 | Thin Section Production | 24 |
| 2.2 | Optical Petrological Analysis | 24 |
| 2.3 | U-Pb Geochronology | 25 |
| 2.4 | Metamorphic Modelling | 28 |
| 2.4.1 | Sample selection and bulk rock XRF data source | 28 |
| 3 | Lithological Discriptions | 30 |
| 3.4 | RG1703 - Lochindorb Garnet Amphibolite | 31 |
| 3.5 | RG1710 – Findhorn Metasediment | 33 |
| 3.6 | RG1714 GMS Glen Gour | 36 |
| 3.7 | RG1716 - Corie Each Pegmatite | 38 |
| 3.8 | RG1718 - Ruthven Semipelite | 40 |
| 3.9 | Deformation Fabrics | 42 |
| 4 | Results | 48 |
| 4.1.1 | RG1703 - Lochindorb Garnet Amphibolite titanite U-Pb | 48 |
| 4.1.2 | RG1710 - Findhorn Metasediment titanite U-Pb | 52 |
| 4.1.3 | RG1716 - Corie Each Pegmatite | 56 |
| 4.1.3.1 | RG1716 Isotope maps | 56 |
| 4.1.3.2 | RG1716 Monazite U-Pb | 57 |
| 4.1.4 | RG1718 - Ruthven Semipelite | 58 |
| 4.1.4.1 | RG1718 Isotope maps | 58 |
| 4.1.4.2 | RG1718 Ruthven Semipelite monazite U-Pb | 59 |
| 5 | Metamorphic Modelling | 60 |
| 5.1 | GMS Glen Gour RG1714 | 60 |
| 5.2 | AB07-27 Leven Schist | 61 |
| 5.3 | Assemblage and pseudosection comparison | 61 |
| 6 | Discussion | 62 |

| | | |
|-----|------------------------------------------------------------------|----|
| 6.1 | Monazite and titanite geochronology of this study | 63 |
| 6.2 | Titanite and monazite U-Pb dates - closure temperature | 63 |
| 6.3 | Limitation of monazite dates | 64 |
| 6.4 | Limitation of titanite U-Pb analyses | 64 |
| 6.5 | Deformation and metamorphism of the Badenoch and Grampian Groups | 65 |
| 6.6 | The nature of the Grampian Shear Zone | 66 |
| 6.7 | Geological significance of Knoydartian dates | 67 |
| 6.8 | Geological significance of Ordovician dates | 68 |
| 6.9 | Future research | 70 |
| 7 | Conclusions | 71 |
| 8 | References | 72 |

INTRODUCTION

1.1 Aims and objectives

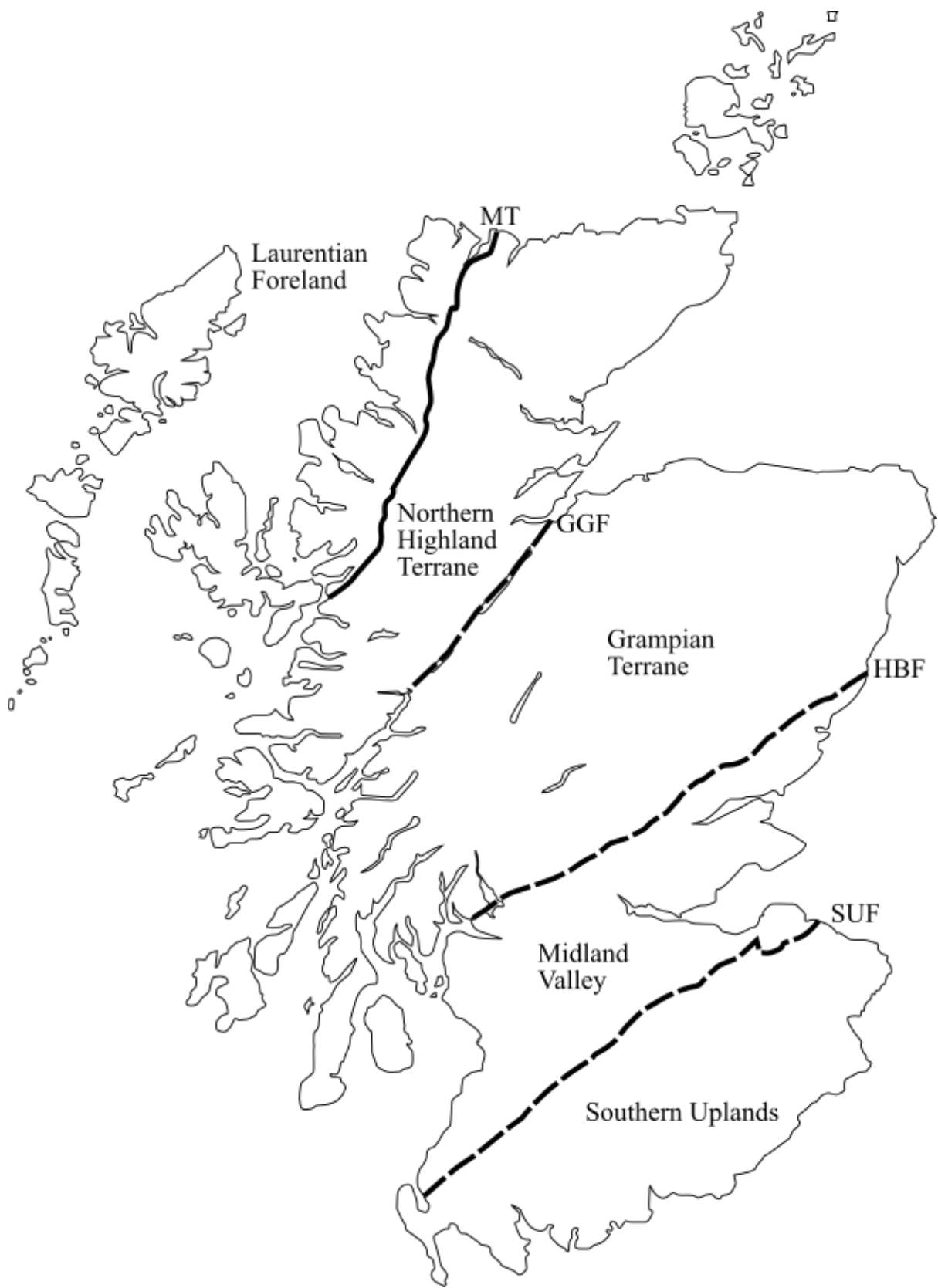
Sedimentary basins are amongst the largest and most economically important geological features on earth. A key problem in our understanding basin geology is how extensional tectonics are accommodated within the underlying basement succession of thick rifted (and subsequently passive) margin successions in both modern and ancient settings. The Neoproterozoic - Cambrian Dalradian Supergroup is a suite of metamorphic rock that were originally deposited as siliciclastic sediments on the rifted/passive Laurentian margin of the Iapetus Ocean. The Dalradian Supergroup sediments are underlain by another suite of metamorphosed sediments referred to as the Badenoch Group. Within the Badenoch Group 840Ma migmatites are crosscut by younger, possibly 806Ma shear zones (Noble et al., 1996, Hyslop and Piasecki 1999) collectively referred to as the Grampian Shear Zone (GSZ). The research presented herein tests the hypothesis that these shear zones represent the mid-

deep crustal expression of regional extension development of the Laurentian margin of the actively spreading Iapetus Ocean during the Tonian period of the Neoproterozoic.

The aims of this study are as follows

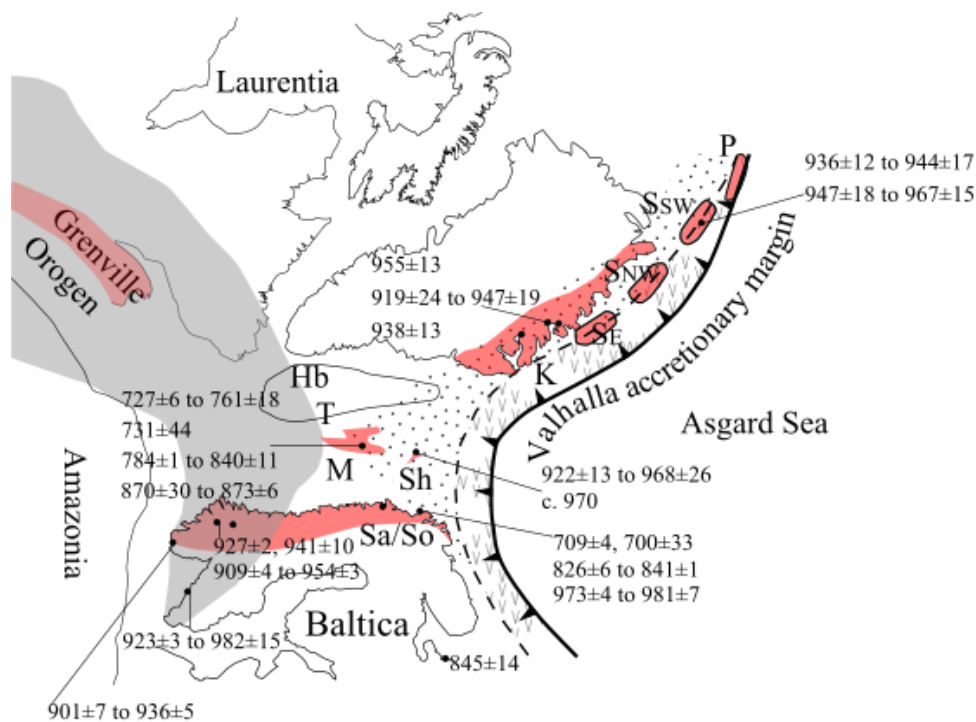
1. Reinvestigate geochronometers from within the Badenoch Group, GSZ and Dalradian Supergroup using modern LA-ICP-MS mapping and U-Pb spot analyses to identify age and structural differences that may be gleaned from geochronometers.
2. Further investigate the deformation within the Badenoch Group, to determine structural and petrological differences between the Badenoch Group and the overlying Dalradian Supergroup.
3. Reinvestigate the GSZ in attempt to unravel its activity over time. Investigating whether the GSZ represents the deep crustal expression of extension during the opening of the Iapetus Ocean or a Knorydarian aged shear zone associated with the Valhalla Orogeny.

1.2 Geology of Mainland Scotland



1.0 Terrane map of Scotland with major terrane bounding faults. MT = Moine Thrust; GGF = Great Glen Fault; HBF = Highland Boundary Fault; SUF = Southern Upland Fault

Traditionally mainland Scotland can be divided into five distinct fault bounded terranes, each with its specific geological history. This study focuses primarily on the rocks of the Grampian Terrane, bounded by the Great Glen Fault to the north and the Highland Boundary Fault to the South, and the Northern Highland Terrane North of the Great Glen Fault. Within the Grampian and Northern Highland Terranes, four Neoproterozoic metasedimentary successions are identified, the Morar, Glenfinnan, and the Loch Eil (Moine) groups of the Northern Highlands and the Dalradian Supergroup of the Central Highlands. The Central Highlands are of particular interest to this study, with the focus being on the relationship between the Badenoch Group of the Central Highlands and the overlying Dalradian Supergroup. The Badenoch Group has been shown to share Neoproterozoic deformation with the Moine of the Northern Highlands. The Moine groups are mostly constrained to the Northern Highlands and represent successions that filled basins on the margin of the supercontinent Rodinia. Lithologies within the Moine 'Supergroup' within Mainland Scotland show deformation during Valhalla Orogen, which is split into two distinct episodes, the Renlandian (980-910 Ma) and Knyodartian (840-680Ma) events (Spencer et al., 2019). The younger phase of metamorphic deformation, the early Knyodartian is recorded within both the Badenoch Group of the Central Highlands and the Moine metasediments within the Northern Highlands North of the Great Glen Fault (Cawood et al., 2010). Attributed to the Valhalla Orogen which represents an accretionary (ocean-continent) collision that saw two cycles of sedimentation and collision split into the Renlandian (960-915Ma) and Knyodartian (860Ma to 730Ma) (Cawood et al., 2015) These are related to, yet separate and distinct from the earlier Grenville Orogen (intra Rodinian continent-continent Orogen from 1090Ma to 980Ma) and the later Caledonian Orogen (200Ma long closure of the Iapetus Ocean, the formation of Pangea and related orogenesis) (McKerrow et al., 2000., Cawood et al., 2010., Hynes and Rivers 2010).



■ Areas affected by later Caledonian metamorphism

Events:

Knoydartian 700 - 770Ma, 780 - 850Ma, c. 870Ma

Renlandian 890 - 950Ma, 950 - 980Ma

1 2 Distribution of Rodinia passive margins affected by the Valhalla Accretionary Orogen. P= Pearya (Ellesmere Island); Ssw = Svalbard south west; SNW = Svalbard north west; Se = Svalbard east; K = Krummedal Succession; Hb = Hebridean Foreland; T = Torridon. (Bird et al, 2018)

The Dalradian Supergroup consists of sediments that were deposited during the rifting of the Iapetus Ocean then underwent metamorphism and deformation during the Ordovician to Silurian Caledonian Orogeny. The Caledonian Orogeny itself is split into three distinct phases of Orogenesis, the 470Ma Grampian Phase, the 450Ma Grampian II, and the 430Ma Scandian Phase (McKerrow, Mac Niocaill, Dwey, ., 2000. Bird et al., 2013).

1.3 Grampian Terrane and Mainland Scotland

1.3.1 Tectonostratigraphy of the Grampian Terrane

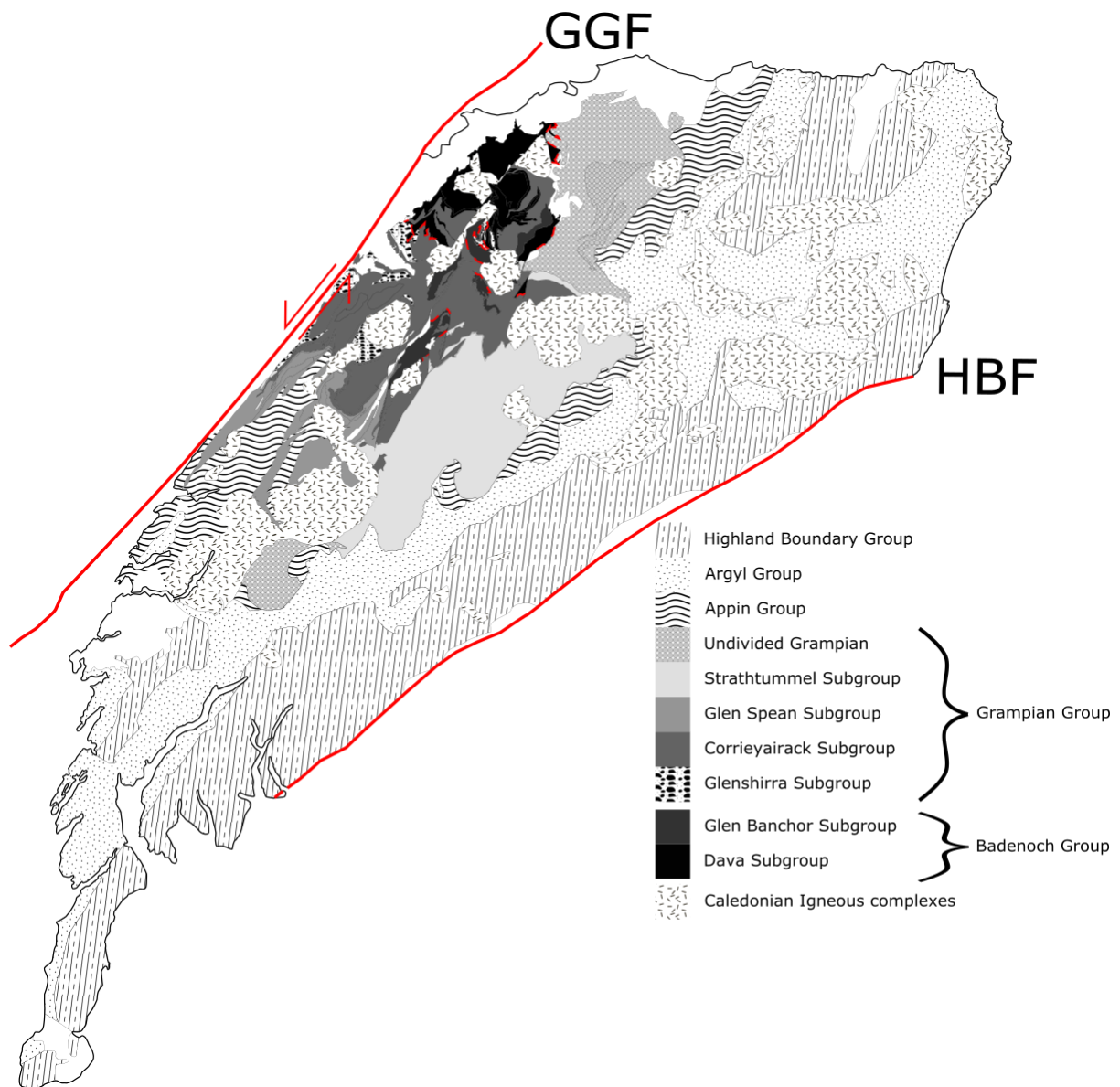
The stratigraphy of the Grampian Terrane is typically split into five groups, with the structurally lowest group, the Badenoch Group, being overlain sequentially by the Grampian, Appin, Argyll, and the Highland Boundary Groups. The latter four groups are assigned to the

Dalradian Supergroup. Most interpretations of the relationship between the Badenoch and the Dalradian state that, the Dalradian rests unconformably upon the Badenoch, with the Badenoch acting as a crystalline basement to the Dalradian sediments prior to Caledonian metamorphism. (Leslie et al. 2013).

1.3.1.1 Badenoch Group Stratigraphy

The Dava succession represents the structurally lowest Sub-Group within the Central Highlands (Badenoch) Group, the group is locally migmatic and is composed of psammites with semipelites and rare quartzites. (Highton et al. 1999). The overlying Glen Banchor Sub-Group is cut by low angle Neoproterozoic shear zones that are host to a suite of foliated pegmatite bodies (Hyslop and Piasecki 1999). The Badenoch Group protoliths are c. 900Ma Neoproterozoic sediments deposited on the margin of the Rodinia supercontinent (Cawood et al., 2015). These lithologies are affected by Neoproterozoic deformation, migmatization within the Dava Sub-Group at 840Ma and shearing and pegmatite emplacement at 806Ma (Highton et al., 1999, Noble et al., 1996).

1.3.1.2 Grampian Group Stratigraphy



13 Map of the Grampian Highlands showing Sub-Groups for the Badenoch and Dalradian Supergroup Groups. Dashed Red lines indicate the location of slide zones associated with the Grampian Shear Zone. (Figure modified from Noble et al, 1996 and Leslie et al, 2013)

The Glenshirra Sub-Group is classified as the basal Sub-Group of the Grampian Group, however, Banks and Winchester 2007 argued it represents a distinct group based on its unique stratigraphy. We have retained it as a sub-group within the Dalradian for simplicity. The Glenshirra Sub-Group represents the earliest phase of post Knoydartian rifting (Banks and Winchester 2007). The sediments of this early phase of rifting led to the deposition of iron rich conglomerates, arkose, and rarer mudstones (Banks and Winchester 2007). The Glenshirra Sub-Group is split into two formations, based on lithological associations across geographical location, these are the Glen Buck Pebbly Psammite and the Garva Bridge

Psammite Formations. Both formations are predominantly comprised of K-feldspar arkosic psammite (Banks and Winchester 2007). Both Formations underlie the Corrieyairack Sub-Group of the overlying Grampian Group, with the contact of the Groups being variably tectonized, in which these shear zones have a top to the NW sense of movement (Banks and Winchester 2007).

Overlying the Glenshirra Sub-Group, the Corrieyairack Sub-Group is composed of micaceous psammites and semipelite that are interpreted as having deep water turbiditic protoliths. The Corrieyairack Sub-Group represents the onset of the main rifting phase for Dalradian basins (Banks and Winchester 2007. Smith et al. 1999). The onset of the Corrieyairack Sub-Group is marked by the Coire nan Laogh Semipelite Formation, representing a regional flooding event that conformably overlies the Glenshirra Sub-Group at Strath Nairn (Smith et al. 1999). Elsewhere such as Northern Glen Banchor and Kincaig the Coire nan Laogh Semipelite Formation rests directly upon the Gneissose lithologies of the Glen Banchor Group, rapid lithological and geochemical changes indicate the presence of an unconformity at the base of the formation (Smith et al. 1999). Above this semipelitic flood deposit are two turbidite deposits, the Loch Laggan, and the Creag Meagaidh Psammites (Smith et al. 1999). The Loch Laggan Psammite is a massive bedded psammite with consistent upward fining sequences, the top of this formation is marked by a fining upwards sequence and the conformable transition into the Ardair Semipelite Formation, which is overlain by the Creag Meagaidh Psammite Formation (Banks et al. 2007, Smith et al. 1999). The overlying Glen Spean Sub-Group contains several sedimentary structures, typical of shallow water deposition, such as dune scale cross bedding, ripple lamination and, lenticular lamination (Banks et al. 2007). The Grampian Group was deposited within two separate basins, these are the Corrieyack Basin and the Strathummel Basin, overlying the Dava and Glen Banchor Sub-Groups of the Badenoch Group respectively (Banks et al. 2007).

1.3.1.2.1 Appin Stratigraphy

The Appin Group is comprised of pelites, semipelites, quartzites, metalimestones and, metadolostones (Stephenson et al. 2013). Within the Grampian Highlands, areas where Caledonian deformation was of lower intensity, onlap relationships between the Appin Group and Badenoch Group are preserved (Smith et al. 1999. Robertson and Smith 1999). Within the Blargie Craig GCR (geological conservation review) site of Leslie et al (2013) Appin Group

stratigraphy provides the clearest sedimentary structures, with all structures consistently younging away from the Badenoch Group. Within this site younger Appin Group lithologies unconformably overstep onto the Glen Banchor Sub-Group, with some 6km of Grampian Group lithofacies not being present (Leslie et al. 2013).

The Appin Group is split into three Sub-Groups, the Lochaber, Ballachulish and, the Blair Atholl Sub-Groups (Stephenson et al. 2013). The Lochaber Sub-Group is a sequence of pelites and semipelites containing lenticular interbedded psammite, with the lower parts of the Sub-Group continuing the shallow marine sedimentary structures of the underlying Grampian Group (Stephenson et al. 2013). Gradually this coarse, siliciclastic shallow marine sedimentation gave way to deeper marine mud dominated lithofacies, with the upper part of the Sub-Group containing tremolitic calcareous rocks that have been interpreted to represent locally developed lagoon facies deposition (Stephenson et al. 2013). The overlying Ballachulish Sub-Group consists of calcareous semipelites grading into tremolitic calcsilicate, further developing into graphitic pelites, the lateral continuation of which attests to the continued stability and slowed subsidence within the basins (Stephenson et al. 2013). With the overlying Blair Atholl Sub-Group continuing the deposition of graphitic pelite containing bands of metalimestone (Stephenson et al. 2013).

1.4 Depositional Age and setting of Badenoch and Dalradian sediments

The available isotopic evidence suggests that the Morar Nappe, Sgurr Beag Nappe of the Northern Highland Terrane, and the Badenoch Group were deposited during the early Neoproterozoic. The deposition of the Morar Nappe occurred 50Ma before the deposition of the Sgurr Beag Nappe (Bird et al 2018). All were subjected to Knoydartian tectonothermal activity, providing a link between the Badenoch Group south of the Great Glen Fault, to the Moine north of the fault (Kinny et al. 2003).

Timing of sedimentation can be constrained by detrital zircon ages, based on the youngest zircons. Sediment provenance can also be calculated using detrital zircon age clusters, constraining the nearby exposed terranes. Using these methods, Cawood et al (2003) found that the Grampian Group and the Badenoch Group produce similar detrital zircon age peaks, with both sharing the distinct lack of Archean detrital zircons. Further stating that this suggests a link between either the sediment source and or the age of sedimentation. With

the 840Ma migmatization age within the Dava Sub-Group of the Badenoch Group (Highton et al. 1999), detrital zircons thus constrain the age of the sedimentation of the Badenoch Group to 900-850Ma.

Two igneous clasts within the Glen Buck Pebbly Psammite Formation of the Glenshirra Sub-Group were dated via U-Pb zircon analyses, a granitic clast gave an age of 1777 ± 7 Ma and a syenitic clast gave an age of 1464 ± 8 Ma, with detrital zircons within the formation giving a unimodal age peak of 1790Ma (Banks et al. 2007). This relatively old provenance is further corroborated by whole rock Nd-analyses (Banks et al. 2007). The igneous clasts within the psammite and paleo-flow indicators suggest that the exposed terrane to the west of the Corrieyairack Basement, to be a 1.8Ga meta-igneous terrane (Banks et al. 2007). The easternmost distal part of the Glenshirra fan has a younger and more varied detrital zircon population, indicating the mixing of the Paleoproterozoic detritus from the west mixing with Mesoproterozoic detritus (Banks et al. 2007). The findings led Banks et al (2007) to conclude that the sediments deposited in the Strathtrummel and Corrieyairack basins, were deposited upon the Glen Banchor Sub-Group, and sandwiched between Grenvillian-Sveconorwegian basement to the east and Makkovikian-Ketilidian (Rhinnian) igneous basement to the west north west. The age of zircons from the eastern margin of the Glenshirra had both Mesoproterozoic 1140Ma and Neoproterozoic 900Ma zircons, with the dominant signature being that of Neoproterozoic zircons (Banks et al. 2007).

The upper part of the Grampian Group is locally conformable with the Appin Group which, if correct means the lower units of an apparently continuous sedimentary stack yields metamorphic ages some 300-200Ma older than the deposition of the youngest units within the stack (Highton et al. 1999).

$\delta^{13}\text{C}$ data of carbonate bodies can be used as a proxy for geochronology as $\delta^{13}\text{C}$ is tied to global climatic events. Within the Dalradian there are several carbonate bodies as well as glaciogenic units associated with the Neoproterozoic glaciation of the Cryogenian (Prave et al. 2009) These units date the deposition of the mid Easedale Sub-Group within the Argyll Group to 600Ma to 551Ma, with the base of the Dalradian to the Port Askaig Tillite Formation spans over 100Ma, acting as a timing constraint from the base of the Dalradian to the base of the Argyll Group (Prave et al. 2009).

1.5 Badenoch Group metamorphism and geochronology

1.5.1 Eclogite Facies deformation

Retrograde eclogite was found within amphibolite pods within the Dava Sub-Group, identified by amphibole plagioclase symplectites and plagioclase coronas surrounding the garnets, with some of the plagioclase coronas containing needles of hornblende radiating from the garnets (Baker 1986). Garnets rimmed by plagioclase coronas are common and were described by Piasecki 1980, found within the GSZ and within the Badenoch Group meta-basite show that eclogite facies may have been widespread prior to later silimanite growth (Baker 1986). The eclogites within the Dava succession may correlate to the eclogitic inliers within the Moine Morar Division, these Dava eclogites are as of yet undated and such a correlation between the eclogites above and below the Great Glen Fault is required (Storey 2008).

1.5.2 D1 Migmatization and Gneissose Deformation

The migmatitic nature of lithologies belonging to the Dava and Glen Banchor successions allows for zircon dating within the leucosomes, which would date the partial melting of those lithologies, this methodology was applied to migmatitic lithologies belonging to the Dava Group (Highton et al. 1999). Three generations of zircons were identified via cathodoluminescence SEM, type 1 neocrystalline zircons were identified as acicular zircons found within both the leucosomes and melanosomes, type 2 neocrystalline zircons with inherited cores found only within the melanosomes and inherited zircons found only within the mesosome (Highton et al. 1999). The U-Pb geochronology of the type 1 acicular zircons gave ages of $840 \pm 11\text{Ma}$ for the upper intercept discordia and a lower intercept of $458 \pm 19\text{Ma}$. The 840Ma represents the migmatization and the development of gneissose banding within Dava Group lithologies and pre-dates the 806Ma shearing event, thus the 840Ma is interpreted to represent the age of D1 deformation (Highton et al. 1999., Noble et al. 1996). While there is no Caledonian zircon growth, the lower intercept is likely to represent metamorphism via channelized fluid flow during the Caledonian (Highton et al. 1999). Kyanite growth associated with the development of D1 fabrics indicates crustal thickening via folding during this time (Phillips et al 1999).

1.5.3 D2 Shearing

Early geochronological work on the Grampian Shear zone was focused on Rb-Sr ages of muscovite porphyroblasts from sheared pegmatites within the shear zone, the ages produced

from the muscovites gave ages ranging from $573 \pm 13\text{Ma}$ to $718 \pm 19\text{Ma}$ (Piasecki and van Breemen 1979). The Badenoch Group, interpreted by some to be a Moine equivalent south of the Great Glen Fault, underwent a D3 Knoydartian garnet amphibolite shearing event dated via Rb-Sr muscovite analysis gave an older age of $749 \pm 8\text{Ma}$ from the Blargie Slide (Piasecki and van Breemen 1979). This age is coeval with the 740-780Ma and the Carn Grom pegmatite and titanite ages within the SW Morar Group of $737 \pm 5\text{Ma}$, these ages all fall within the younger age ranges for Knoydartian metamorphic activity (Piasecki and van Breemen 1979, Tanner and Evans, 2003, Cawood et al., 2015). The younger muscovites ages are now thought to be a result of incomplete resetting during the Ordovician reworking (Noble et al 1996).

Further Rb-Sr muscovite and whole rock geochronology of the sheared pegmatites within the 'Grampian slide' gave ages of $740 \pm 40\text{Ma}$, the large errors on this Knoydartian age are thought to be a result of Caledonian overprint (Piasecki and van Breemen 1983). This 740Ma age was interpreted to represent the age of kyanite sillimanite grade ductile thrusting and the development of subsequent shear fabrics (Piasecki and van Breemen 1983).

High precision monazite U-Pb geochronology, using chemical dissolution mass spectrometry yielded shearing and crystallization ages of $806 \pm 3\text{Ma}$, $808 \pm 11\text{Ma}$, and $804 \pm 13\text{Ma}$, with a lower intercept of 440Ma, with the 806Ma age associated with syn-shearing pegmatite crystallization. The Glen Banchor and Dava Sub-Group lithologies structurally lower and just above the Grampian Shear Zone must predate this 806Ma age (Noble et al 1996), these being the An Stac Psammite and Semipelite which have been sheared and the overlying Creag Liath Psammite formation of the Glen Banchor Sub-Group. The sillimanite within the sub Dalradian basement is believed to have grown during a decompression event, which followed the higher pressure kyanite growth conditions (Smith et al. 2011). Sillimanite growth has not only affected the pre-Dalradian basement but lithologies within the Grampian and Appin Groups as well (Smith et al. 2011).

1.6 Structural Deformation within the Grampian Terrane

1.6.1 Structural Deformation within the Badenoch Group

S1 fabrics within the Badenoch Group are gneissose banding and migmatization, with migmatization primarily affecting the Dava Sub-Group (Leslie et al, 2013). No major F1 folds have been found, rare intrafolial folds and low angle discordance between the gneissose

fabric and compositional banding suggests that early large scale recumbent fold structures do exist (Stephenson et al. 2013). D1 gneissose banding is generally concordant with compositional banding and may represent the original bedding (Stephenson et al. 2013).

S2 Fabrics within the Badenoch Group are the development of schistosity and the mylonites associated with the Grampian Shear Zone, with local phylonite development, these S2 shear fabrics are associated with fluid flux along the shears (Phillips et al. 1999).

1.6.2 Structural Deformation within the Dalradian

Caledonian deformation within areas where the Badenoch Group and the overlying Dalradian strata are present is variable and appears to be influenced in part by the basin morphology (Leslie et al. 2013).

Within the Glen Roy area, the Grampian and Appin Groups went through a progressive D1 to D2 deformation, D1 is marked by the development of large scale recumbent folds, bedding parallel S1 fabrics and shear zones along the Grampian Appin boundary (Phillips et al. 1999). These early D1 structures were then deformed by D2 upright open to tight NE trending folds (Phillips et al. 1999).

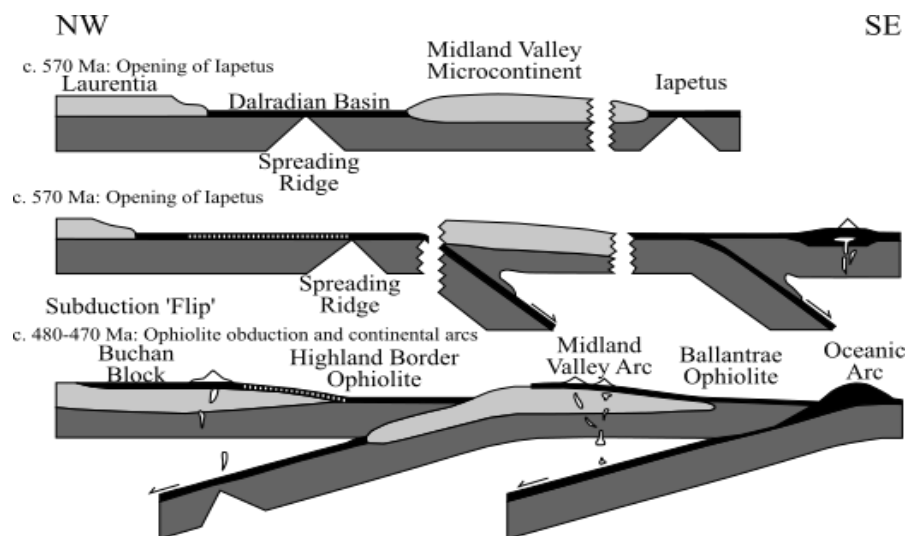
1.6.3 Structural Deformation of the Geal-Charn - Ossian Steep Belt

The intensity and complexity of structural deformation within the steep belt is unique, with three main phases of deformation recognised (Robertson and Smith 1999). The first phase of deformation within the steep belt led to the advancement of large scale isoclinal folds with amplitudes of several kilometres, this deformation coincides with the development of a penetrative schistosity, extreme attenuation of fold limbs and, shear zones (Leslie et al. 2013). The slides are marked by the development of platy fabrics in discrete zones up to 20m thick (Leslie et al. 2013).

This first phase of deformation was modified by a second phase of close to isoclinal folding oblique to the first phase of deformation, this later phase was coaxial and coplanar in the north of the steep belt (Leslie et al. 2013). The early stages of this D2 deformation is marked by prograde kyanite growth, fluid movement during the reactivation of D1 shears led to the overprinting of kyanite by sillimanite (Leslie et al. 2013).

1.7 Tectonic setting of deformation within the Grampian Terrane

Although the Neoproterozoic Grampian Group is composed of similar lithologies to the Moine lithologies north of the Great Glen Fault, it is included within the Dalradian Supergroup based on stratigraphic, structural, and metamorphic continuity (Smith et al. 1999). The Badenoch Group has produced Knoydartian dates confirming the presence of Precambrian deformation within the Grampian Terrane, of the Central Highlands (Noble et al. 1996., Highton et al. 1999). However, within the Dalradian Supergroup of the Grampian Terrane only 475-460Ma Grampian Orogeny deformation has been found. This paradox, wherein discrete tectonometamorphic thermal events are known and can be identified within, what was suggested to be a continuous stratigraphic succession is a key problem within Highland geology. Supporting the identification of the Badenoch Group representing a poly-metamorphic basement succession uncomfortably overlain by the sediments of the Grampian Group (Smith et al. 1999, Chew, 2009).



1 4 Summary of the Grampian Orogeny within Scotland. Modified from Tanner 2014.

1.8 Further Neoproterozoic deformation within the North Atlantic region outside of the Central Highland Terrane

Neoproterozoic metamorphic events within the North Atlantic region are usually associated with the Valhalla Accretionary Orogen, which itself is related to the breakup of Rodinia and the clockwise rotation of Baltica by 95° (Cawood et al. 2016). Neoproterozoic deformation

outside of Scotland associated with the Valhalla Orogen is primarily found within Norway, though Neoproterozoic deformation within the Arctic region is found elsewhere, such as the margins of the Siberian craton that have been associated with the Valhalla Orogen. One such event is the emplacement of the Litlefjrod Granite within Finnmark, dated via U-Pb discordia of zircons giving the age $804 \pm 19\text{Ma}$ (Aitcheson et al. 1991). The Granite Cuts the Sørøy succession, detrital zircons within the succession constrain its deposition from 910Ma to 840Ma (Kirkland, Daly and Whitehouse 2007).

Cawood et al. (2003); 23 - Noble et al. (1996); 24 – Piasecki and van Breeman (1983); 25 Halliday et al. (1989) and Dempster et al. (2002); 26 - Cutts et al. (2009a), Cutts et al. (2009b); 32 – Kinny and Strachan (unpublished data); 27 - Cutts et al. (2009a), Cutts et al. (2009b) and Jahn et al. (2017); 28 - Walker et al. (2020); 29 - Walker et al. (2017); 30 – Watts et al. (2000); 31 – Kaalsbeek et al. (2000); 32 – Strachan et al. (1995); 33– Leslie and Nutman (2003); 34 – Jensen (1993); 35 - Andresen et al. (2007); 36 – Balashov et al. (1996); 37 – Petterson et al. (2009); 38 – Balashov et al. (1995); 39 – Maika et al. (2008); 40 – Gasser (2013) 41 – A.N. Larionov, unpublished data in Johansson et al. (2005); 42 – Gee et al. (1995), see also Johansson et al. (2004), Johansson et al. (2000); 43 – Johansson et al. (2000); 44 – Knoll (1982); 45 – Malone et al. (2017); 46 – Makja et al. (2021); 47 – Trettin et al. (1982); 48 – McClelland et al. (2012); 49 – Kirkland et al. (2007); 50 – Kirkland et al. (2006); 51 – Roberts et al. (2006); 52 – Pedersen et al. (1989).

Within Scotland, Neoproterozoic deformation is primarily found within the Moine north of the Great Glen Fault associated with the Knoydartian events (Cutts et al. 2010). Knoydartian deformation 850 – 700Ma tectonometamorphism has been found within Moine lithologies, having undergone multiple tectonothermal events, with all Moine lithologies having undergone significant Caledonian overprint (Cutts et al. 2010, Bird et al. 2019).

The Moine lithologies are divided into two nappes by the Sgurr Beag Thrust, the Moine Nappe containing the Morar Group and the Sgurr Beag Nappe containing the Glenfinnan Group and the Loch Eil Group (Chew and Strachan 2013). Until recently the Moine was regarded as a Supergroup with no significant metamorphic or isotopic break within the Moine, this has recently been challenged by Bird et al (2019) with the new isotopic data for a tectonometamorphic event occurring within the Morar Group. This data was the first evidence for the Renlandian Orogeny within mainland Scotland with prograde garnet ages of 940-950Ma from the Morar Group Meadie Pelite.

The recent findings that question the Moine as a Supergroup may have implications for Neoproterozoic ages within the Sub Grampian basement and accurate correlations of this basement to the Moine north of The Great Glen Fault.

The Knoydartian (830 – 725Ma) mid-Neoproterozoic tectonothermal events within the Moine have been shown via in situ monazite dating within chemically distinct garnet zones via LA-ICP-MS (Cutts et al. 2010). This method yielded monazite ages within prograde garnet, producing two Neoproterozoic ages, 800-780Ma and the younger Neoproterozoic age of 724 ± 6 Ma, with the latter corresponding to SIMS zircon age of 725 ± 4 Ma obtained from leucosomes within the sample (Cutts et al. 2010). With the older monazite ages within prograde garnet that grew under conditions of 5-6kbar and 600-650°C and the younger monazites within poikiloblastic garnet containing quartz, rutile, staurolite, and biotite gave pressure formation up to 9kbar and temperature of 650°C (Cutts et al. 2010). The 730-725Ma

being 60-90Ma younger than the older 800-780Ma prograde deformation is significant and that the Morar has been subjected to two Neoproterozoic orogenic events (Cutts et al. 2010).

The finding of Renlandian age prograde garnet via Lu-Hf garnet geochronology and LA-ICP-MS garnet composition mapping gave prograde Renlandian 950Ma 6-7kbar and 600°C garnet growth (Bird et al 2018). The garnets also produced ages of $840 \pm 29\text{Ma}$ and $705 \pm 30\text{Ma}$ which corresponds to previous orogenic prograde Knoydartian ages (Bird et al. 2019. Cutts et al. 2010). Both the Renlandian and Knoydartian deformation is linked to the Valhalla Orogen (Spencer et al. 2019), with the orogeny theorised to be the product of the rotation of Baltica with associated magmatism coming in two waves the Renlandian 980-910Ma and the Knoydartian 840-680Ma (Spencer et al. 2019).

The Sgurr Beag Nappe of the Northern Highland Terrane as well as other successions such as the Badenoch that have undergone Knoydartian deformation is interpreted to have been deposited in basins that formed due to the steepening or retreat of subduction zones within this section of Rodina prior to renewed Knoydartian accretion (Bird et al. 2018). The detrital zircon data sets for the lower Dalradian Sub Groups, the Grampian, Appin and the possible sub Dalradian basement, the Badenoch Group, with the lower units of the Glenfinnan and the lithologies within the Morar Group shows possible linkage of the Morar Group with the Badenoch Group while ruling out the Glenfinnan (Kirkland, Strachan and Prave 2008). The lowest unit of the Grampian Group, the Garva Bridge Psammite of the Glenshirra Sub-Group produces detrital zircon peaks like the Morar Group and Badenoch Group, providing a possible link. However, as of yet no pre-Caledonian metamorphic ages from the Grampian and Appin Groups have yet been produced (Kirkland, Strachan and Prave 2008). The Glen Buck pebbly psammite, the proposed basal unit of the Glenshirra Sub-Group has a restricted zircon age population, with the top units showing little similarity to Moine lithologies, except for a similar detrital zircon profile to the Glen Urquhart Psammite, of the Moinian Glen Urquhart Succession (Cawood et al. 2004, Kirkland, Strachan and Prave 2008).

The stabilised Valhalla succession is overlain by mixed siliciclastic, carbonate, and volcanic units, as seen in the Dalradian and the Eleonore bay Supergroups which have inferred bases of 760Ma (Cawood et al, 2016, Prave et al. 2009). Within northern Norway, the Kalak nappe records younger syn-deformational magmatism at 710-670Ma, and magmatism at 600Ma, 570-560Ma and 530-520Ma (Cawood et al. 2016).

2 METHODOLOGY

2.1 Sample Preparation

2.1.1 Sample collection

A total of 36 samples were collected by Rachel Gosling a PhD candidate during a period of fieldwork in 2017. These samples encompass lithologies within the Badenoch Group, Grampian Sub-Group, and Appin Sub-Group, as well as samples focused on the lithologies sheared within the Grampian Shear Zone, including pegmatites from within the shear zone.

The samples dated within this study RG1703, RG1710, RG1716, RG1718 were selected for U-Pb analysis for the presence of geochronometers within the produced thin sections. These geochronometers were monazite and titanite, of which samples RG1703 and RG1710 contained significant quantities of titanite while samples RG1716 and RG1718 contained monazites suitable for LA-ICP-MS mapping and U-Pb spot analyses.

2.1.2 Thin Section Production

A selection of the samples collected in 2017 already existed as thin sections. Included in the processed set are two samples from Martin Smith (BGS).

To produce the thin sections rock samples were cut, parallel to lineation and perpendicular to the foliation, into slabs using a diamond edge saw. These slabs were then inspected for microstructures and mineralogical content, areas of microstructural and mineralogical interest are then highlighted by surrounding them with a rectangle of permanent ink.

These rectangles are then cut out of the slab and ground down to a thickness of roughly 2-3mm thick. Cuttings are mounted to a glass slide using an epoxy resin. These slide-mounted sections are then polished down to 30µm using a lapping plate, micrometer, and optical microscope. A thickness of 30µm is known to be achieved through the optical properties of marker minerals at 30µm, such as muscovite and garnet.

2.2 Optical Petrological Analysis

Optical microscopy analysis of thin sections was performed using a GX Microscopy series XPL1500 microscope. Optical microscopy was used to characterise the petrology, microstructures, and the associations between the two.

All sections were scanned using a GT vision GMXPRIMESCAN slide scanner. These scans are set at 10,000 dpi, to be saved as JPG files, the exposure setting from 0-100 is set independently for each slide.

2.3 U-Pb Geochronology

To constrain the timing of monazite growth within samples RG1716 and RG1718, titanite growth within samples RG1703 and RG1710 were analysed for U-Th-Pb masses using Laser Ablation Inductively Coupled Plasma Mass Spectrometry (LA-ICP-MS). This was undertaken in the Laser Ablation Geochemistry facility at the University of Hull using a RESOLUTION SE compact 193nm Excimer laser with a Laurin technic dual volume sample cell, coupled with an Agilent 8800 Triple Quadrupole mass spectrometer.

Prior to U-Pb analyses larger monazite grains (>100µm) were mapped for Major and REE zonation using laser ablation imaging. The produced maps (Ca, Ce, Cr, Dy, Eu, Fe, Gd, Hf, K, Lu, Mg, Nd, Pb, Rb, Si, Sm, Sr, Th, Ti, U, Y, Yb, Zr) were then used to guide spot analyses locations to minimize the effect of mixing different compositionally distinct mineral domains.

For monazite analyses the Bananeira (Gonçalves et al., 2016) and the 'Stern' (Palin et al., 2013) monazite standards were used for monazite analyses while the MKED1 (Spandler et al., 2016) titanite standard was used for titanite analyses, with NIST 610 and 612 glass standards used as the secondary reference material. The published individual isotopic age estimates for the Bananeira monazite standard are presented within the following table.

Table 1 Age estimates taken from (Gonçalves et al., 2016)

| | Age Estimates | | | | | | | | |
|---------|-----------------|------------|----------------|---------|----------------|---------|-----------------|------------|------|
| | 207Pb/ 206Pb | 2s (Ma) | 206Pb /238U | 2s (Ma) | 207Pb /235U | 2s (Ma) | 208Pb/ 232Th | 2s (Ma) | rho |
| Average | 497.4 | 56.0 | 504.5 | 8.1 | 503.3 | 8.5 | 491.9 | 16.5 | 0.78 |
| SD | 13.3 | 1.4 | 2.4 | 0.1 | 2.9 | 0.3 | 4.1 | 0.3 | 0.02 |
| RSD% | 2.68 | 2.57 | 0.48 | 1.35 | 0.58 | 3.29 | 0.84 | 1.85 | 2.21 |

The age of the Bananeira monazite was calculated at 507.7 ± 1.3 Ma. Analyses of the standards produced ages that are consistent with (Gonçalves et al., 2016; Spandler et al., 2016). The measured age of the Bananeira monazite was consistent with the published data. However, 3 analyses show elevated 07/06 perhaps indicating regions with elevated initial Pb values.

The published age for the monazite standard ‘Stern’ is 512.1 ± 1.9 (2SD) calculated using data gathered via ID-TIMS. With individual isotopic ages shown in the following table. The monazite standard Stern produced an age of 514.25 ± 0.41 Ma. All analyses are consistent with the published data. Both standards are consistent with published data. However, there may be issues with the monazite Bananeira.

Table 2 Age estimates taken from (Palin et al, 2012)

| | Age Estimates | | | | | |
|---------|---------------|---------|------------|---------|------------|---------|
| | 207Pb/206Pb | 2s (Ma) | 206Pb/238U | 2s (Ma) | 207Pb/235U | 2s (Ma) |
| Average | 486.5 | 1.9 | 510.8 | 0.4 | 506.5 | 0.7 |

Table 3 Published U-Pb age ratios taken from (Spandler et al, 2016).

| | Age Estimates | | | | | |
|---------|---------------|--------|------------|--------|------------|--------|
| | 207Pb/206Pb | 2s (%) | 206Pb/238U | 2s (%) | 207Pb/235U | 2s (%) |
| Average | 0.09465 | 0.0190 | 0.26538 | 0.0244 | 3.4632 | 0.0403 |

For the titanite analysis of sample RG1703 MKED1 produced an age of 1515.97 ± 1.7 Ma. For the titanite analysis of sample RG1710 MKED1 produced an age of 1515.76 ± 1.3 Ma. For both of the titanite analysis MKED1 was consistent with published data.

For all of the runs the primary mineral standards were within error margins of published data. There may be some minor issues with the monazite Bananeira as it seems to have some initial Pb content within some spot analyses.

Within Iolite4.1 baseline splines were calculated using the less than automatic selection function using the totalbeam channel. Spot ablation analyses were checked and changed as necessary spot by spot, using the selections within the time series window. Sample group splines were checked and changed as necessary within the time series window. Then the U-Pb geochronology DRS scheme was run with linear with exponential fit type using the chosen mineral standard (Paton et al., 2010, Paton et al., 2011) Finally QA/QC modules were ran using the Concordia age and secondary check modules.

All ages reported are within absolute uncertainty 2σ using Iolite4.1. (See tables 8, 9, 10 and 11 in the Appendix under section Iolite4.1 Output data) for the U and Pb isotope ratio data collected from standards during LA-ICP-MS runs.

Run data would be further trimmed post Lolite4.1. Reasons for removing spot data from the Age analyses would include erroneous errors, Pb or U content, spot data would be considered erroneous if factor a of 10 greater or less than the rest of the spot data within a given run. Erroneous spots typically occurred due to misidentification of a given grain or a misplaced ablation spot in relation to the target grain, ie on the grain edge or on an adjacent mineral. Another reason for erroneous spots would be the selection of a false peak in iolite4.1, if a given grain contained multiple age domains down hole. The spot peak data would fluctuate downhole. Within Lolite4.1 peaks were trimmed to either the greatest peak value available. However, if a given peak value was thin a flatter region of the spot peak would be selected. If spots were outside of a given trend or cluster they would be omitted to further clarify the age of said trend or cluster. The criteria for this was whether the spots error ellipse was twice removed from said cluster or isochron.

Laboratory and sample preparation

| | |
|--------------------------------------|------------------------------------------------------|
| Laser Ablation Geochemistry Facility | University of Hull |
| Sample Type | In situ monazites |
| Sample Preparation | Cleaned using high purity pressurised N ₂ |

Laser Ablation system

| | |
|--------------------------|----------------------------------------|
| Make, Model and type | RESOLUTION SE compact |
| Ablation cell and volume | Laurin technic dual volume sample cell |
| Laser wavelength | 193nm |
| Pulse width | 5ns |
| Fluence | 4 (titanite) 2.5 (monazite) |
| Repetition rate | 10Hz |
| Ablation duration | 30s |
| Spot diameter | 30µm (titanite) 16µm (monazite) |
| Carrier gas flow rate | |

ICP-MS instrument

| | |
|----------------------------|--------------------------------------------------|
| Make model and type | Agilent 8800 Triple Quadrupole mass spectrometer |
| Sample introduction | Laser |
| RF power | |
| Make-Up Gas flow | Ar |
| Detection system | |
| Masses measured (Monazite) | 204, 206, 207, 208, 232, 235, 238 |

Masses measured (Titanite) 42, 90, 204, 206, 207, 208, 232, 235, 238
Dwell times

Data Processing

| | |
|-----------------------------------|-----------------------------------------------------------------|
| Gas Blank | Baseline time length |
| Calibration strategy | All standards note primary standards |
| Data processing package used | Iolite4.1 |
| Mass discrimination | 232/238 monitored in NIST610 |
| Common Pb correction | Nominal for titanite runs |
| Uncertainty level and propagation | All ages are reported with an absolute uncertainty of 2δ |
| Quality control (Monazite) | Bananeiro weighted mean = 514.01 ± 0.56 MSWD 11.5 |
| Quality control (Monazite) | Stern weighted mean = 509.78 ± 0.49 MSWD 3.5 |
| Quality control (1710 Titanite) | MKED1 weighted mean = 1515.77 ± 1.3 MSWD 0.86 |
| Quality control (1703 Titanite) | MKED1 weighted mean = 1512.37 ± 1.97 MSWD 0.59 |

Table 4 Laboratory and sample preparation methods. Ablation System, instrument parameters and data processing parameters. Modelled after (Gonçalves et al., 2016)

2.4 Metamorphic Modelling

Two pressure-temperature (P-T) pseudosections were calculated using version 15.5 of Theriak-Domino programme suite (de Capitani and Petrakakis, 2010), using the Holland and Powell dataset (2011; ds62). Calculation of P-T pseudosections using the geologically realistic MnCFMASHTO system.

The modelling for this system uses the a-x relationships of White et al. (2007) for silicate melt; Tinkham et al. (2001) for garnet, cordierite, staurolite, and alkali feldspar; a combination of White et al., (2014a) and White et al., (2014b) for biotite; for chloritoid; Coggon & Holland (2002) for muscovite and paragonite; and Holland & Powell (2003) for plagioclase, a combination of White et al., (2000) and White et al (2014) for ilmenite, and Holland and Powell (2011) for epidote.

2.4.1 Sample selection and bulk rock XRF data source

Metamorphic modelling of two samples collected for previous studies was carried out during this project. The sample B11 [NN 5999 9512] was collected 700m north of Blargie Farm for a previous PhD at the University of Hull (Hyslop 1992). The second sample modelled is AB07-27 [NN 2611 8032], the garnetiferous Appin Group Leven Schist at Glen Spean (Bird et al 2013).

The data for sample B11 was provided by Martin Smith as an excel document which contained XRF data from all of the samples collected by Hyslop, sample B11 was selected for modelling due to its proximity to sample RG1714 [NN 6009 9518] and a similar distance from the shear

zone as mapped by Hyslop, with B11 85 m NW of the shear zone and RG1714 70m NW of the shear zone. See figure 0-3 of the appendix for the locations of Hyslop's samples and sample RG1714. Sample RG1714 was selected due to its proximity to samples from the data set provided. Sample RG1714 is a sheared semi-pelite proximal to the shear zone exposed north of Blargie. Samples from Blargie are discussed further within Hyslop and Piasecki 1999.

3 LITHOLOGICAL DISCRPTIONS

Table 5 Table Sample name with location data and notes

| Sample Name | Group | Sub-Group | Lithology | Grid Ref | Notes |
|----------------------------------------|----------|---------------|-----------------------|-----------------|---------------------------------------------------------------------------------------|
| RG1703 – Lochindorb Garnet Amphibolite | Badenoch | Dava | Garnet Amphibolite | NH 9870 3126 | Garnet Amphibolite associated with the Lochindorb Shear Zone |
| RG1710 – Findhorn Metasediment | Badenoch | Dava | Findhorn metasediment | NH 9883 4900 | Lithology interpreted as a metasediment sampled from the River Findhorn |
| RG1714 - GSZ Glen Gour | Badenoch | Shear Zone | Sheared Semipelite | NN 6009 9518 | Semipelite sampled from the Shear Zone north of Blargie Farm |
| RG1716 – Corie Each Pegmatite | Badenoch | Shear Zone | Sheared Pegmatite | NN 6640 9958 | Shear Zone pegmatite sample from north of the River Calder 3 miles west of Newtonmore |
| RG1718 – Ruthven Semipelite | Grampian | Corrieyairack | Ruthven Semipelite | NH 6333 2749 | Sample taken from South of Loch Ruthven. Part of the Ruthven Semipelite Formation |

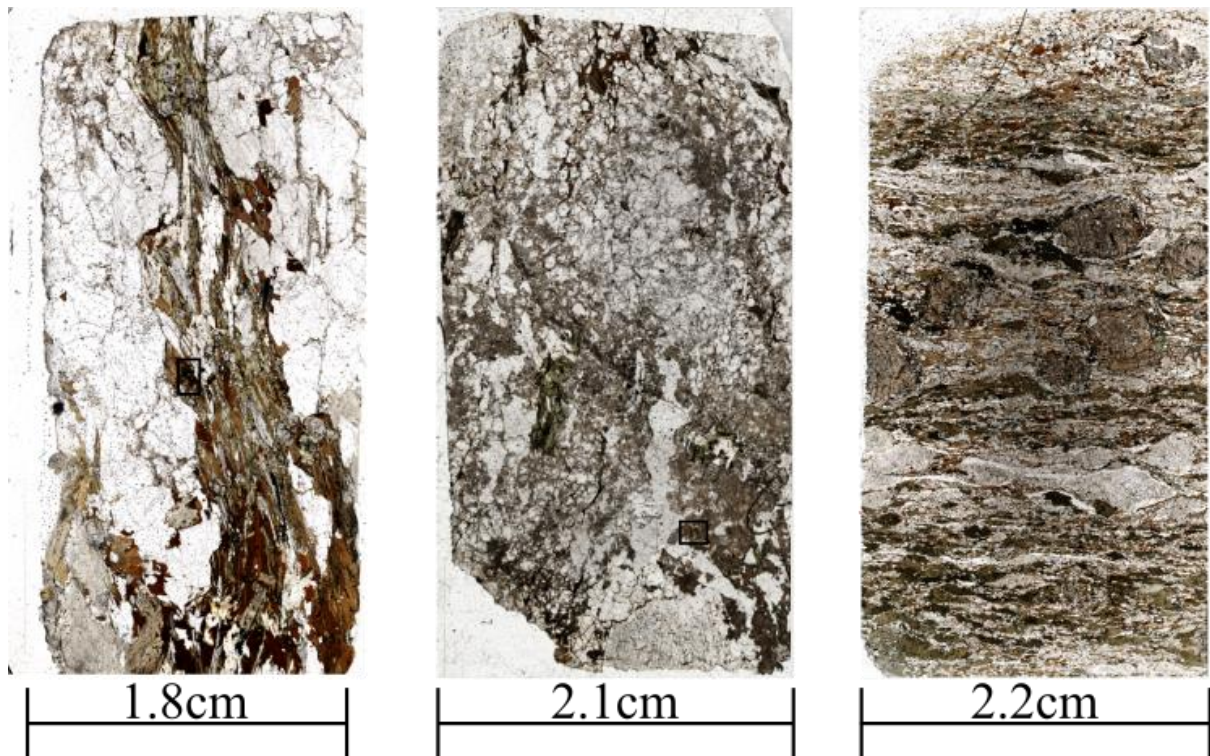


Figure 3 1 Slide scans. From left to right RG1718c, RG1716, and RG1703. The black boxes on RG1718c and RG1716 highlight the large monazites that were ablated for element maps and U-Pb spot analyses

RG1703 - Lochindorb Garnet Amphibolite

This sample was collected at Lochindorb [NH 97154 36445] close to the GSZ [NH 9767 3074], though within the area the GSZ is difficult to locate, with a migmatitic Dava Sub-Group lithology passing upwards into more flaggy Dalradian metasediments (Bird & Gosling, pers. Comm.). The amphibolite was sampled within the Dava units. In the field, the lithology was dark in colour with garnets up to 0.5cm in diameter, and feldspars and amphiboles up to 0.5cm in length (Bird & Gosling, pers. Comm.).

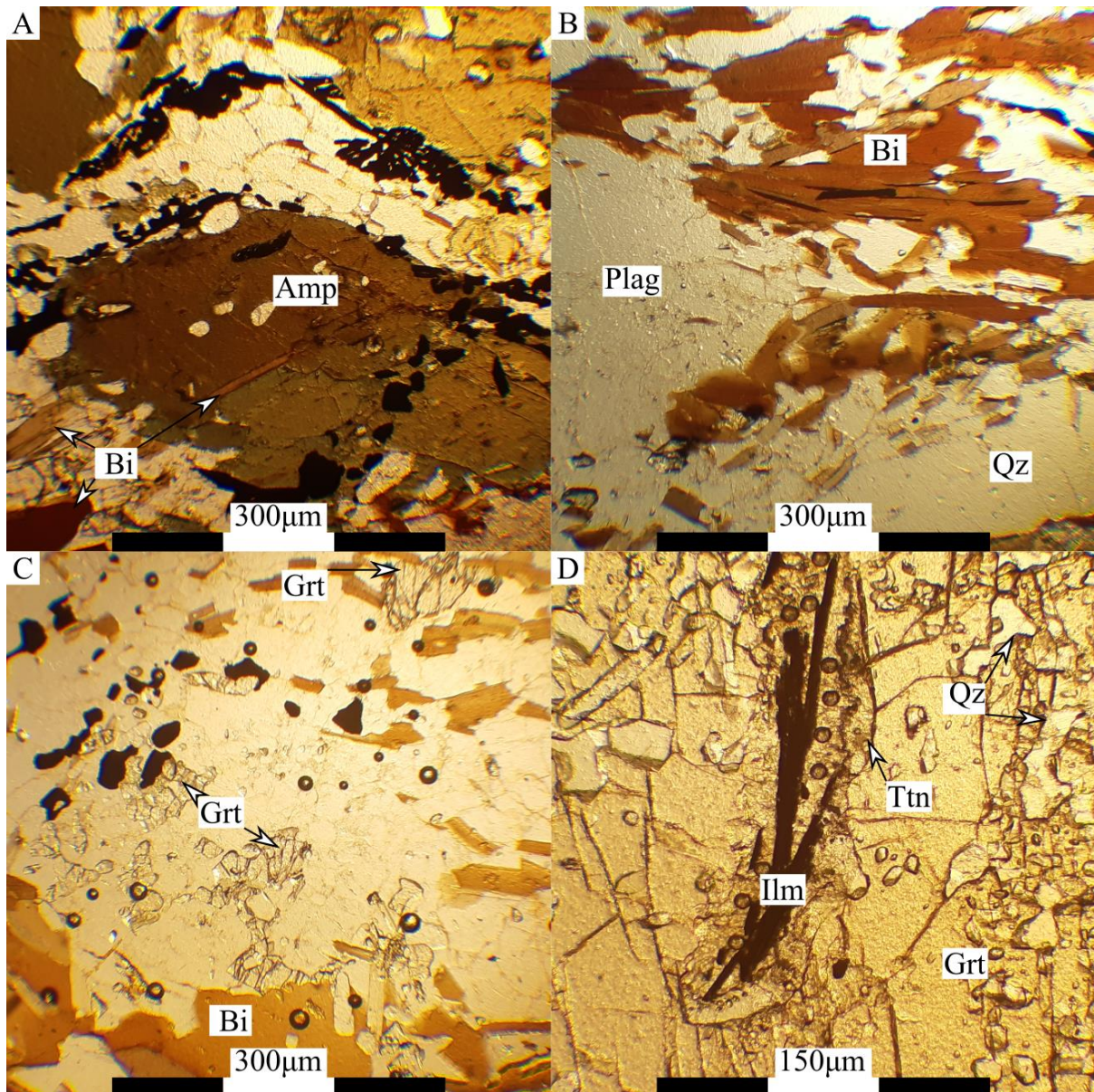


Figure 3-2 Image panel. Image A (PPL) Amphibole with quartz, titanite and opaque inclusions. Of note is the wrapping of the Amphibole by the opaque phase both externally and internally. Image B (PPL) Plagioclase porphyroblast wrapped by biotite and a quartz vein. Image C (PPL) Garnets from the area of semipelitic composition within the slide. Note that the biotites and opaque phase wraps what is likely to have been a garnet porphyroblast, now replaced by plagioclase. D. Example of titanite wrapping ilmenite within a garnet porphyroblast. The titanite contains ablation pits, note the titanites rough appearance, which is distinct from the diamond shaped titanite population.

In thin section, the sample displays 4 main mineralogical domains (Figure 4-2), a zone containing large (0.5cm) garnets, a zone of semi pelitic composition, a zone containing large (0.3cm) rounded feldspars mantled by quartz and an amphibolite zone dominated by amphibole, See Figure 3-2-A for the Garnetiferous Amphibolite, 3-2-B for the rounded feldspars mantled by quartz, held within biotite rich band within amphibolite, 3-2-C for the region of pelitic composition with garnet clusters showing relict mantling and 3-2-D for titanite rimming ilmenite within the large garnet porphyroblasts of the amphibolite. Of the

four listed compositions, the semi pelitic composition is distinct in that it lacks amphibole which is present in all the other compositions. The minerals which denote the main fabric within the sample are biotite, amphibole, and an opaque phase, likely ilmenite. With biotite and the opaque phase wrapping the larger minerals within the section.

Garnets within the sample have developed as large (largest diameter 4.7mm) porphyroblasts, however, there are patches of small (50µm) grain like garnet crystals. The smaller garnets occur within a portion of the section that is absent of amphibole and contains a mineralogy typical of semipelitic composition. The porphyroblastic garnets within the section contain a core, consisting of garnet surrounding ilmenite, titanite and quartz and outer rims which contain fewer inclusions of biotite and rhombus-shaped titanites, see figure 3-2-D. These large garnets are wrapped by amphibole, feldspar, opaques, with biotite present within the strain shadow of the garnets see figure 3-1 slide 3 for assemblage wrapping the garnet porphyroblasts.

Titanite within the sample shows two distinct morphologies, euhedral titanites and highly anhedral titanites. Euhedral titanites are found within the matrix and as inclusions within the amphibole and outer rims of the garnets (see figure 3-2-A for titanite inclusions within amphibole) whereas the highly anhedral titanites are restricted to garnet cores (see figure 3-2-D). These anhedral titanites are consistently associated with intergrowths of ilmenite. Titanite can form due to the breakdown of ilmenite and a calcium bearing phase (Harlov et al., 2006). Because the titanite population present within the garnet cores is distinct in its appearance and its mineralogical relations, the age data gathered from these titanites can only predate or date the growth of these garnet cores, providing a maximum age for garnet growth within the sample.

3.1 RG1710 – Findhorn Metasediment

This sample was collected 660m NNW of Relugas Farm [NH 99169 48464], within the field, this lithology was correlated to the Dava Group, and referred to as the Findhorn Dava Group metasediment. (Bird & Gosling, Pers. Comm.).

Within thin section, this lithology displays a predominantly planar fabric with separation of plagioclase (commonly microcline), antiperthitic texture plagioclase within the leucosome bands (Figure 3-3-B), amphibole, plagioclase, quartz, biotite, titanite and rutile within the

melanosome (Figure 3-3). Within section, rutile is only present as acicular rutile hosted within biotite along cleavage planes and as small cores to titanite (figure 3-3-A). Some biotite within the sample shows intergrowth with quartz (figure 3-3-D). Amphiboles range in size up to 4mm, the amphiboles within section are seen forming vermicular intergrowth with quartz on a small scale (figure 3-3-C), with larger amphiboles hosting round quartz intergrowths.

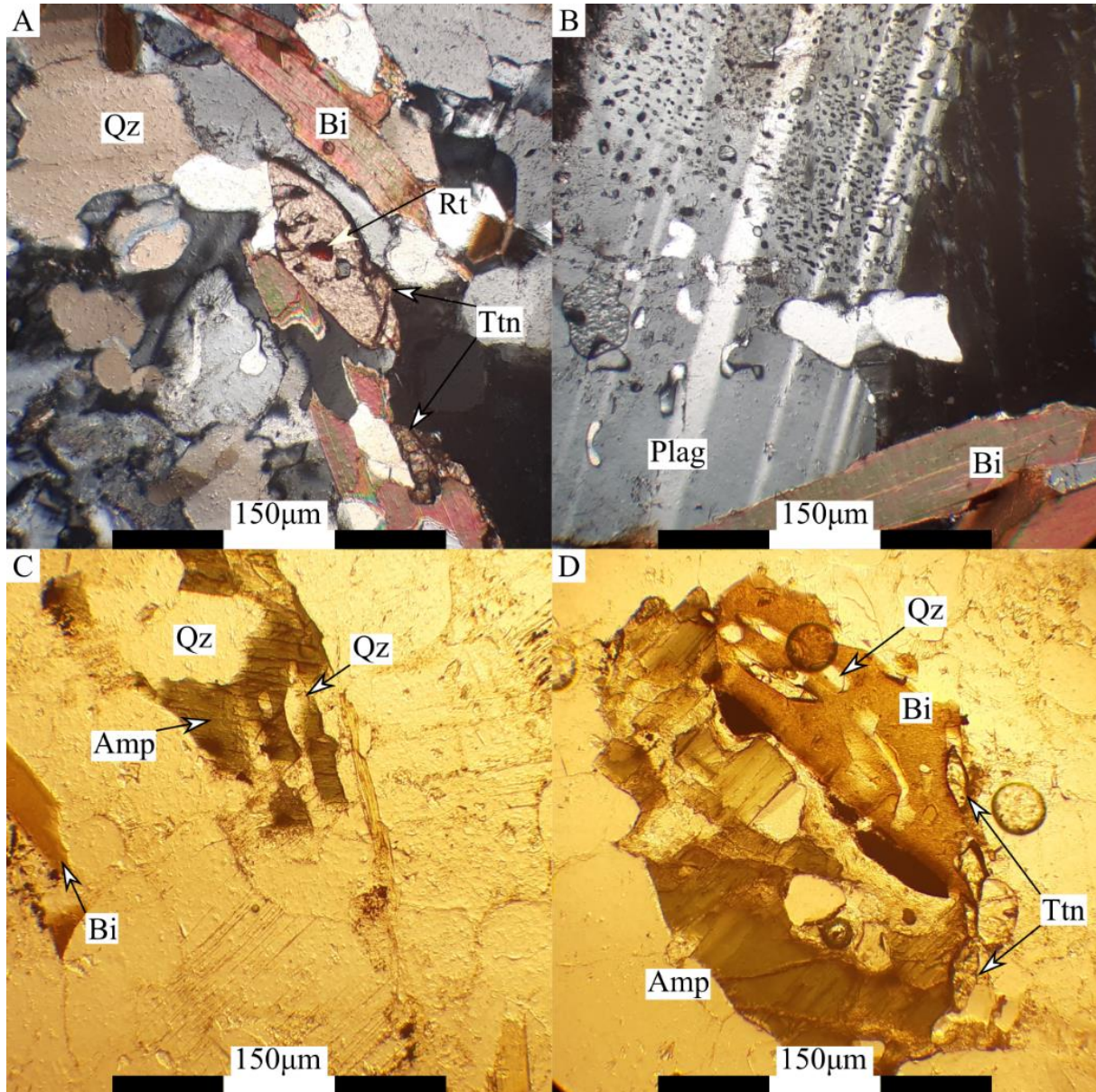


Figure 3-3 Image panel of mineral relationships from sample RG1710. Image A (XPL) Shows a notably large 70µm titanite grain with a rutile inclusion within the centre of the titanite. Image B shows a large titanite (150µm), this titanite is one of two titanites within the three produced sections that displays twinning. Within the biotite are titanite inclusion which are more typical of the slide. Image C shows the typical mineralogy of the slide, being quartz, hornblende, biotite and smaller titanites.

The presence of rutile cores within titanite indicates the breakdown of rutile into titanite as a retrograde reaction (see figure 3-3-A). Within the slides there appear to be two titanite

populations, determined by size, mineralogical relationships, and twinning. The first population is the rarest, large (150 μ m) titanites which display lamellar twinning. The second are titanites within the fabric, biotites and amphiboles, these titanite range in size, reaching up to 50 μ m, typically of diamond shape (see figure 3-3-A and 3-3-D respectively). The presence of acicular rutile within biotite could indicate high Ti content within the biotite.

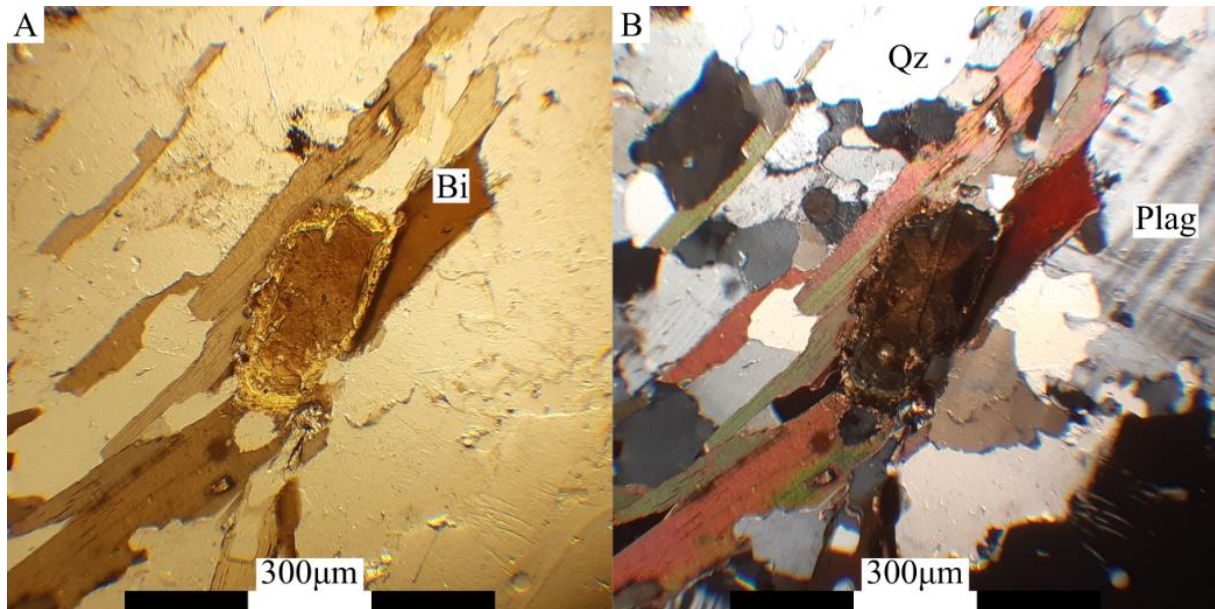


Figure 3-4 Brown phase showing cyclic twinning. Every occurrence of this brown phase is rimmed by the yellow phase.

Figure 3-4 shows a brown accessory phase rimmed by another yellow phase, this brown phase shows cyclic twinning. This is interpreted to be a pseudomorph of cordierite replaced by this brown phase. Cordierite is often rimmed by yellow alteration product pinite. This was followed by the complete alteration of the cordierite perhaps by a second generation of pinite, within section, not all cordierite has undergone complete alteration such as the example within figure 3-4. This brown phase is radioactive as seen by the radiation damage of adjacent biotites (see 3-4-A), therefore this brown phase is interpreted to be allanite.

The presence of rutile inclusions within titanite (3-3-A), vermicular quartz intergrowths with amphibole and biotite (3-3-C and 3-3-D respectively) as well as cordierite pseudomorphs indicate a previous higher grade mineralogy (see 3-4 A and B), with cordierite indicative of granulite facies metamorphism. With the biotite quartz and amphibole quartz intergrowth themselves likely being the reaction products of retrograde metamorphism. It is plausible therefore that the antiperthite textures within this lithology can be explained through a reduction temperature causing exsolution of orthoclase and plagioclase within the lithology.

Elsewhere within the Badenoch Group rutile inclusions within titanite is evidence for pre-existing eclogite facies deformation (Simon Cuthbert, pers comm). Within the Badenoch Group typically, these retrograde eclogites are podiform and are composed of calcic-amphibole and plagioclase with some biotite and relics of garnet. Within these relict eclogite pods, garnets are often replaced by hornblende and Ca-plagioclase kelyphite. Of key interest to sample RG1710 Findhorn metasediment the abundance of titanite as an accessory phase which contain tiny cores of rutile, which is attributed to eclogite paragenesis. Where the Badenoch Group is strongly migmatitic these pods of relict-eclogite are completely transformed to hybrid biotite-hornblende rocks with variable feldspars and quartz, with garnet completely disappearing (Simon Cuthbert Pers Comm). This information suggests evidence for a relict eclogite within the Findhorn Badenoch outcrops.

Perhaps this possible pre-existing granulite facies mineral assemblage is related to these podiform retrograde eclogites.

3.2 RG1714 GMS Glen Gour

This sample was collected 770m north of Blargie Farm [NN 6004 9441]. The lithology is sheared by a NE SW running outcrop of the GSZ, with this sample being collected 75m from the core of this shear zone (Bird & Gosling, Pers. Comm., Hyslop 1992). Within this area the semi-pelitic lithology is interpreted to being the Glen Gour host rock which is progressively sheared. The Glen Gour pegmatite was not seen, the lack of the Glen Gour pegmatite was interpreted as this outcropping of the shear zone being too structurally high for the pegmatite to occur (Martin Smith, pers comm.).

Mylonitised garnetiferous pelite, composed of muscovite, quartz, biotite, garnet, ilmenite, chlorite and a porphyroblastic opaque phase. Muscovites within the sample form mica fish, with cleavage planes sub parallel to the main fabric. The mica fish population is commonly overprinted by a later muscovite population that formed muscovite books with cleavage planes at sharp angles to the main fabric (see figure 4-4-B).

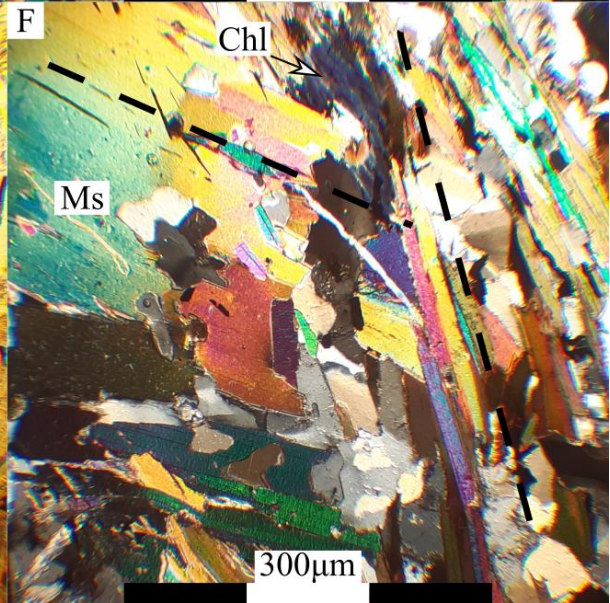
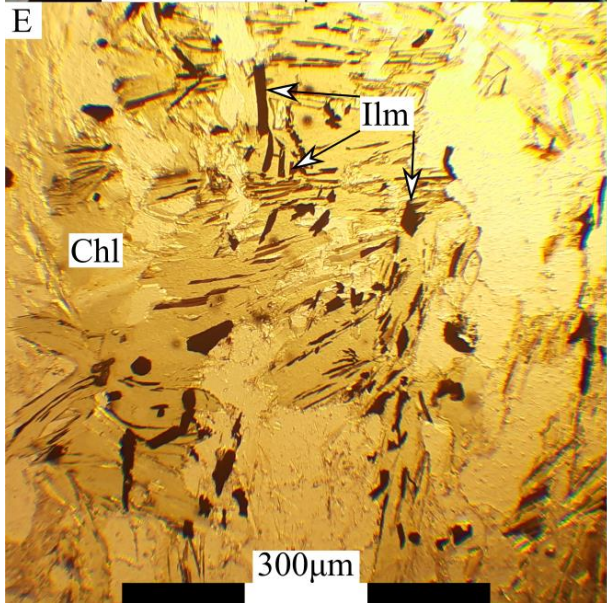
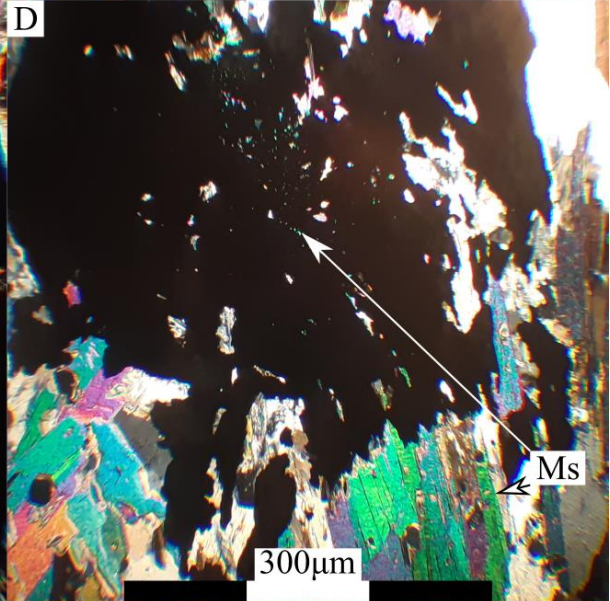
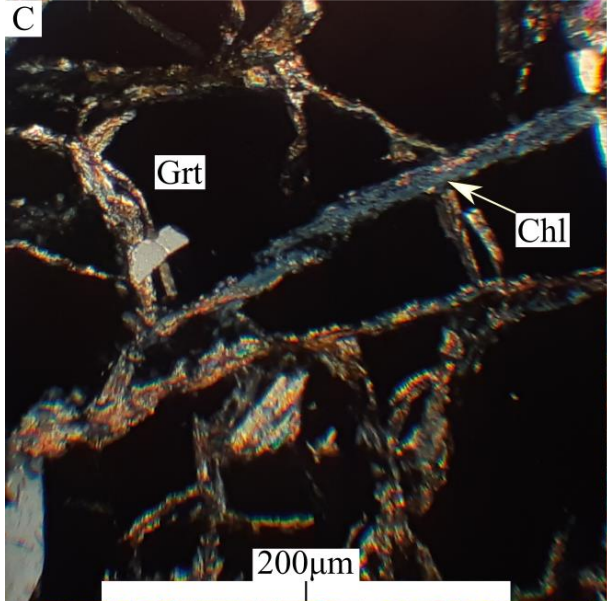
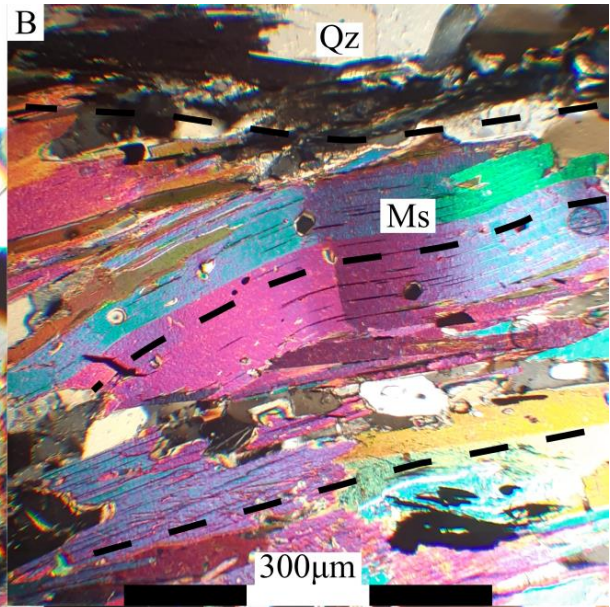
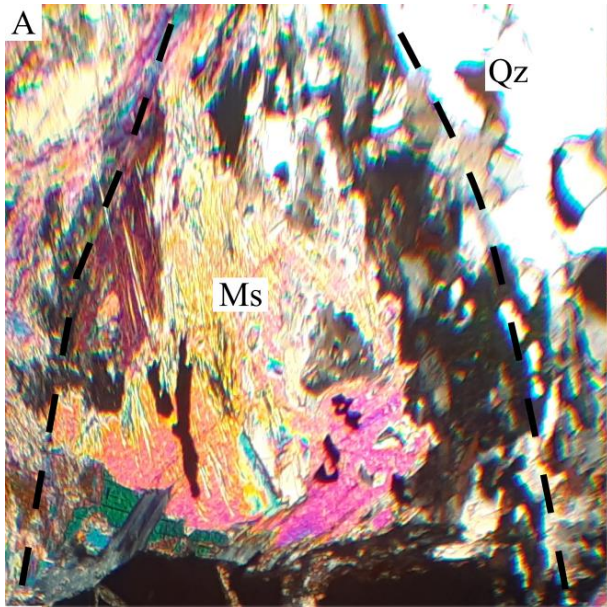


Figure 3-5 Image panel from sample RG1714. A. Garnet with strain shadow. Muscovite mesh within strain shadow. Chlorite growing in garnet fractures. B. Folded muscovite fish, with cleavage planes sub-parallel to main fabric. C. Opaque porphyroblast muscovite inclusions indicate phase grew after the nearby fabric XPL. D. Ilmenite and chlorite mesh with no fabric visible. E. Late muscovite book grown at a sharp angle to the main fabric.

Within the sample muscovite, biotite and quartz indicate the mylonitic fabric, in which muscovite fish are connected by mats of matrix sized (up to 140µm across and 1370µm in length,) muscovite grains. A second population of muscovite is seen replacing the muscovite aligned to the mylonitic fabric (see figure 3-5-E), this muscovite population commonly replaces pre-existing muscovite fish as thick (270µm) muscovite books. The cleavage of the younger muscovite population is at high angles (30° to 60°) to the main fabric. Garnet porphyroblasts often form large (4.5mm) clusters of smaller (>2.9mm) garnets, which are broken down further into smaller (>1240µm) fragments by breakdown into chlorite along pre-existing fractures (see figure 3-4-A). Chlorite is most associated with garnet and muscovite, with chlorite replacing garnet along fractures, and partially replacing some muscovites (see figure 3-5-A and E), with larger (450µm) mats of chlorite with ilmenite inclusions. Opaque porphyroblasts are seen within the sections, this opaque population contains inclusions of the surrounding minerals indicating the phase is younger than the mylonitic fabric (see figure 3-4-C).

3.3 RG1716 - Corie Each Pegmatite

This sample was taken 5km west of Newtonmore. The sample is interpreted as being a segregation pegmatite formed during shearing of the pelitic host rock (Bird & Gosling, pers. comm.).

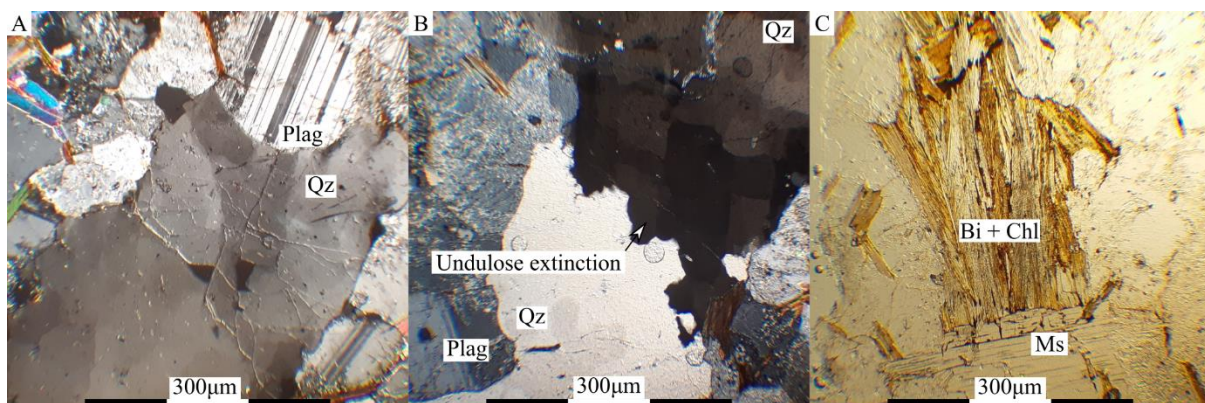


Figure 3-6 Image A shows an undeformed, rounded plagioclase grain nearby undulose quartz grain in XPL. Image B shows the typical relationship between chlorite replacing biotite. The image also contains a typical muscovite

In thin section (Figure 3-1 and Figure 3-6), the mineralogy is dominated by plagioclase of variable sericite content, quartz with undulose extinction and biotite that has variably been broken down into chlorite (see figure 3-6 image A and image B). The biotite and plagioclase grains display little evidence of shearing. Quartz forms large mat-like grains with undulose extinction and irregular grain boundaries indicating grain boundary migration indicative of higher temperatures and strain rates. These quartz mats typically are limited in size only by the surrounding biotite and plagioclase.

Most of the feldspars within the sample have undergone some degree of sericitisation, with many feldspar grains being almost completely replaced by sericite (see figure 3-6). Most biotites within the slide are at least partially replaced by chlorite, and in some places have been completely replaced by chlorite (Figure 3-6). The degree of sericitisation of plagioclase as well as the breakdown of biotite shows the sample has undergone some retrogression, likely driven by fluids.

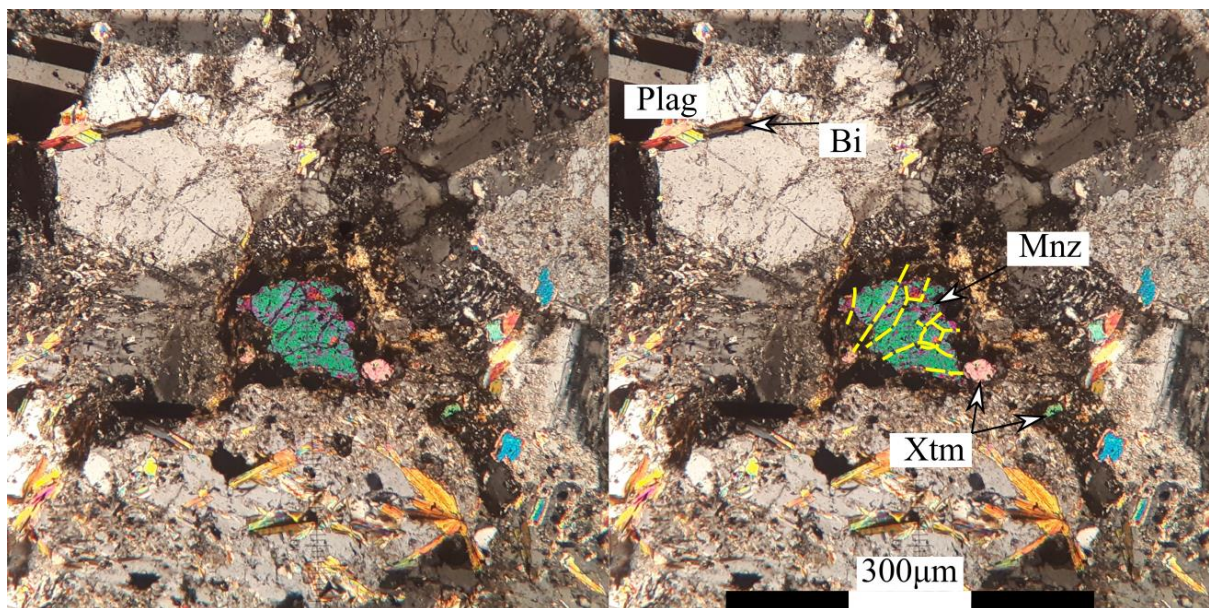


Figure 3-7 Monazite from RG1716 that was mapped and dated. The image on the right highlights the surrounding minerals and fractures within the monazite grain.

Figure 3-7 shows a large monazite from RG1716, it is surrounded by isotropic minerals and sericite. A grain of the isotropic mineral was mapped by LA ICP-MS, this map revealed a high ~40% Ca content indicating that these grains are likely to be small grains of fluorite, minor amounts of fluorapatite and a brown phase which is possibly allanite. The monazite also has a large xenotime grain within its direct vicinity. It should be noted that monazite, xenotime,

fluorapatite and fluorite partition REE's between them, with fluorite preferentially taking up REE's at lower temperatures (Shironosova and Kolonin 2013). The presence of fluorite and fluorapatite on the outer edges of the monazite indicates a degree of metasomatism of the monazite grain, supported by the degree of sericitisation of the surrounding feldspars. The proximity of the xenotime grains to the larger monazite grain may indicate a relationship with the xenotime having formed from fluid that extracted Y from the monazite grain.

3.4 RG1718 - Ruthven Semipelite

In the field, this lithology is a stromatic migmatite 340m NEE from Stac Gorm [NH 6304 2730] south of Loch Ruthven. The unit is comprised of psammite bands within which are bands of micaceous psammite separated from garnetiferous pelitic bands which contain pink orthoclase feldspar rock (Bird & Gosling, pers. comm.).

This lithology can be split into two mineralogical compositions. The composition of the melanosome and leucosomes. The melanosomes are primarily composed of biotite, muscovite, and garnet, with grains of fluorapatite and retrograde chlorite. The leucosomes are composed of quartz and sodic plagioclase, with a single occurrence of a kyanite grain, surrounded by small micas.

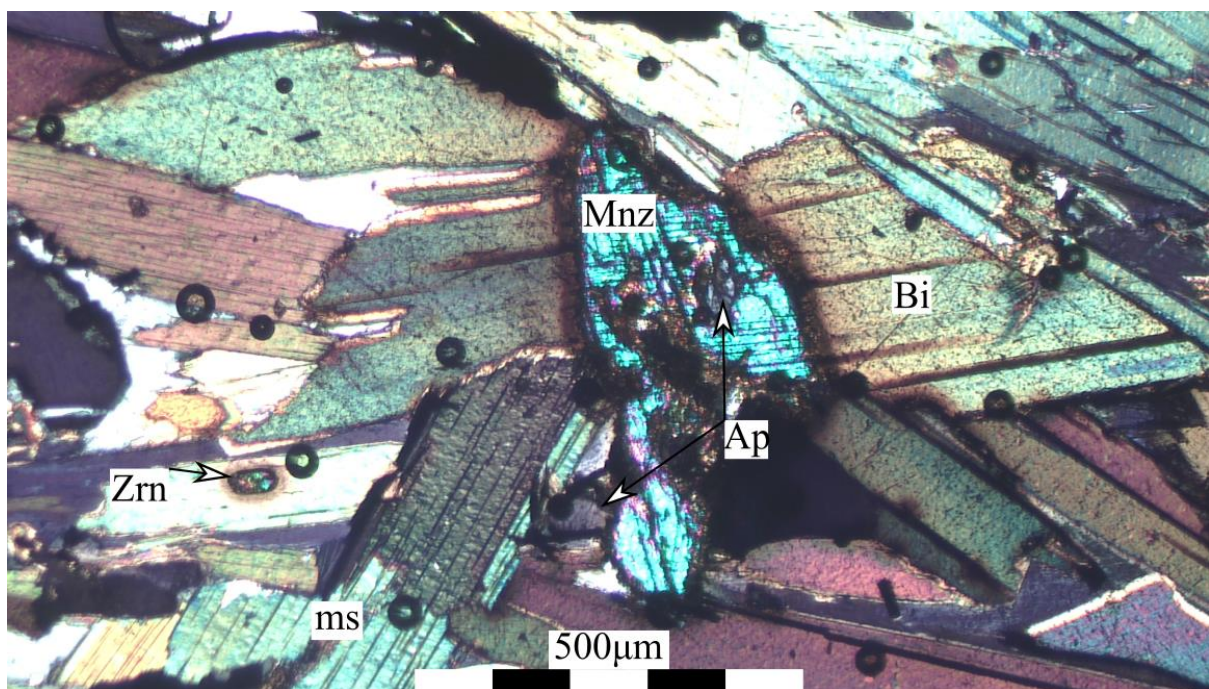


Figure 3-8 Photomicrograph of the mapped and dated monazite grain from slide RG1718c. Image is in XPL.

All monazites present within the sample are associated with apatite (Figure 4-8). There are two monazite populations within the sample, one population is composed of small (>30µm) granular monazites included within larger apatite grains, these monazites form as inclusion clusters within the apatite grains. Of the other monazite population only one grain was found, the mapped and dated monazite. This monazite is notably larger than the other monazites within the sample, contains a smaller apatite grain within and a small apatite grain directly adjacent to it. This monazite has grown within the centre of a biotite book and the centre of the grain appears to have undergone some reaction. Monazite is also associated with both biotite and muscovite within the pelitic layers. The presence of monazite as small inclusions within apatite/fluroapatite grains may indicate a reaction between the apatite population and REE rich fluids as the origin for the metamorphic monazite population within the sample.

Monazite, fluorapatite, biotite, muscovite, garnet, and chlorite are restricted to the melanosomes. It is common for garnets to have chlorite retrograde reaction rims (see image B in Figure 3-9).

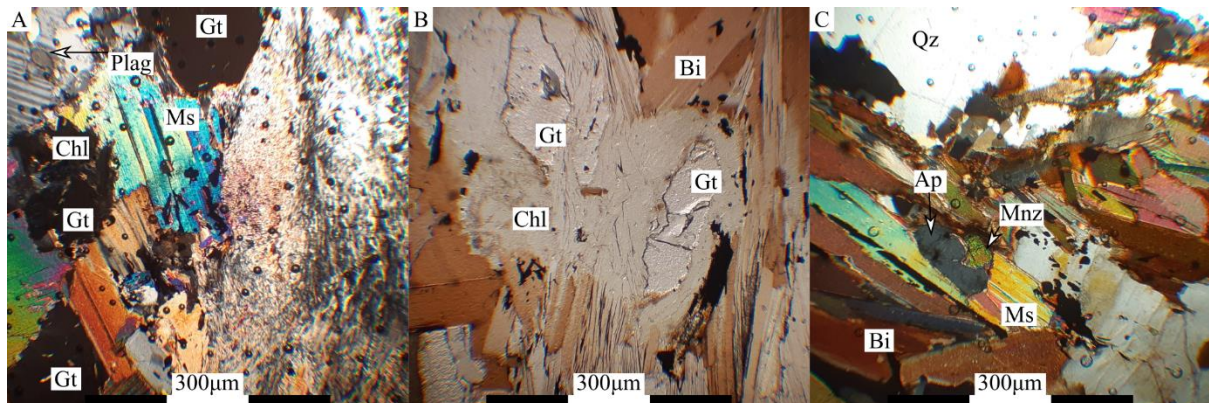


Figure 3-9 Image panel of typical mineral relationships within sample RG1718. Image A shows garnets adjacent to muscovite, the image also shows a region of mica breakdown into small individual mica plates. Image B chlorite reaction rim around garnets. Image C shows the relationship between fluorapatite, monazite, biotite, and muscovite.

3.6 Deformation Fabrics

3.6.1 The Badenoch Group

3.6.1.1 RG1710 Findhorn Metasediment

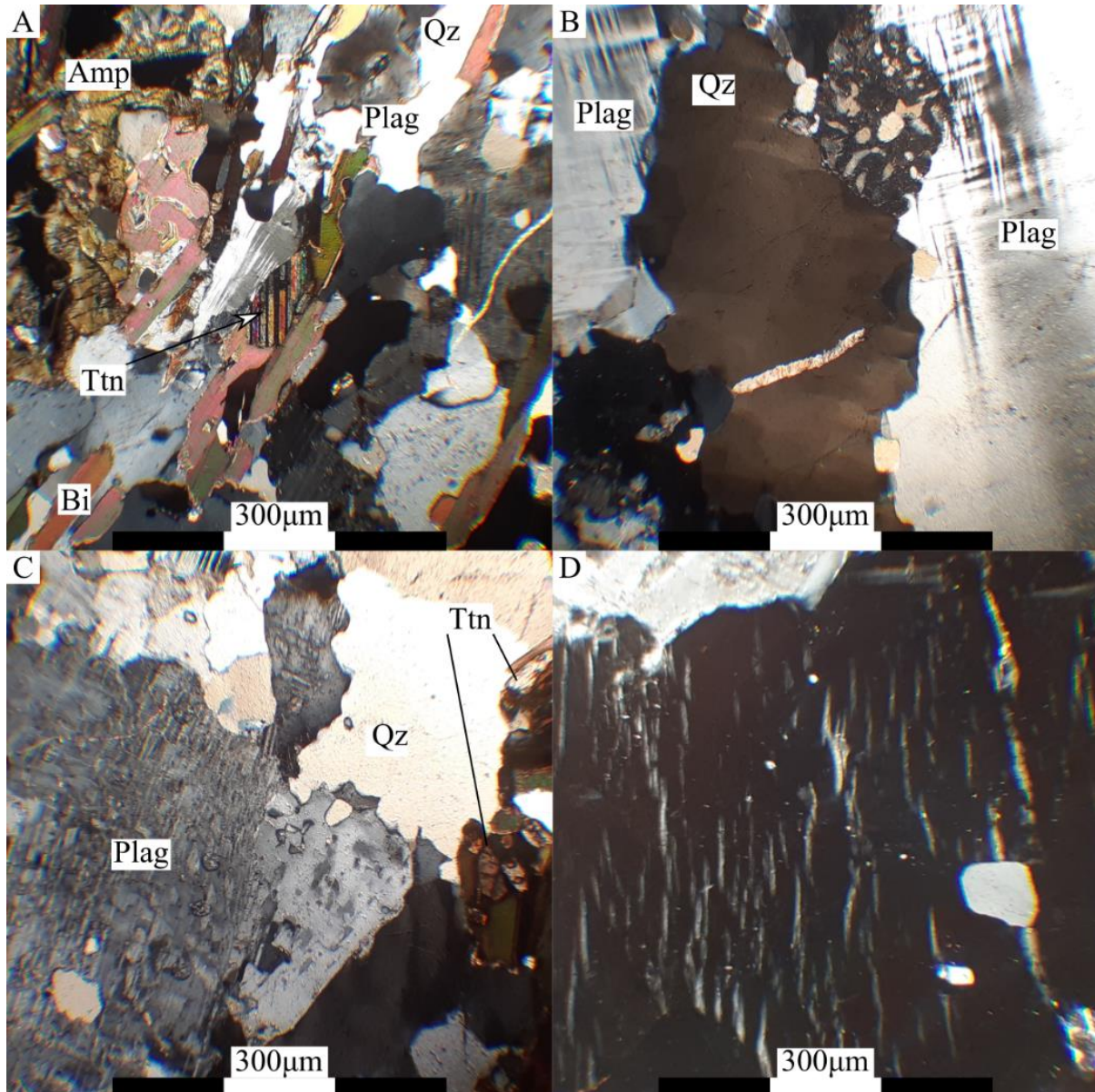


Figure 3--10 XPL photomicrographs of sample RG1710. Image A shows the predominant linear fabric defined by titanite (lamellar twinning) and biotite. Quartz and plagioclase display lobate grain boundaries. B. shows elongate sub-grains within central the quartz grain, not smaller grains on quartz edge indicative of SGR. C Elongate plagioclase grain adjacent to quartz grains within the pale gneiss bands showing lobate grain boundaries, plagioclase grain shows exsolution texture with possible existing perthitic texture or cross hatched twinning. D. Flame perthite texture.

Within sample RG1710 biotite and titanite define the fabric within the dark gneissose bands. This fabric gently wraps the adjacent pale bands consisting of variable feldspar content

(typically plagioclase and microcline endmember plagioclase) and quartz. The presence of flame perthite within large feldspar grains (>300µm) as well as kinked twinning of feldspar grains is indicative of greenschist facies deformation with high differential stress (Passchier and Trouw, 2005). The growth of nodular myrmekite (figure 4-9 image B) is upper green schist to amphibolite facies deformation, within temperatures ranging from >500°C to 600°C (Harlov and Wirth 2000).

The lobate grain boundaries of quartz and plagioclase grains may indicate grain boundary migration (see figures 3-3-A mineral labelled QZ and 3-4-B mineral labelled Plag). Grain Boundary Migration (GBM) within feldspar is indicative of deformation temperatures greater than 800°C. The development of elongate sub-grains within quartz is due to sub-grain rotation (SGR) (figure 3-10-B central quartz grain) is indicative of deformation within the temperature range from 390°C to 530°C (Stipp et al., 2002). Large elongate quartz and feldspar grains are frequently surrounded by smaller grains which is indicative of SGR (figure 3-10-B small quartz grains adjacent to central grain).

The presence of flame perthite (figure 3-10-D) is associated with greenschist facies deformation, as opposed to the granulite deformation temperatures required for feldspar GBM. The presence of flame perthite which is indicative high differential stress at greenschist facies deformation. The lobate grain boundaries may be the result of a pre-existing intergrowth texture within the quartz plagioclase matrix rather than high deformation temperatures (>800°C) required for GBM deformation of feldspar. The presence of anti perthite texture within the feldspars (figure 3-3-B) along with the intergrowth textures of quartz-biotite (figure 3-3-D) and quartz-amphibole (figure 3-3-C) indicate a drop in temperature and a change in mineralogy within the lithology. These intergrowth textures of the quartz and feldspar (figure 3-3-B) may explain the lobate boundaries of the feldspars (figure 3-4-B), rather than the grain boundary migration which would require temperatures in excess of 800°C. Taking the intergrowth textures into account the presence of both flame perthite (figure 3-10-D) and myrmekite nodules (3-10-B), and the dominance of SGR within feldspar and GBM and SGR within quartz indicates greenschist to lower amphibolite facies deformation occurring after retrogression from a higher grade mineralogy.

3.6.2 The Grampian Group

3.6.2.1 RG1718 Ruthven Semipelite

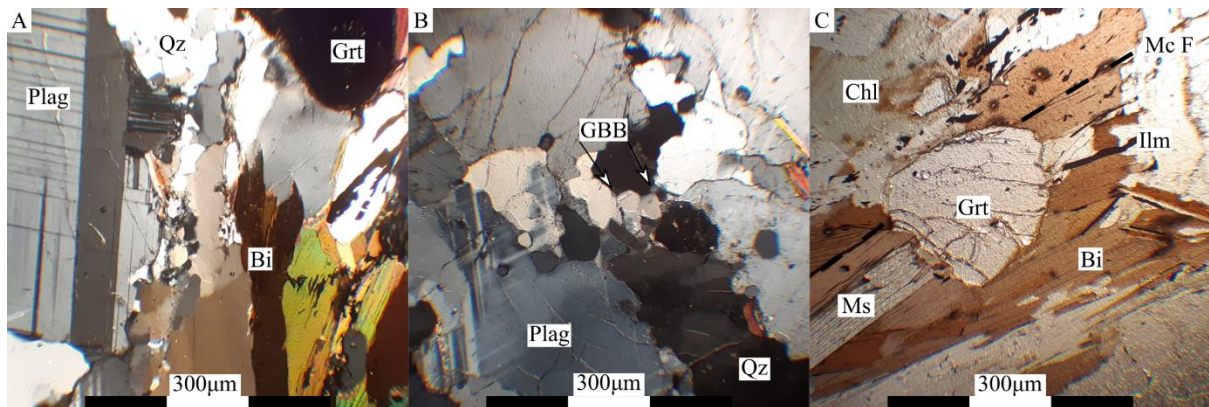


Figure 3-11 Photomicrographs of sample RG1718. A XPL, leucosome (left) adjacent to melanosome mineralogy (right). B XPL, leucosome mineralogy of quartz and plagioclase, quartz so weakly defined internal subgrains. C PPL, melanosome mineralogy of biotite, garnet, muscovite chlorite and ilmenite. Mc F denotes the black dashed line which shows the mica cleavage orientation. Note that this mica orientation is not affected by the garnet.

Within thin section of the Ruthven Semipelite the fabric within the melanosome is linear and defined by the mica content and ilmenite. Garnet overprints the linear mica fabric (Figure 3-11-C) showing garnet growth after the development of said fabric. Within the leucosome large (1.5mm) plagioclase grains have grown, with quartz shows grain boundary bulging (GBB) (see figure 3-11-B arrows point to undulating grain boundary with the adjacent extinct quartz grain).

3.6.3 The Grampian Shear Zone

3.6.3.1 RG1703 Lochindorb Garnet Amphibolite

The deformation fabrics within sample RG1703 are defined by a predominantly linear fabric to which quartz, biotite, amphiboles, and opaque phases are aligned (see sample 3-12-B and D). This linear fabric wraps the garnet and plagioclase porphyroblasts. Within the garnetiferous portion of the section minerals reach a greater grain size, the quartz minerals within the garnetiferous region show little internal deformation and are equant in shape adjacent to garnets and show grain boundary migration further away from the garnets while outside of this region quartz is amoeboid in shape or forms smaller (<50µm) grains.

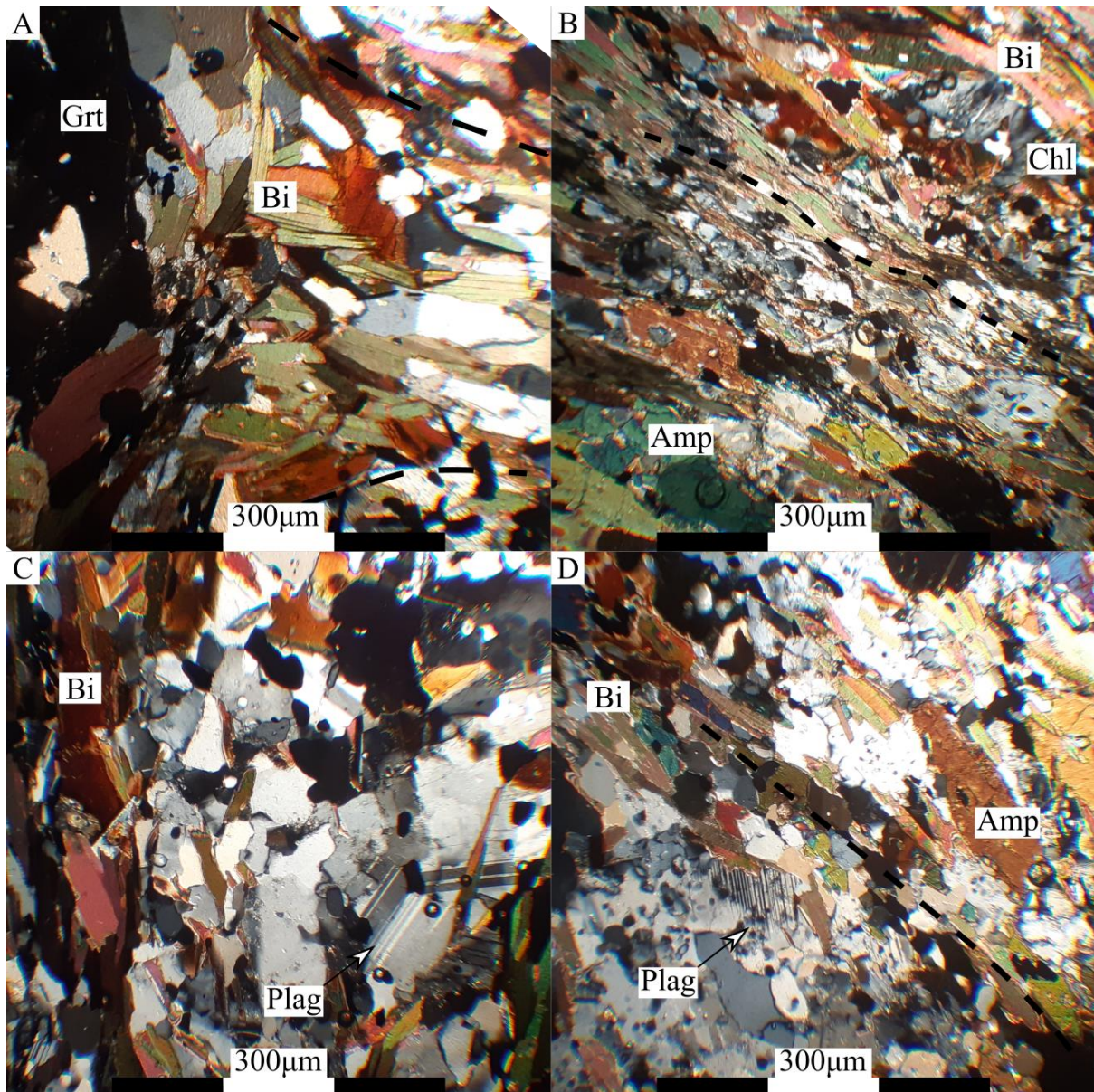


Figure 3-12 Photomicrographs in XPL of sample RG1703. A Garnet (left) strain shadow with undeformed quartz and larger grain size. B Crenulated fabric defined by biotite and quartz, notable smaller grain size due to grain size reduction of quartz and biotite, image from garnet free zone. C Plagioclase biotite and quartz within garnet zone. Quartz and plagioclase show grain boundary migration. D Linear fabric defined by amphibole and biotite; smaller quartz grain size due to grain size reduction.

The difference in grain size, grain boundary shape and internal quartz grain deformation seen within the sample indicated heterogeneous strain within the lithology. Regions with garnets (figure 3-12-A) show lower strain rates and larger grain size than regions without (figure 3-12-B and D), this may be due to garnetiferous regions consisting of interconnected garnet porphyroblasts strain shadows, causing increased deformation in garnet free regions. Within the sample, quartz shows both grain boundary bulging (Figure 3-12-C) and grain size reduction (Figure 3-12-B), this is indicative of both low temperature deformation and high strain rates.

However, because of the heterogeneous strain rates within the sample the high strain rate grain boundary reduction cannot be used to indicate high strain rate deformation across the lithology.

3.10.1.1 RG1714 GMS Glen Gour

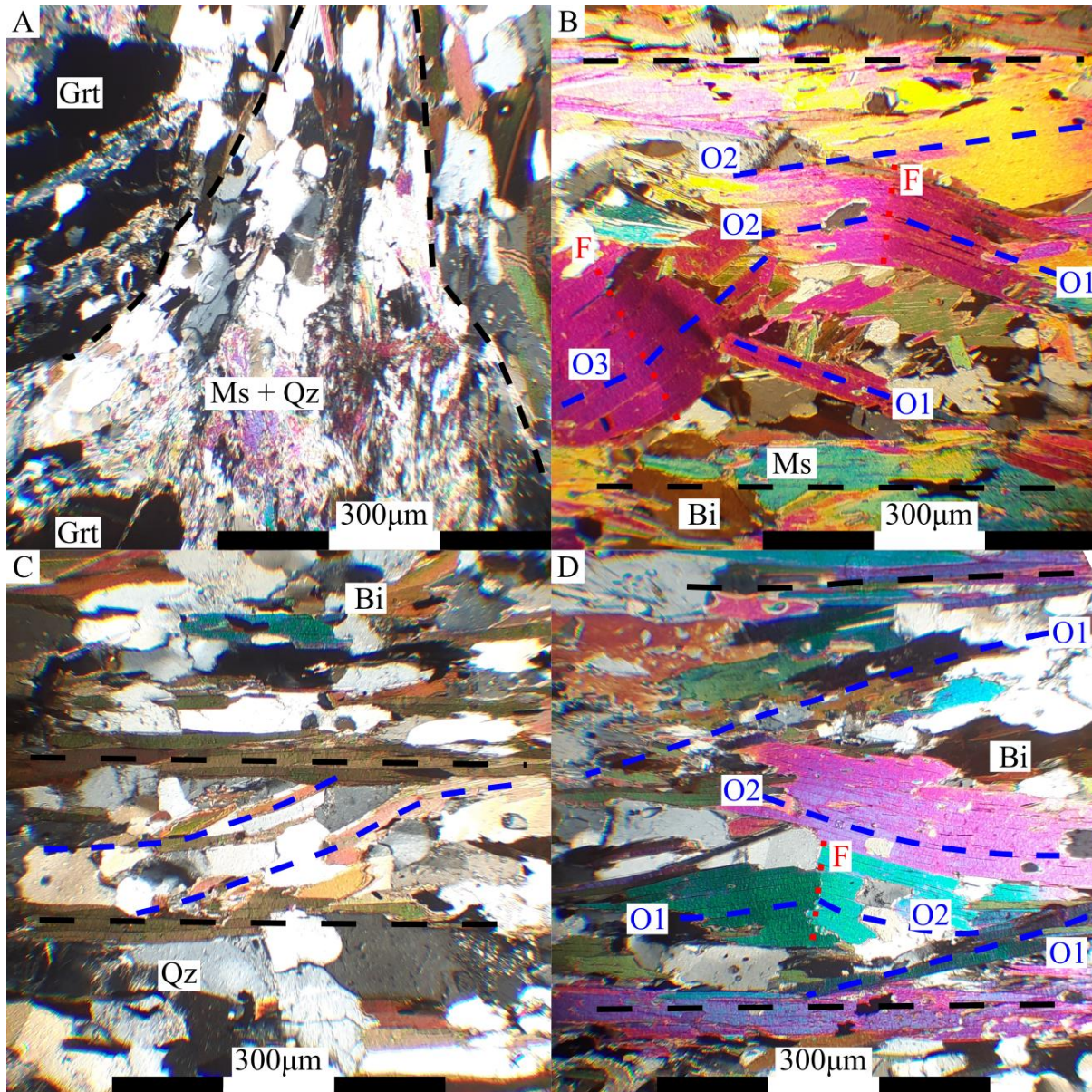


Figure 3-13 XPL image panel. A, quartz and disaggregated muscovite strain shadow from nearby garnet porphyroblast. B, Multiple orientations of muscovite cleavage with two folded muscovites. C, Biotite displaying 2 fabric orientations O1 as defined by the black dashed lines and O2 defined by the blue dashed lines. In black the main mylonitic foliation, in blue secondary biotite orientations at small angles to the main foliation. D, Folded muscovite fish with two preferred cleavage orientations.

Sample RG1714 is a pelitic mylonite that contains mica fish, garnet porphyroblasts display well-developed strain shadows of quartz and disaggregated muscovite (figure 3-13 B and D). The garnet population are commonly elongate, with one garnet within section displaying a

rounded rectangular shape within the thin section. The muscovite fish population appears to have two favoured cleavage orientations, indicating reactivation of the shear zone (figure 3-13-B). Some of the mica fish within the thin section are folded with fold angles of ranging from 175° to 165° . Quartz and plagioclase have deformed into elongate equigranular interlobate grains (figure 3-13-C). The folding of muscovite fish into multiple orientations at small angles to the mylonitic foliation indicates multiple episodes of shearing affecting this sample.

3.10.1.2 RG1716 Corie Each Pegmatite

Sample RG1716 contains plagioclase porphyroblasts (8mm width in section) mantled by quartz and plagioclase (figure 3-1 central slide, base image contains the plagioclase porphyroblasts). The plagioclase within the porphyroblast mantle is sericitized while the porphyroblast is relatively unaffected by sericitisation.

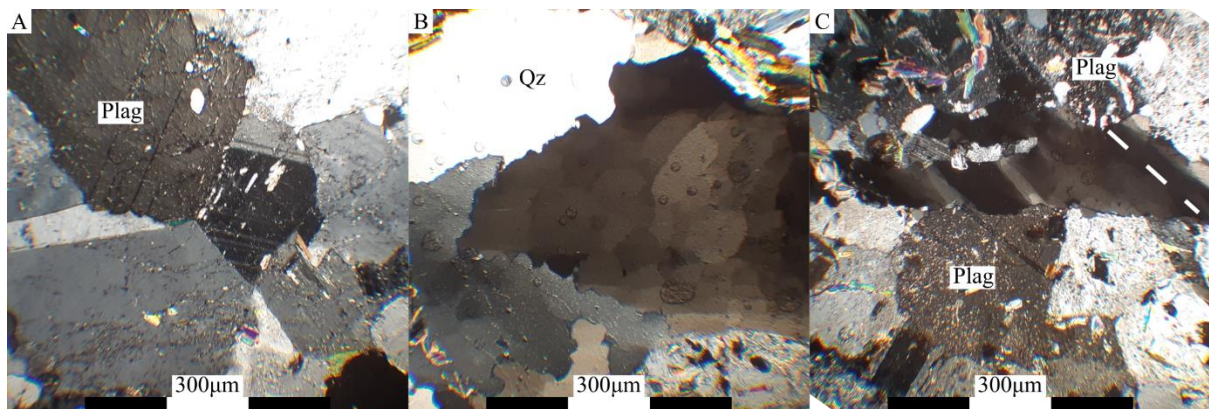


Figure 3-14 XPL photomicrographs of RG1716. A shows granoblastic plagioclase grains. B Shows large (500µm) quartz grain with well-developed blocky sub-grains. C. shows an elongate quartz grain bounded by plagioclase, the sub-grains within the quartz are elongate and a high angle to the fabric that runs horizontally across the image.

Plagioclase unrelated to the porphyroblasts within section are equigranular, granoblastic in texture while quartz grains are seriate-interlobate in texture (figure 3-14). Within the section, quartz grains show 2 types of internal sub-grain, equant, checkerboard sub-grains (figure 3-14-B) and elongate ribbon sub-grains (3-14-C). The presence of two forms of quartz deformation are indicative of heterogeneous strain, with checkerboard sub-grains indicating low strain rates and ribbon sub-grains forming due to sub grain rotation indicative of moderate strain rates and temperature during deformation.

The presence of granoblastic plagioclase apparently unaffected by mylonitisation seen at outcrop and hand specimen scale indicates the pegmatite was emplaced during shearing and thus is a syn-shear pegmatite body.

4 RESULTS

4.1.1 RG1703 - Lochindorb Garnet Amphibolite titanite U-Pb

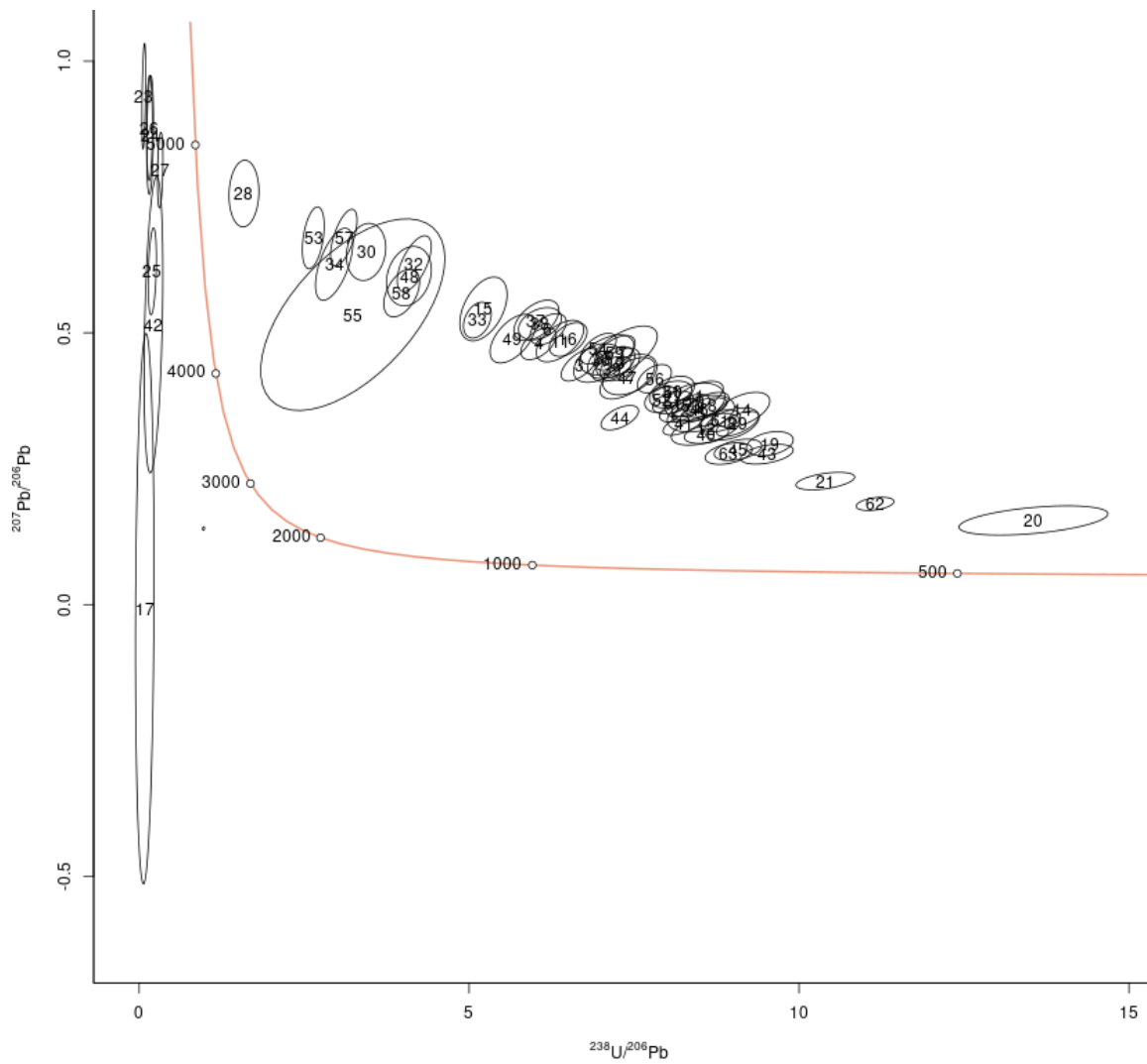


Figure 4-1 Complete RG1703 U-Pb titanite dataset Terra-Wasserburg plot. Produced from 39 analysed grains.

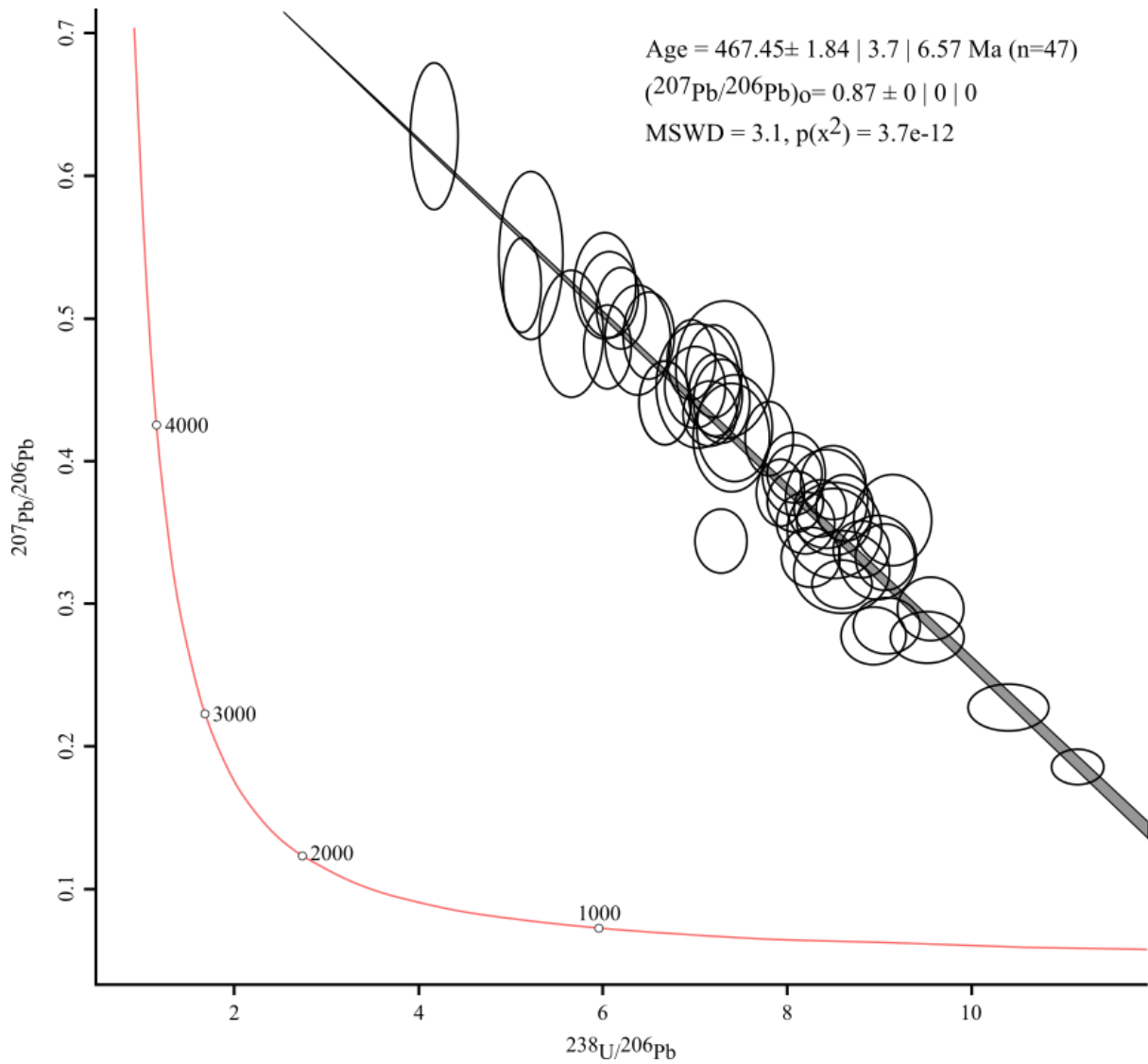


Figure 4-2 Discordia plot from Sample RG17103. The discordia was used to work out the initial Pb value of the titanites. Erroneous and over dispersed analyses removed (See section 2.3 for clarification on spot omission). See the difference between figure 6-4 and 6-5 for omitted spots. Seven spots were over dispersed due to their negligible U contents and plotted to the left of the concordia.

A Terra-Wasserburg plot used to calculate the initial Pb values for titanites within sample RG1703. The discordia transects the concordia at $467.45 \pm 1.84\text{Ma}$ (MSWD 3.1 $p(X^2) = 3.7e^{-12}$ n = 47).

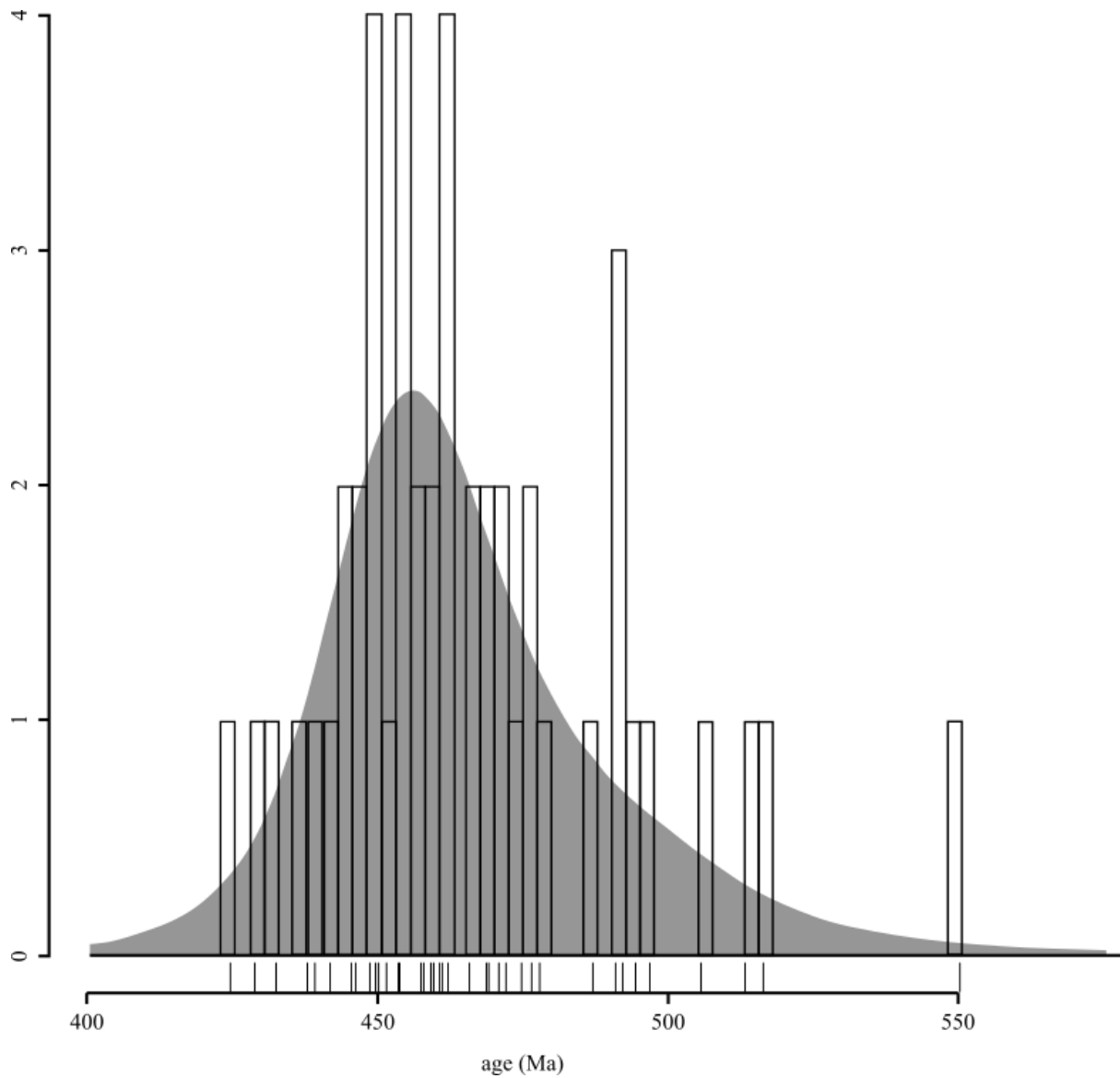


Figure 4-3 KDE (Kernel Density Estimation) plot of sample RG1703. Post nominal Pb correction.

The above KDE (Kernel Density Estimation) plot of initial Pb corrected titanite U-Pb ages shows the dominant age clusters, at 450Ma, 460Ma and 470Ma.

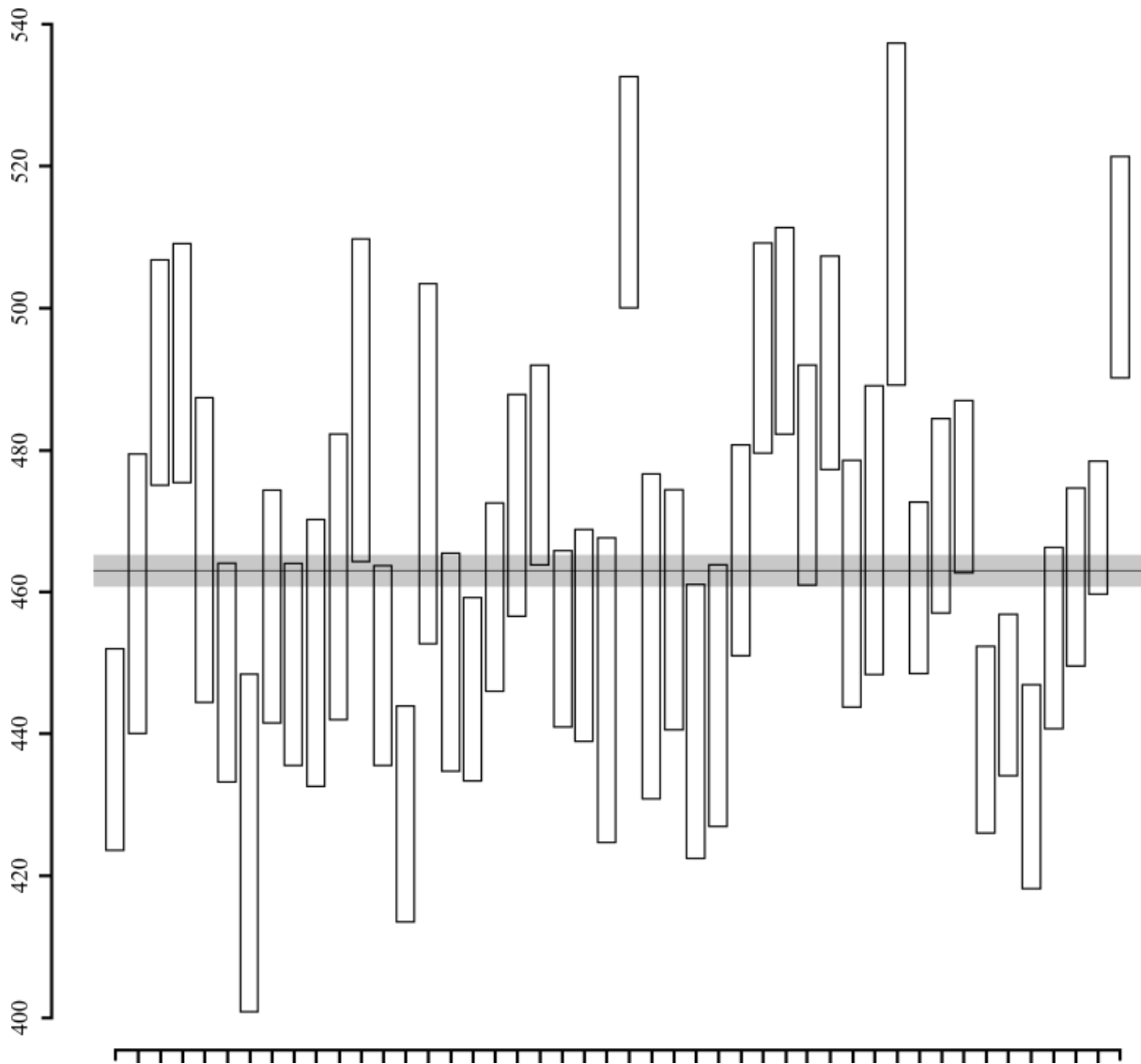


Figure 4-4 Weighted mean plot of data from sample RG1703. Black dots within the bars are over the centre of the age bar. Post nominal Pb correction.

The weighted mean plot shows the weighted mean age of $463.05 \pm 1.15\text{Ma}$ ($n=46$) with an MSWD of 6.73.

4.1.2RG1710 - Findhorn Metasediment titanite U-Pb

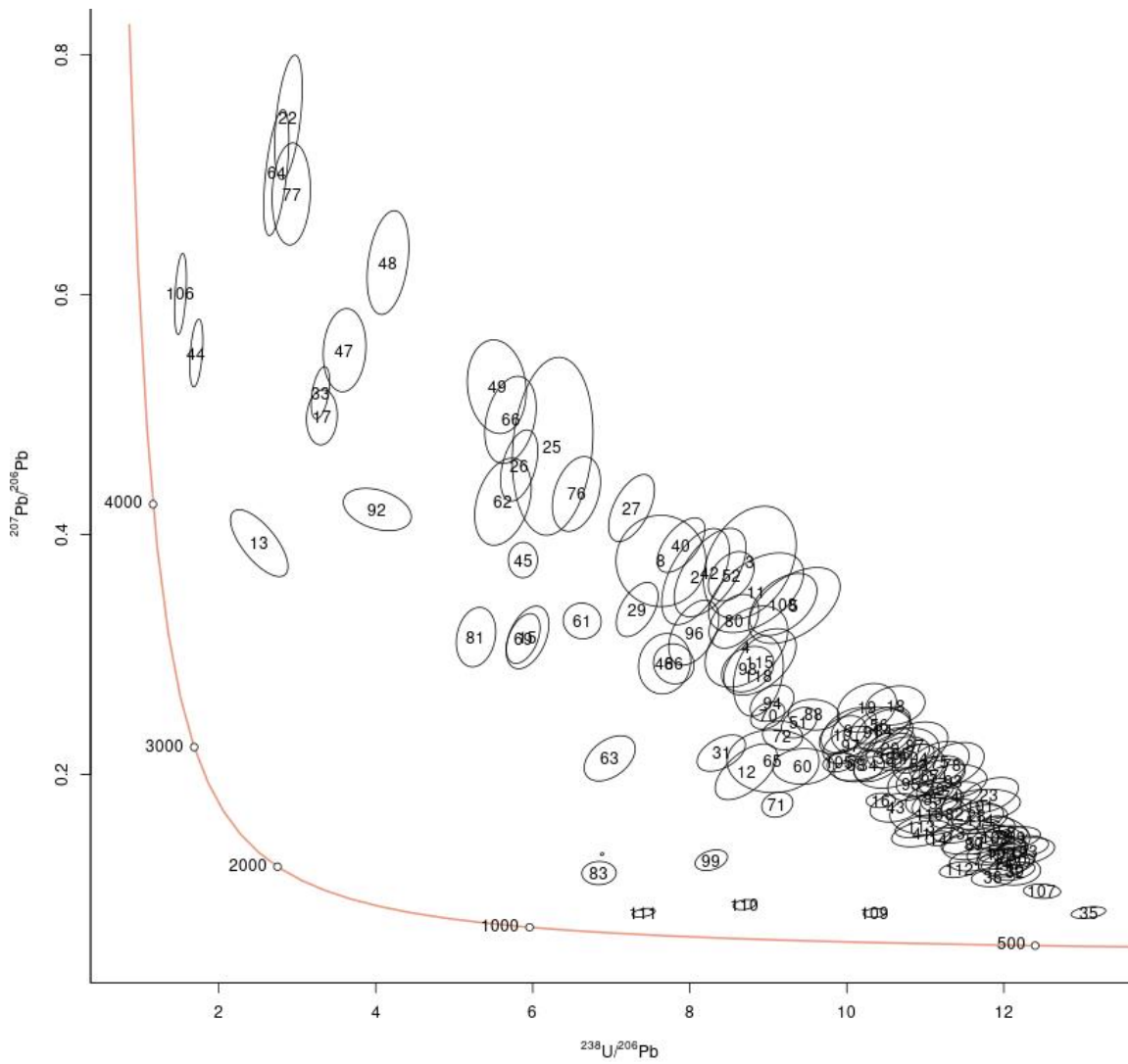


Figure 4-5 n = 118. RG1710 titanite U-Pb Terra-Wasserburg Plot

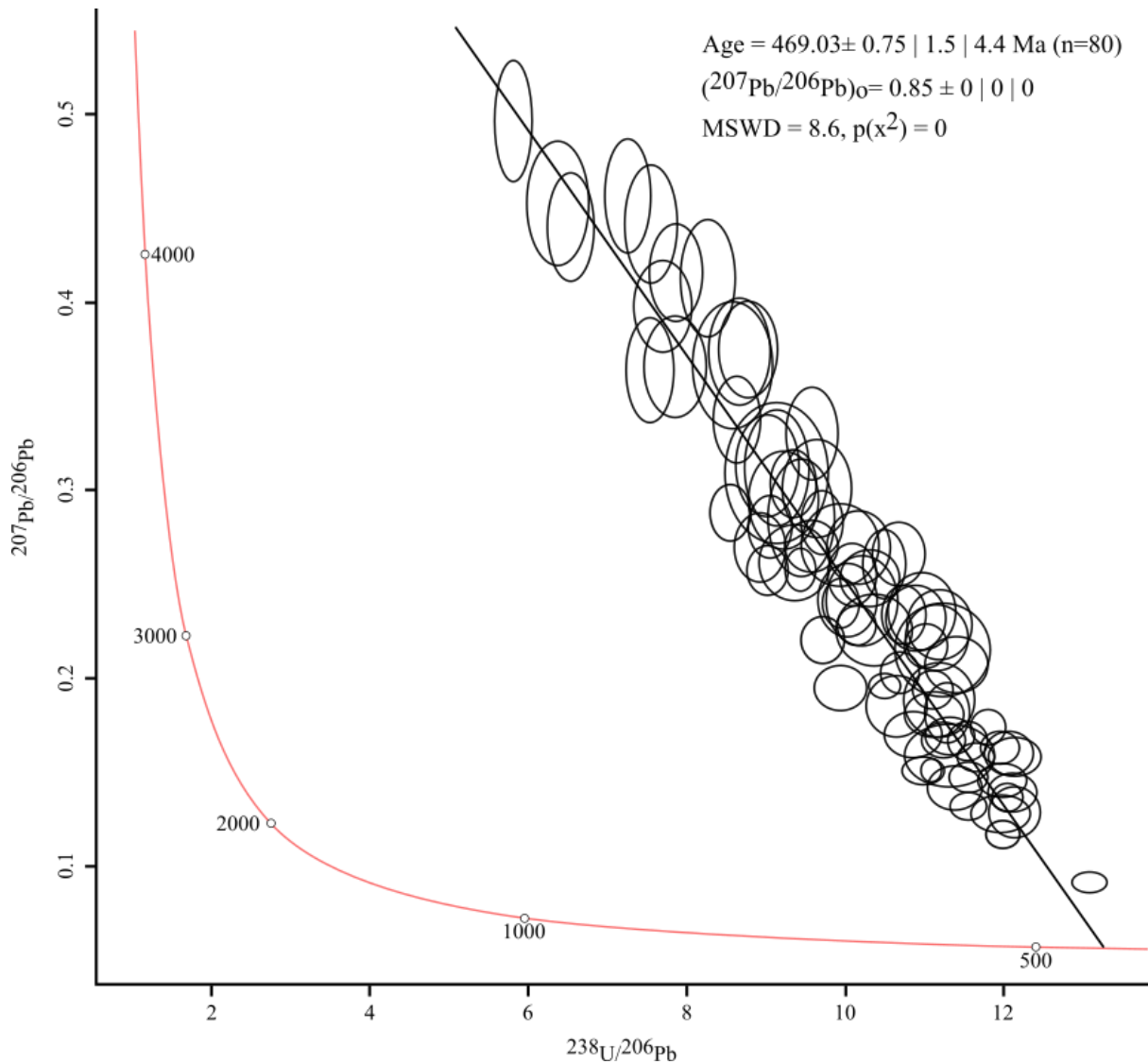


Figure 4-6 Discordia plot of sample RG1710. The Discordia was used to calculate the initial Pb value. 38 Analyses were omitted to correct for overdispersion of the spots as well as the reasons given in section 2.3.

82 individual grains were ablated for U-Pb analysis, these 82 grains gave 121 total spots. Of which 4 analyses from 2 grains were not titanite, as indicated by U/Pb ratios less than 0.5. 37 analyses have been omitted from the above plot.

The Terra-Wasserburg discordia plot for sample RG1710 gave an initial Pb value of 0.85. A discordia age value of $469 \pm 0.3\text{Ma}$ (n=80) was also produced from this plot. With an MSWD of 8.6 showing a significant degree of over dispersion.

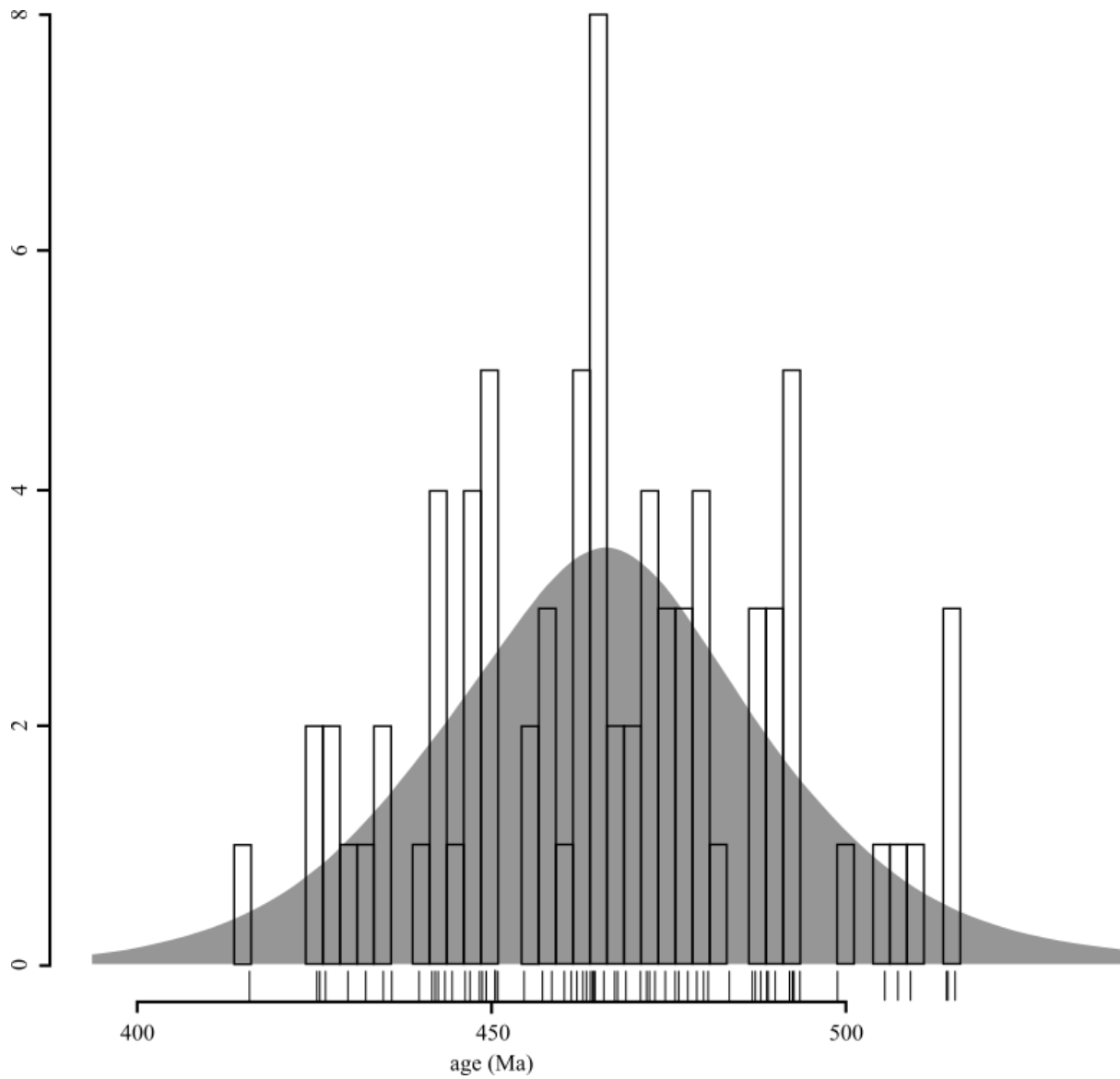


Figure 4-7 KDE plot of sample RG1710. Post nominal Pb correction.

The KDE plot of the Pb corrected age values reveals 3 main age pulses; 485Ma to 480Ma, the main age pulse of 475Ma to 460Ma and the final age pulse of 450Ma to 440Ma.

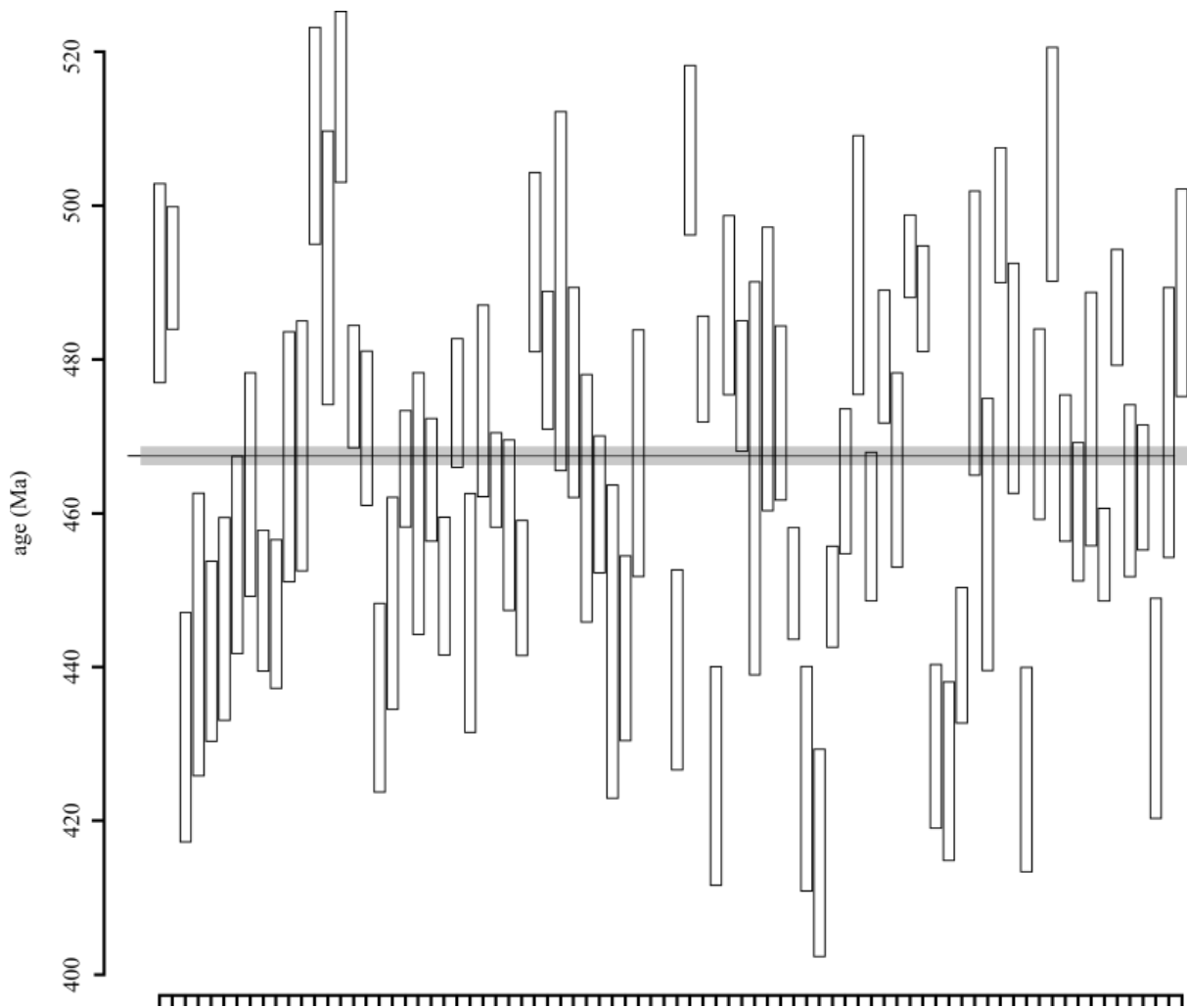


Figure 4-8 Weighted mean plot of Pb corrected age data from sample RG1710.

The weighted mean plot produced an age of $467.52 \pm 0.6\text{Ma}$ ($n=80$) with an MSWD of 15.6. The range of ages shows a high degree of over dispersion.

4.1.3 RG1716 - Corie Each Pegmatite

4.1.3.1 RG1716 Isotope maps

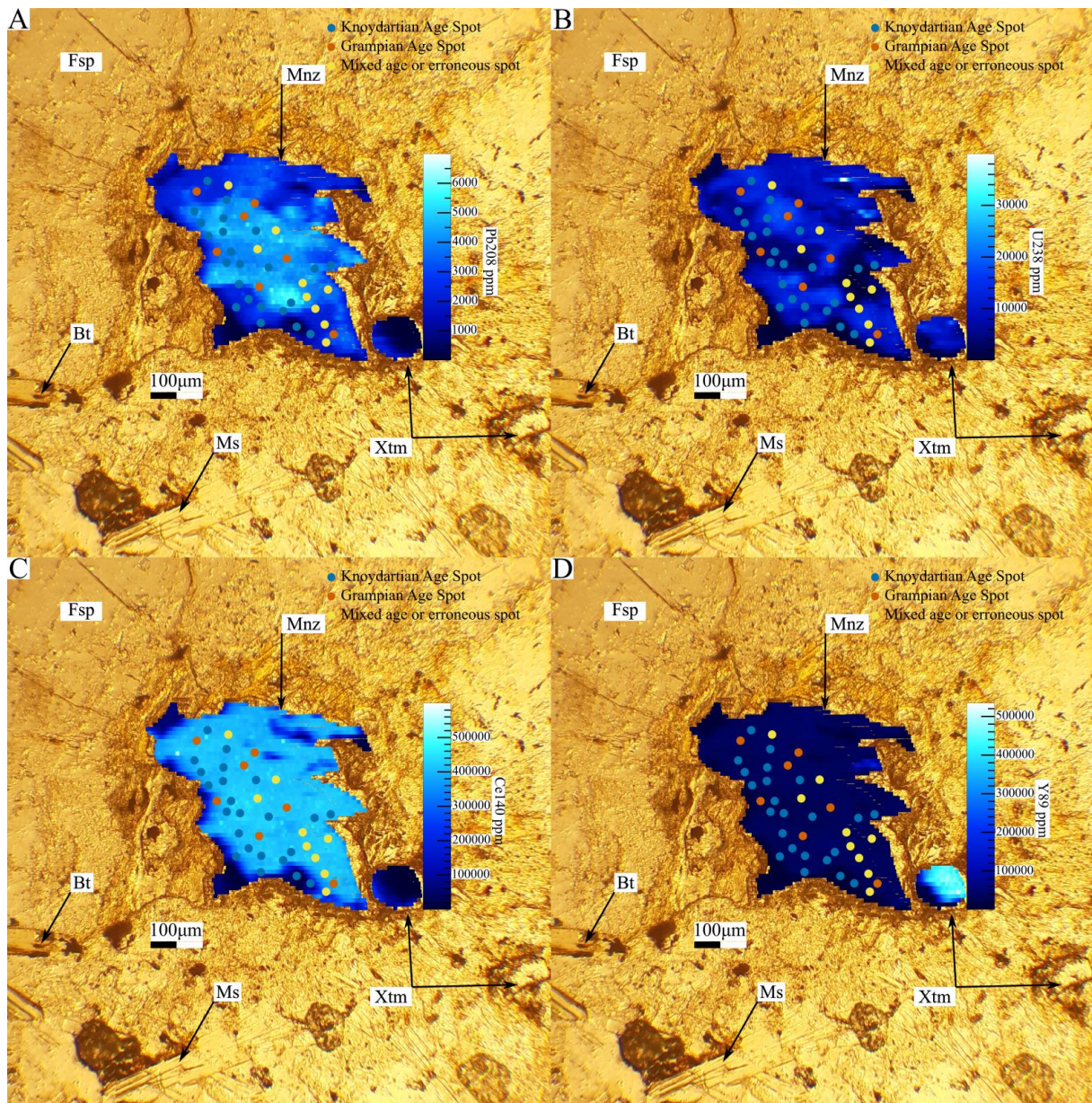


Figure 4-9 RG1716 Pb (panel A) U (panel B) Ce (panel C) and Y (panel D) isotope maps over a PPL microphotograph of the mapped dated monazite.

LA-ICP-MS element maps produced from the monazite within sample RG1716 show complex patchy zoning with U, Pb and HREE's. Elements such as Ce, Nd, Sm show which parts of the map are monazite in composition. Adjacent to the main mapped grain were two smaller grains, one of which was mapped. Mapping revealed this adjacent grain to be xenotime based on the

high Y content. The Pb element map is useful to separate the older high Pb core of the mineral grain from the younger age mineral domains.

4.1.3.2 RG1716 Monazite U-Pb

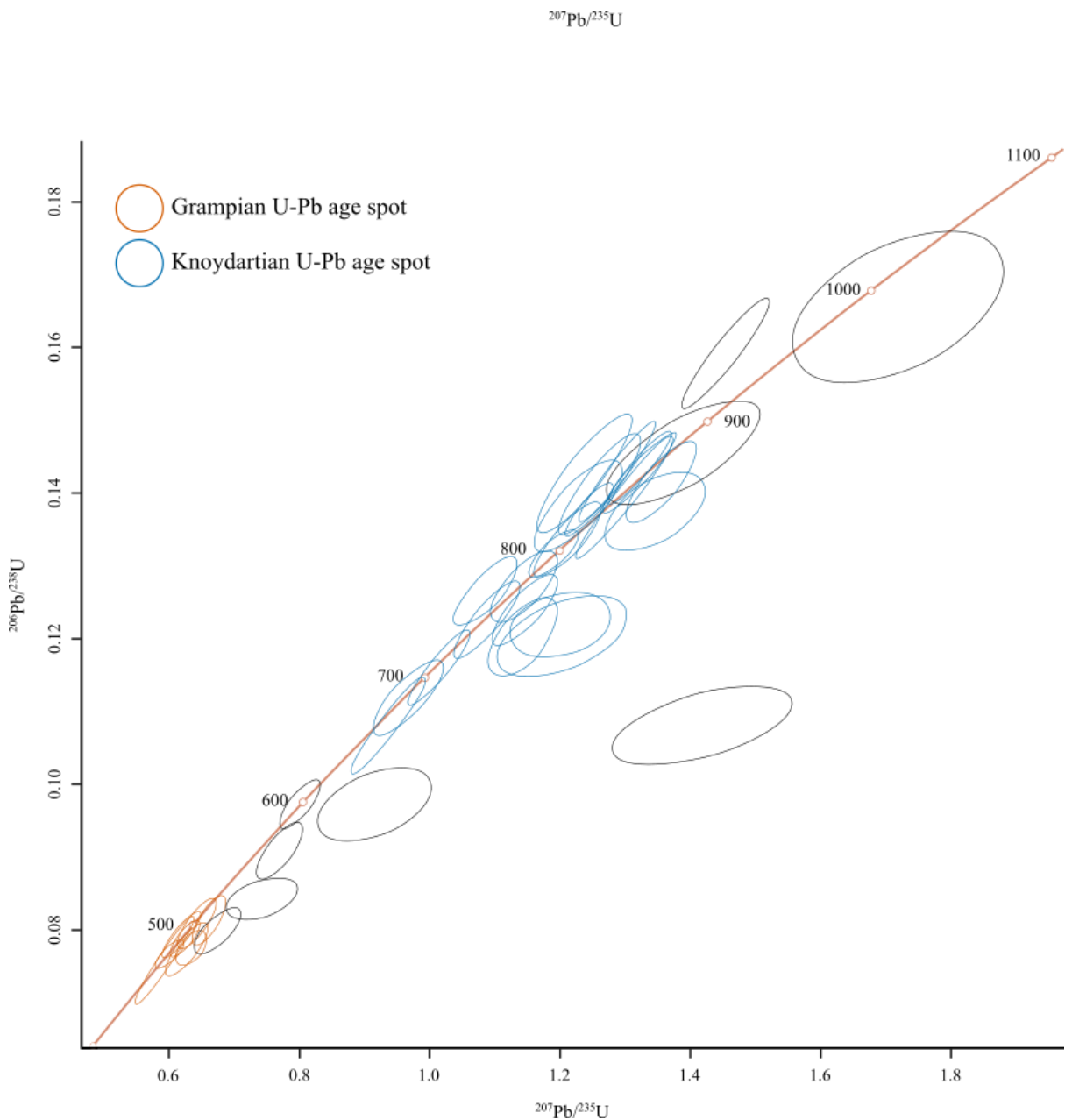


Figure 4-10 U Pb concordia of the dated monazite from sample RG1716

The monazite within sample RG1716 produced a spread of ages. A clear Grampian cluster of $485.85 \pm 2.63\text{Ma}$ (MSWD = 4.9, $p = 0.026$ $n = 5$) and a spread of individual ages from 847Ma

to 605Ma. Of these older ages, a clear grouping from $824 \pm 2.73\text{Ma}$ (MSWD 9.7 $p(X^2) = 0.0019$ $n = 12$) to $751.81 \pm 3.56\text{Ma}$ (MSWD = 3.2 $p(X^2)$ $n = 8$) can be picked out, of which all analyses bar two spots are within the age range of the Knoydartian 850 to 680Ma (Spencer et al. 2019). Spots within these age clusters plot both to the right and the left of the concordia.

Many spots, particularly spots of possible Neoproterozoic age are discordant, with spots plotting both to the left and right of the concordia.

4.1.4 RG1718 - Ruthven Semipelite

4.1.4.1 RG1718 Isotope maps

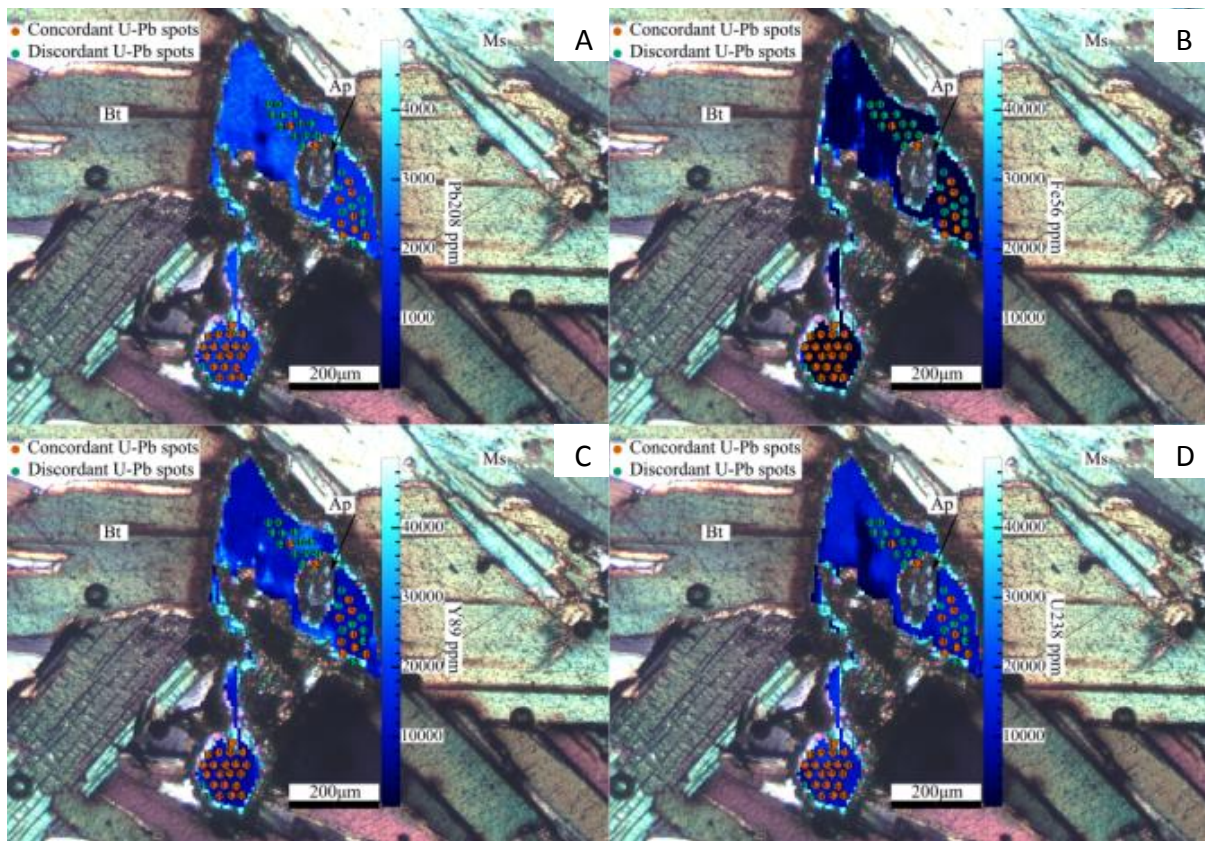


Figure 4-11 Isotope (Pb - A, Fe - B, Y - C and U - D) maps of the analysed monazite from sample RG1718 Ruthven Semipelite overlain over an XPL photomicrograph of the same monazite. Note the region of depleted U and Pb, with elevated Fe. This region was interpreted as a fluidised fracture.

Mapping the large monazite grain within sample RG1718 revealed the grain to be nearly homogenous, except for a region of depleted LREE and U, this region also showed elevated Fe and Hf and is likely a fracture within the grain, along which fluid precipitation occurred. The other region of interest is a patch of elevated HREE's, this region gave ages that plotted to the right of the concordia and showed variable increase in Pb values.

4.1.4.2 RG1718 Ruthven Semipelite monazite U-Pb

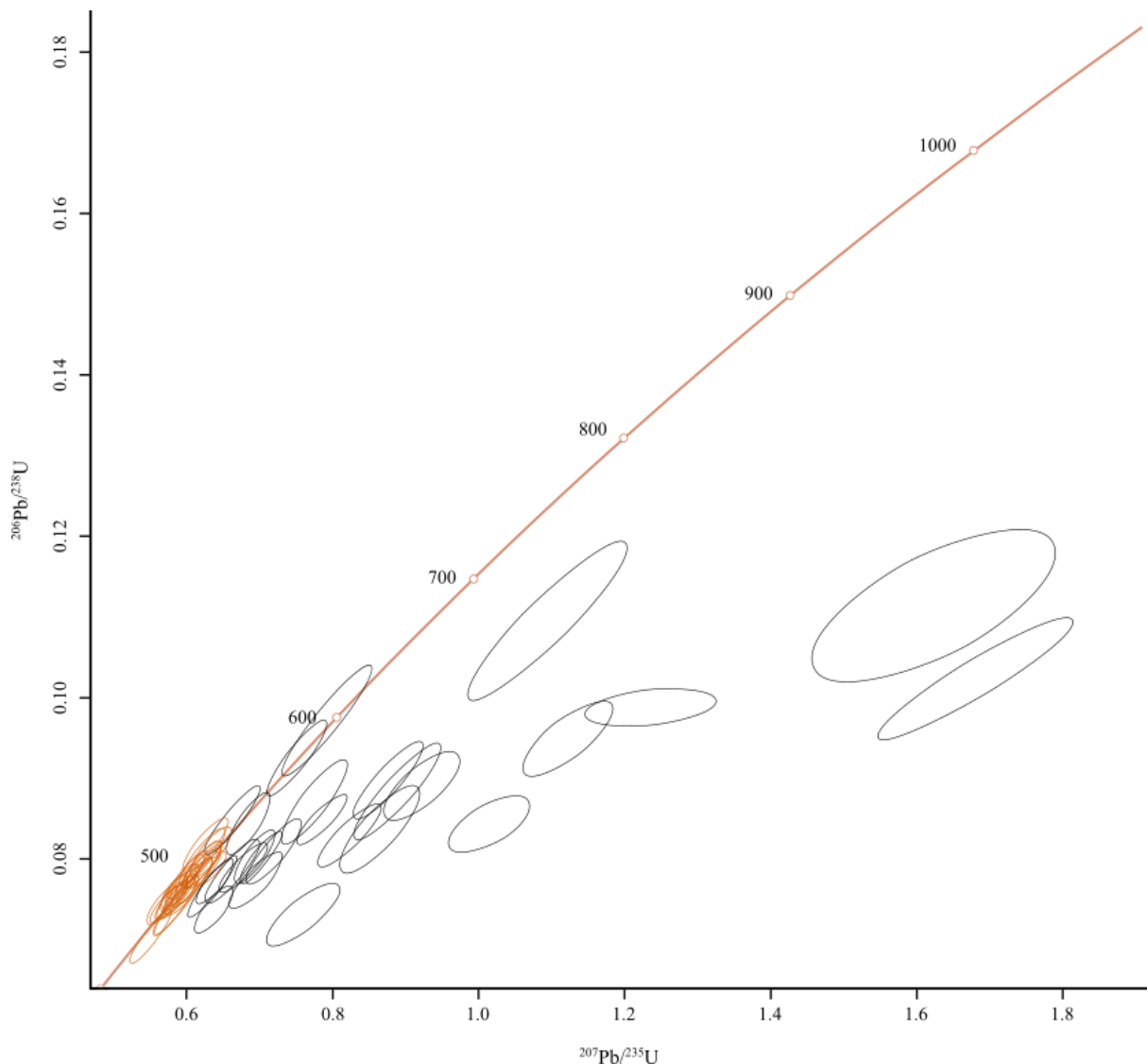


Figure 4-12 U Pb ages from sample RG1718 that showed no or little excess Pb. The black ring to the left represents a spot that shows no excess Pb but is significantly older than the 440Ma age cluster

Age spots from the Ruthven Semipelite produced a spread of ages that cluster around $475.03 \pm 1.11\text{Ma}$ ($\text{MSWD} = 0.98$ $P(X^2) = 0.32$ $n = 25$). The monazite also produced 4 older age spots outside of the main cluster that gives a date of $589.3 \pm 13.5\text{Ma}$. The spots that plot to the right of the concordia are associated with a region of elevated HREE.

The Discordant U-Pb spots when using a discordia analysis produces a lower intercept age of $475.51 \pm 2.84\text{Ma}$ and an upper intercept age of $3004.7 \pm 58\text{Ma}$ ($\text{MSWD} = 9.4$ $P(X^2) = 0$). This likely represents an inherited grain with an age of 3Ga.

5 METAMORPHIC MODELLING

5.1 GMS Glen Gour RG1714

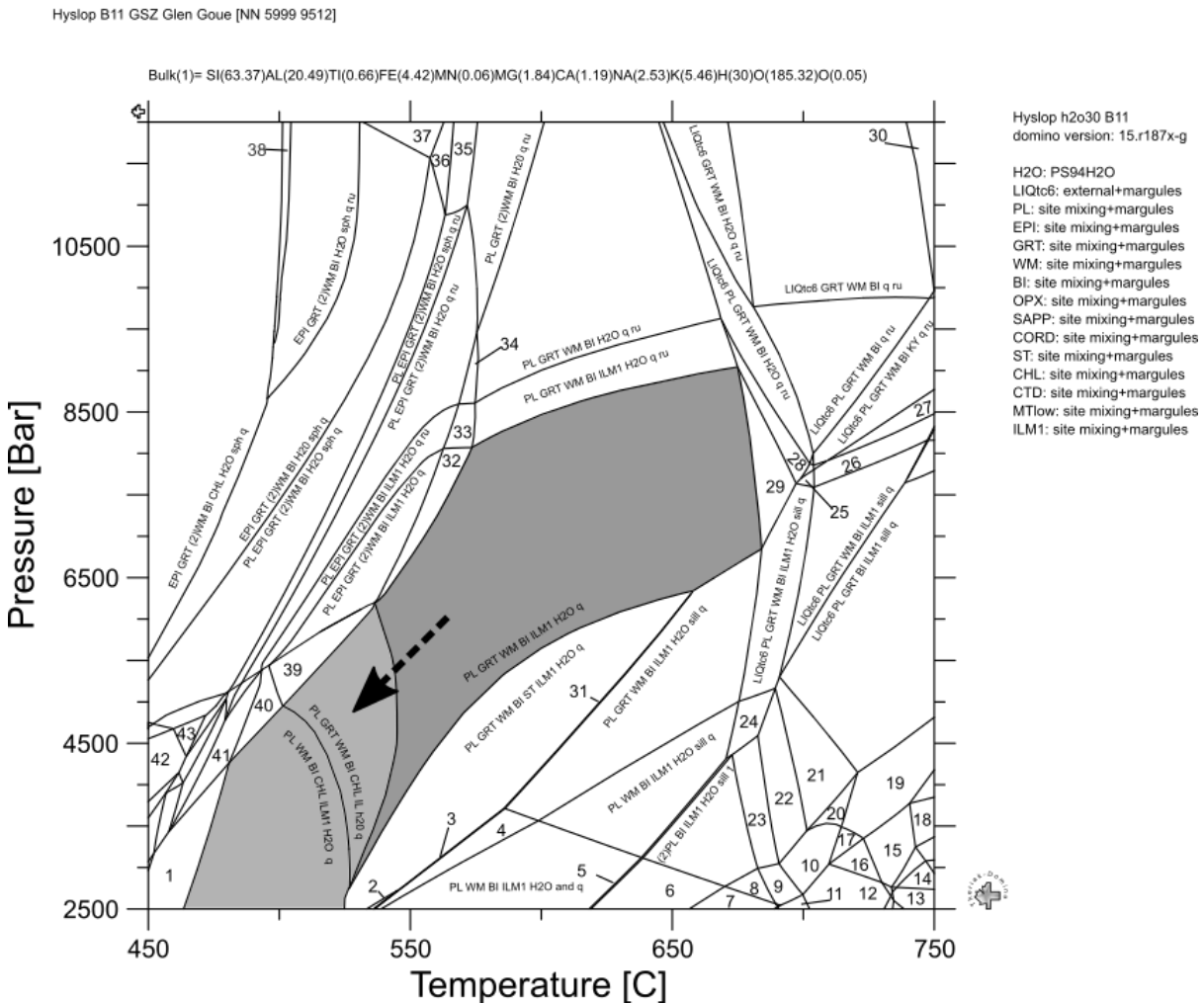


Figure 5-01 Pseudosection produced using Theriak Domino for XRF data from Hyslop (1992) sample B11. Moles of H₂O were in excess of H₂O totally from LOI. 0.05 moles of oxygen added to the system. Darker grey indicates peak assemblage while lighter grey reflects retrograde assemblage. Arrow indicates retrograde reactions.

The GMS Glen Gour is a muscovite – biotite – garnet – quartz - ilmenite mylonitic pelite with retrograde chlorite and muscovite replacing garnet and biotite. Unfortunately, the mineralogy of this sample falls within the largest stability fields within the produced pseudosection, and there for accurate temperature and pressure estimates cannot be determined by the produced pseudosection.

5.2 AB07-27 Leven Schist

AB07-27 Leven Schist [NN 2611 8032]

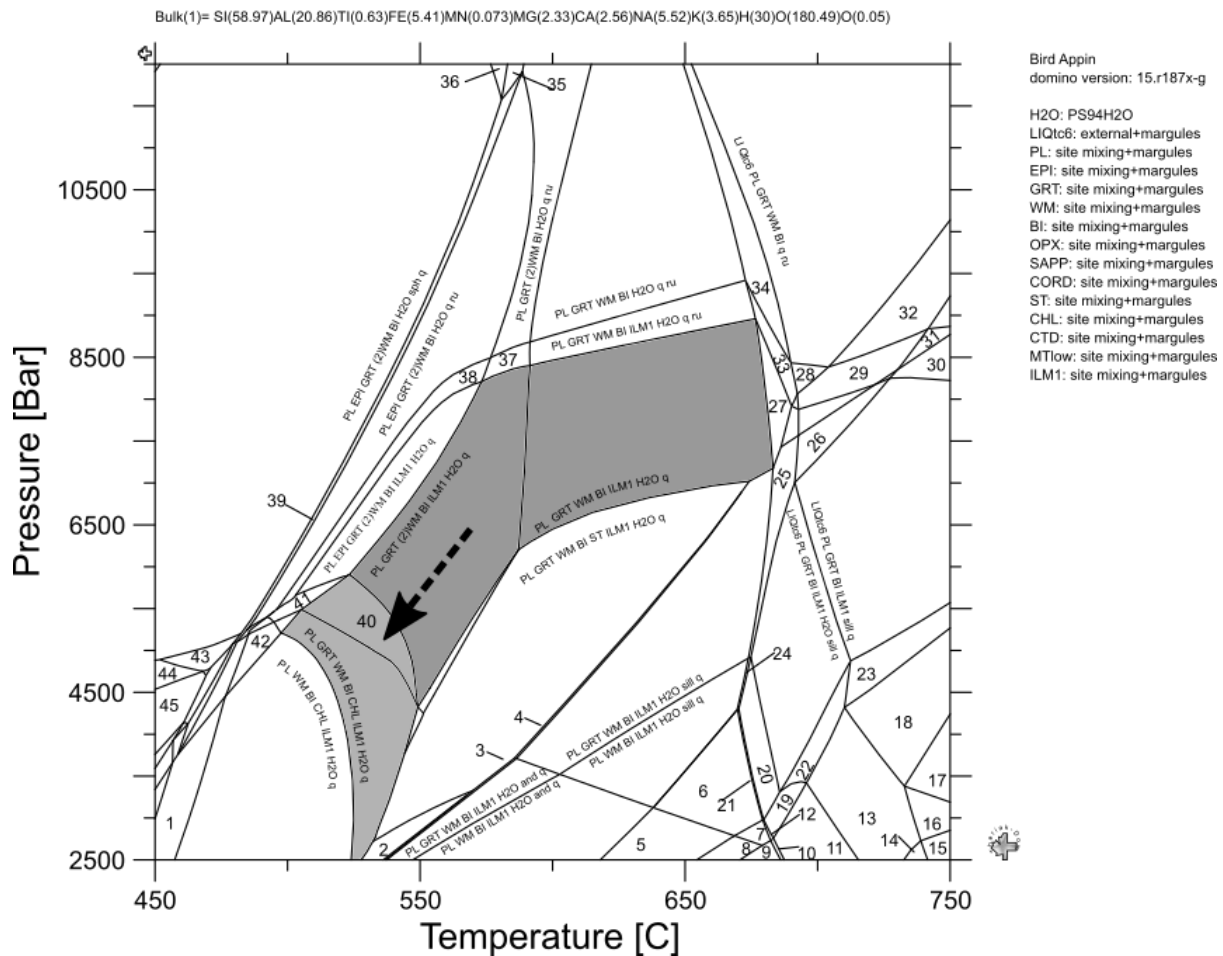


Figure 5-2 Pseudosection produced using Theriak Domino for XRF data collected by A. Bird for Bird et al., (2013). Moles of H₂O were in excess of moles as calculated using LOI. 0.05 moles of O of excess was applied to the system. Darker grey indicates peak assemblage while lighter grey reflects retrograde assemblage. Arrow indicates retrograde reactions.

Sample AB07-27 is a biotite – garnet – muscovite - quartz schist, with an accessory opaque phase Bird et al (2013), the opaque phase is assumed to be ilmenite for the purposes of study. Unfortunately, the mineralogy of this sample falls within the largest stability fields within the pseudosection, and there for accurate temperature and pressure estimates cannot be determined by the produced pseudosection. However, the larger staurolite stability field produced within this pseudosection somewhat reduces the range of pressures and temperatures that produced the peak mineralogy of this sample.

5.3 Assemblage and pseudosection comparison

Both the mineral assemblages within the samples and the pseudosection produced for the samples are remarkably similar, the produced models cannot be used to determine a significant difference in pressure and temperature of deformation between the samples.

6 DISCUSSION

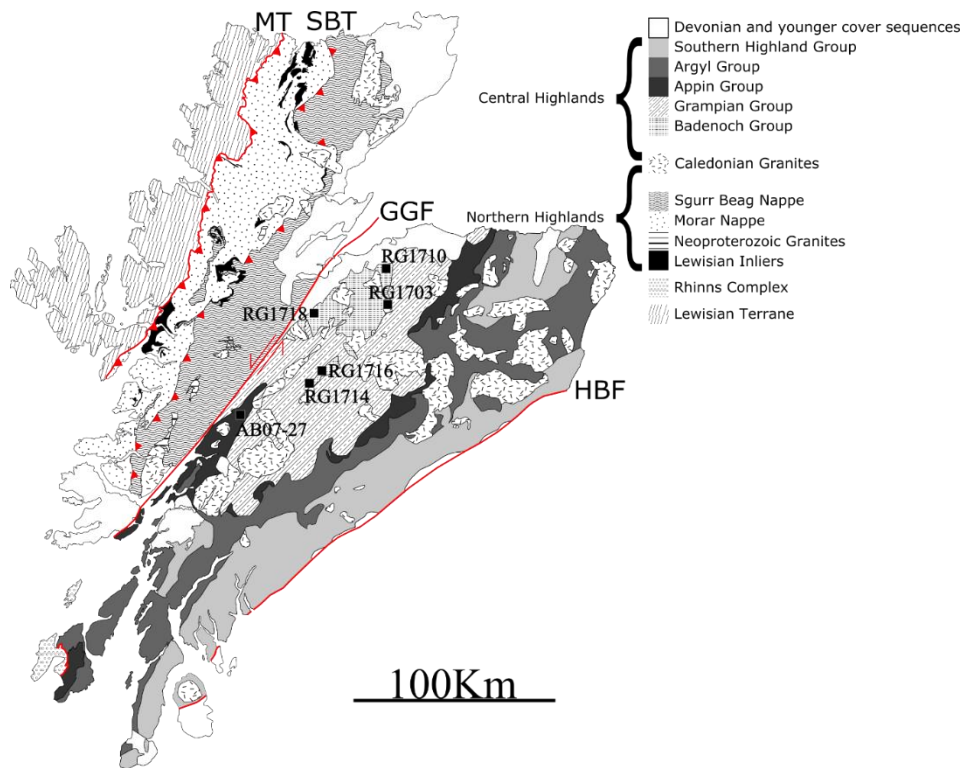


Figure 6-1 Group map of the Northern and Central Highlands. Dated and modelled samples from this study within the map. (Bird et al, 2013)

As stated previously the aims of this study are as follows.

1. Reinvestigate geochronometers from within the Badenoch Group, GSZ and Dalradian Supergroup using modern LA-ICP-MS mapping and U-Pb spot analyses to identify age and structural differences that may be gleaned from said geochronometers.
2. Further investigate the deformation within the Badenoch Group, to determine structural and petrological differences between the Badenoch Group and the overlying Dalradian Supergroup. To
3. Reinvestigate the GSZ in attempt to unravel its activity over time. Investigating whether the GSZ represents the deep crustal expression of extension during the opening of the Iapetus Ocean or a Knoydartian aged shear zone associated with the Valhalla Orogeny.

6.1 Monazite and titanite geochronology of this study

The titanite U-b analyses of Lochindorb Garnetiferous Amphibolite RG17103 and Findhorn metasediment RG1710 this study Gave ages of 467Ma and 469Ma, respectively. The monazite U-Pb data from within study gave varied ages. With sample RG1716 Corie Each pegmatite producing Knoydartian ages from the oldest age spot 998Ma (large errors, low U compared to all other analyses with a similar Pb content). Oldest Knoydartian age of 877 ± 16.4 Ma (younger age range within error ellipse overlaps with the 824Ma cluster. The younger Knoydartian cluster of 752Ma shows activity within the GSZ after the initial development of the Corie Each Pegmatite. The dated monazite from sample RG1718 Rutheven Semipelite produced a clear metamorphic monazite age of 475.03 ± 1.11 Ma.

6.2 Titanite and monazite U-Pb dates - closure temperature

Closure temperature is a function of Pb diffusivity within the mineral lattice of a given mineral. Above a given minerals closure temperature, Pb will diffuse through the mineral, below this temperature the mineral is considered closed and the Pb contents will be locked in (Ganguly and Tirone 1999). Factors independent or in conjunction with temperature can also affect Pb diffusion, such as fluid grain interactions (Taylor et al., 2014, Grand'Homme et al., 2016).

Closure temperatures are determined experimentally using either natural samples or synthetic samples, the closure temperature of a grain is a product of Pb diffusivity with temperature and grain size. The closure temperature of monazite at 10 μ m is in excess of 900°C, over 100 μ m $^{\circ}$ C monazite has a closure temperature in excess of 1000°C (Cherniak et al., 2004). The closure temperature for titanite determined via combined titanite closure age and Ti, Zr in titanite thermobarometry gave a closure age of 750°C (Spencer et al., 2013).

6.3 Limitation of monazite dates

Due to the size of monazites analysed within this study ($>100\mu\text{m}$), the closure temperature would be more than the temperature conditions studied here. However, fluid and mineral alterations lead to patchy lobate mineral domains within monazite and xenotime, HREE oxides such as thorite may be deposited within new mineral domains, leading to these domains being depleted of the HREE (Putins, A 2009., Taylor et al 2014). Fluid alteration of monazite and subsequent redistribution of Pb and Th phases can occur due to the influx of low temperature $<320^\circ\text{C}$ fluids, with these fluids affecting the U-Th-Pb systems within the mineral (Seydoux-Guillaume et al., 2012). During low-temperature fluid alteration monazite loses U, while Th is redistributed within the mineral and deposited as thorite (Seydoux-Guillaume et al., 2012). The same process seems to affect Y, with Y extracted from monazite during low-temperature fluid alteration and depositing as xenotime (Seydoux-Guillaume et al., 2012).

Monazite typically contains negligible amounts of common Pb, and commonly, contains 4-12% ThO_2 , though the variety cheralite can contain up to 30% ThO_2 (Deer, Howie and Zussman 2013), this large Th content may affect U-Pb ages within monazite analyses due to intermediate daughter disequilibrium from intake of ^{230}Th into its crystal structure leading to an increased amount of radiogenic ^{206}Pb relative to the initial levels of ^{238}U (Parish 1990).

While it is typical for monazite to contain negligible common Pb within its crystal structure, monazite grains can contain significant quantities of common Pb. Within monazite grains common Pb is usually situated within grain fractures, where (Th-U) silicate inclusions may precipitate as a result of fluid-mediated partial alteration of monazite grains. With common Pb within natural monazite occurring within pre-existing within grain fracture networks (Seydoux-Guillaume et al., 2012).

6.4 Limitation of titanite U-Pb analyses

Titanite incorporates Pb into its mineral structure, this Pb is referred to as common Pb. This non-radiogenic Pb portion must be accurately accounted for to produce meaningful U-Pb ratios (Kirkland, et al 2017). Common $^{207}\text{Pb}/^{206}\text{Pb}$ can be accurately determined by regressing through the data on a semi total Pb/U isochron to the y-intercept (Storey et al., 2006).

An issue with dating metamorphic titanite is determining whether the minerals present formed due to retrograde or prograde reactions. This can be determined through observation of petrological relations, which are typically driven by Ti loss of other minerals such as high Ti biotite, or breakdown of Ti bearing phases such as rutile (Essex and Gromet 2000). Titanite is only reset at the highest grades of a sample, multiple populations of titanite may be present in a sample, and these can be identified through size, colour and petrological relations (Aleinikoff et al., 2002).

Recoil from α decay within a crystal lattice from elements such as U or Th causes the changes in the crystalline structure within a mineral (Salje et al., 2011). Within titanite the accumulation of damage from α decay causes the mineral to swell by 3%. However, these structural changes are reduced when the titanite is heated above 301°C, causing the annealing of damaged regions (Salje et al., 2011). Amorphization of titanite is relatively low when compared to other geochronometers (such as zircon), this is seemingly due to the lower amounts of radiogenic contaminants within titanite, Th seems to be the main element that causes radiation damage within titanites (Salje et al., 2011).

Due to the deformation temperatures of the samples, the titanites dated are unlikely to have undergone significant radiation damage, any that did occur is likely to have been significantly annealed. Further, the temperatures of metamorphic deformation may have led to Pb loss within the titanites, however, this is unlikely as the temperature required for Pb loss within titanite is 750°C, ages are to be associated with grain morphology and petrological associations rather than Pb loss events.

6.5 Deformation and metamorphism of the Badenoch and Grampian Groups

The presence of rutile inclusions within titanite (Sample RG1710) indicates a higher facies (eclogite) peak mineral assemblage for that lithology, the higher temperature and pressure assemblage probably formed Knoydartian deformation, indicating that higher temperatures or pressure deformation occurred during the Valhalla Orogen. This higher peak grade may be linked to the eclogites of Baker (1986), where the relict eclogites within migmatitic Badenoch Group lithologies the eclogite has been transformed to hybrid biotite hornblende rocks (Simon Cuthbert Pers. Comm.). The samples discussed within this thesis from both the

Badenoch Group and Grampian Group lithologies underwent amphibolite facies metamorphism. The modelled samples both share similar peak metamorphism mineral assemblages with large variance in the possible temperature and pressure of peak assemblage formation. The metamorphic models produced cannot be used to glean differences between the GSZ, Badenoch Group or the Dalradian Supergroup.

6.6 The nature of the Grampian Shear Zone

The ages produced from the RG1716 monazite show a large spread of Knoydartian resetting of the grain. The oldest age the growth of the mineral could either be the oldest spot age within a cluster or the age produced by the cluster, 877Ma or 824Ma. The shear zone cuts migmatites within the Glen Banchor Sub-Group, these are interpreted to have formed at 840Ma (Highton et al., 1999). Because the shear zone cuts said migmatites the structure must be younger than migmatization. Ages Older than the migmatization at 840 ± 11 Ma of Highton et al., (1999), can be explained through two separate processes, the first being that the dated monazite incorporated age domains inherited from the RG1716 Corie Each sheared pegmatite host rock. The other possible explanation for ages older than 840Ma is the uneven distribution of U and Pb within the grain due to differential rates of fluid mobilisation of elements within the grain particularly of U and Pb see figure (6-11).

With 840Ma migmatization as the upper possible limit for mylonitisation and pegmatite growth the age cluster of 824Ma. The shear zone shows multiple periods of movement, reflected by the younger Knoydartian and Grampian age clusters of 752Ma and 485Ma, with reactivation of the shear zone possibly occurring during the late Knoydartian and Grampian Orogeny. This shear reactivation is reflected in the deformation of mica fish showing multiple preferred cleavage orientations. The younger ages produced by the monazite may not reflect reactivation and movement along the shear zone and may instead reflect periods of fluid mobilisation along the shear zone.

The presence of Grampian age titanite rimming ilmenite inclusions within the garnet cores of sample RG1703 the Lochindorb amphibolite indicates ilmenite breakdown during the Grampian Orogeny. This occurred before the growth of garnet within the lithology. These garnets have well-developed strain shadows causing localised strain reduction within the sample, this episode of shearing must have occurred after growth indicating a period of

shearing younger than titanite inclusions. Therefore, the evidence shows that the GSZ was active during both the Knoydartian and the Caledonian Orogenies.

6.7 Geological significance of Knoydartian dates

The previously studied monazites from within the GSZ, from the A'Buidhean mylonitic pegmatite and Lochindorb mylonitic pegmatitic body and host mylonite produced ages of 808Ma, 806Ma and 804Ma (Noble et al., 1996). The analytical technique used within this study mineral dissolution U-Pb MS of 'pristine' monazite grains, with the largest studied being broken into fragments. The intermediate grains from Lochindorb post washing with HNO₃ were reduced to skeletal 40µm fragments. Mineral dilution MS U-Pb analyses for monazite is a limited analytical approach due to the tendency of monazite to recrystallize due to fluid grain interactions. These dates have been assigned to the Knoydartian Orogeny on the grounds of the U-Pb ages produced.

The lower intercepts provided within Noble 1996 paper are of 431Ma and 430Ma, these lower intercepts are linked to Ordovician reworking of Grampian Deformation.

The maps produced from LA-ICP-MS mapping of the RG1716 monazite show distinct patchy growth domains (figure 6-11 images A and B). Figure 6-11 shows that the distribution of ages is not directly linked to U and Pb grain domains, this is likely due to U redistribution within the monazite grain during fluid interactions. These maps also show that while similar, the U and Pb domains of the mineral do not perfectly overlap, with an area with U less than 200ppm while maintaining relatively high levels of Pb. The U map produced shows a U hot spot situated near a within grain fracture, this hotspot likely occurred as a result of the deposition of U silicates within grain fractures during fluid mediated alteration of the monazite grain, causing within grain U to be deposited within fractures.

Knoydartian ages from sample RG1716 sheared pegmatite are spread over a wide range, this may be due to several pulses of fluid flow or metamorphic growth during the Neoproterozoic. This conclusion is further supported by the spread of ages produced from the Neoproterozoic domains of, $824.73 \pm 4.05\text{Ma}$ (n=6), $816.64 \pm 4.36\text{Ma}$ (n=4), $799.57 \pm 5.68\text{Ma}$ (n=2), $761.26 \pm 4.43\text{Ma}$ (n=4) $711.84 \pm 9.65\text{Ma}$ (n=1). This data presented within this thesis suggests an initial growth of monazite at 824Ma, followed by fluid mediated alteration of this 824Ma monazite population during Neoproterozoic shearing up to 711Ma. This fluid

interaction has occurred over a 140Ma period, this spread of age clusters is likely a result of fluid flux possibly due to movement along the GSZ.

Further supporting the claim that the monazite has undergone fluid alteration is the grains cracked pitted appearance. The grains association with nearby xenotime and low Y content indicates alteration by low-temperature fluids extracting Y and depositing the nearby xenotime grains. This along with the fluorite adjacent to the grain indicate low temperature (~400°C) fluid alteration. Further supporting this claim is the near-total sericitization of the feldspars directly adjacent to the monazite.

These Neoproterozoic ages produced within this thesis are of Knoydartian age. Knoydartian ages within Scotland are associated with the onset of a second phase c.840Ma of deformation and sedimentation within the Valhalla Orogen (Cawood et al., 2010). The secondary phase of Knoydartian ages (c. 750Ma) are associated with the opening of the Iapetus Ocean and local mafic and felsic igneous activity (Cawood et al., 2010). The contacts between the basement lithologies affected by the Valhalla Orogen such as the Badenoch Group and sediments associated with the opening of the Iapetus Ocean such as the Grampian group are often highly tectonised (GSZ) (Cawood et al., 2010).

The Corie Each pegmatite RG1716 monazite sample records ages associated with both the secondary phase of the Valhalla Orogen (c. 840Ma) and the opening of the Iapetus Ocean (c. 750Ma). This indicates that the shear formed during Valhalla Orogen and was reactivated during the secondary phase of the Knoydartian to accommodate the rifting Iapetus Ocean and the subsequent deposition of the Dalradian Supergroup.

6.8 Geological significance of Ordovician dates

Ordovician dates have been obtained from samples RG1703, RG1710, RG1716 and RG1718. The dated monazite from within sample RG1718 is associated with biotite and two smaller apatite inclusions. The surrounding biotites appear to have undergone some degree of metamictisation/fluid alteration, as there is a patch of broken-down minerals containing both biotite and monazite appearing as a disaggregated mesh. The dated monazite is unique, in its size morphology and petrological relations, of particular interest, is its unique relationship with apatite. While monazite is commonly associated with apatite within the sample, this is typically as small, rounded clusters of monazites within larger apatite grains. The dated

monazite is unique as it developed into a large pristine monazite, with notable cleavage and distinct faces. This indicates the possibility of two periods of monazite growth.

The U-Pb data from the RG1718 monazite can be split into three groups, one consisting of monazites that cluster around $475.67 \pm 1.12\text{Ma}$ (MSWD = 1.7 $p = 0.2$ $n = 24$), two significantly older spots that gives an age of 575.5Ma and the spots that show excess ^{207}Pb when compared to ^{206}Pb . The first group shows a significant spread of ages, from Grampian to Grampian II ages. The MSWD of 1.7 could be explained by a long-lived growth period for the monazite from the Grampian Orogeny to the Grampian II Orogeny. New monazite growth on detrital grains found within previous monazite studies found that monazite growth on pre-existing monazite occurs within amphibolite facies metamorphism (Rubat et al., 2001). Therefore, the age of 475.67Ma from this monazite represents the age of prograde amphibolite facies metamorphism within the Ruthven Semipelite. Furthermore, the distinct lack of Neoproterozoic monazite growth on top of this relict grain indicates that the Grampian lithology the Ruthven Semipelite has not undergone Neoproterozoic deformation.

The element maps of this mineral show a region within the monazite of higher Y and Dy, this region likely predates the surrounding monazite, as garnet growth would intake most of the Y within the system.

The Ordovician overprint within the RG1716 monazite at $484.72 \pm 2.67\text{Ma}$ (MSWD = 0.97, $P(X^2) = 0.32$, $n = 5$), is significantly older than the Ruthven Semipelite monazite. This indicates that the basement lithologies and deformation of the GSZ during the Caledonian Orogeny occurred before monazite formation and amphibolite grade deformation within the overlying Grampian Group of the Dalradian Supergroup.

The titanite geochronology of this study produced two Grampian ages of 472Ma and 468.03Ma. The titanites dated from within sample RG1710 are small rhombus shaped titanites, typical of metamorphic titanite populations. The ages of 468Ma show prograde growth of titanite within a calc-silicate lithology during the Grampian orogeny. The presence of rare rutile inclusions within this titanite population would be indicative of a retrograde reaction of rutile into titanite. For metamorphic rutile to be present within the lithology before the 468Ma titanite population the lithology must have undergone higher grade

metamorphism previously. This event either could have occurred early during the Grampian Orogeny or as a part of Knoydartian deformation of Dava Group sediments.

Dated titanites within sample RG1703 were all Garnet inclusions and associated with ilmenite. These 472Ma titanites, and their strong association with ilmenite, with some of the titanites rimming ilmenite indicates prograde metamorphism into greenschist facies. Later amphibolite facies deformation is indicated by the large garnets that host the titanite and ilmenites within their cores. This put a maximum older age for garnet growth within this lithology at 472Ma. The development of garnet strain shadows within the lithology and grain size reduction of quartz outside of the strain shadows shows reactivation of the shear zone after the growth of these garnets.

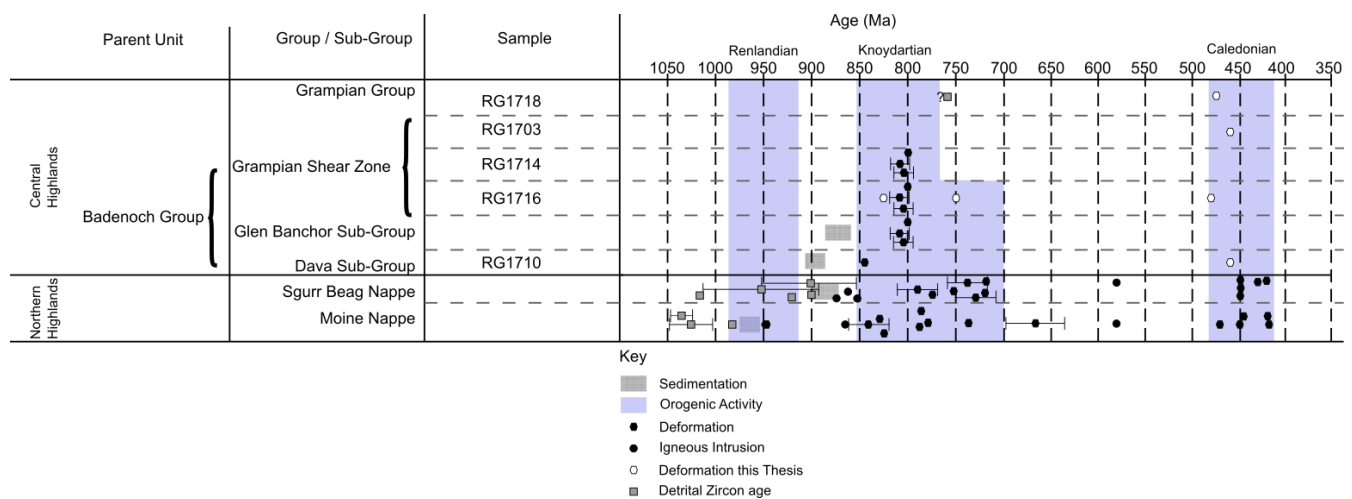


Figure 6-2 Timeline of recorded deformation of the samples. With Nappes of the Northern Highlands to compare. See figure 3-5 for references of this figure.

6.9 Future research

Two pegmatite populations are observed within the GSZ, smaller pegmatite lenses and larger pegmatite sheets. A study into the potential age differences of these pegmatite populations may gleam useful insight into the development of the GSZ.

Sample RG1716 Corie Each Pegmatite contained monazite and xenotime. If garnets exist within the lithology then Garnet, monazite, xenotime thermobarometry would provide useful data on the temperature and pressure of the minerals during formation and therefore the temperature and pressure within the GSZ during a period of the growth of these minerals.

Sample RG1718 Ruthven semipelite contains apatite grains that host clusters of granular monazites. Geochronology applied to both phases could help reveal the nature of monazite

and apatite petrological relations while providing further geochronological data of this lithology. Because this lithology is migmatitic, zircon analysis could reveal the age and nature of migmatization with the lithology.

Mylonitised pegmatites from the GSZ are host to both large mica fish and books. Ar-Ar and Rb-Sr geochronology could be applied to these mineral populations. This has been done before by Piasecki and van Breemen (1979), however, with modern analytical techniques such as LA-ICP-MS the geochronology from this approach could be updated.

The nature of the retrograde eclogites within the Badenoch Group is poorly understood as to date there has been no analysis of the geochronology of these eclogites. Garnet compositional mapping and geochronology could constrain this elusive early eclogite facies deformation within the Badenoch Group.

7 CONCLUSIONS

The complexity of the Grampian Shear Zone as recorded by monazite is greater than previously thought. Monazite from the deformed Coire Each pegmatite gave a range of Knoydartian ages from 824Ma to 711Ma, with early Grampian overprint of 485Ma. The formation of the RG1716 sheared pegmatite sample occurred at 825Ma during the first phase of the Knoydartian. The long period of Knoydartian deformation along with the isotope maps and directly surrounding mineralogy and fractured texture of this grain indicates polyphase deformation and dissolution re-precipitation during both the Valhalla Orogen and the opening of the Iapetus Ocean. While the data from this monazite indicates formation during the Knoydartian Orogenic and sedimentary cycle attributed to the Valhalla Orogen, the monazite also contains evidence of dissolution re-precipitation (adjacent fluorite and lobate U distribution within grain) and the likely reactivation of the GSZ to accommodate the deposition of the Dalradian Supergroup during the opening of the Iapetus Ocean.

Monazite from within the Ruthven Semipelite, Grampian Group, Corrieyairack Sub-Group, records only Caledonian deformation through the Grampian Orogeny to the Grampian II orogeny. The isotope maps of this grain indicate a degree of overprint, which increased Pb, Y and HREE within a patch of the grain. Reduction of U, Pb and REE's within the centre of the grain with an increase in major elements indicates dissolution re-precipitation after the grains initial formation.

Titanite from within the Findhorn Dava Group Metasediment records titanite formation or overprint during the Grampian Orogeny. Rutile inclusions within titanite indicate a higher-grade metamorphic mineral assemblage that predates these titanites. Further petrological evidence supports the claim of a pre-existing higher-grade mineralogy, biotite quartz intergrowth, amphibole quartz intergrowth and relict cordierite and cordierite pseudomorphs. The presence of cordierite strongly indicates granulite facies deformation. This high-grade deformation may be linked to the relict eclogites seen elsewhere within the Badenoch Group.

Within the Lochindorb Garnet Amphibolite titanite reaction rims surrounding ilmenite record the reaction between ilmenite and another phase at 467Ma late Grampian Orogeny. These titanite ages predate or date the growth of garnet cores within this lithology.

From the evidence provided herein, we propose that shearing associated with the Grampian Shear Zone was initiated during Valhalla Orogenesis at 824Ma as dated by monazite U-Pb spot analyses. The spread of Knoydartian ages (824Ma to 711Ma) and lobate HREE mineral domains within the monazite is indicative of fluid dissolution re-precipitation of the monazite throughout this period. Both the Grampian age monazite U-Pb cluster from the Corie Each Pegmatite sample (RG1716) and the Grampian age of titanite inclusions within the sheared Lochindorb garnet amphibolite (RG1703) show reactivation of the shear zone during the Caledonian orogeny. Ultimately, we propose that the Grampian Shear Zone is a Knoydartian age shear zone that underwent reactivation during the Caledonian orogeny.

8 REFERENCES

Aitcheson, S.J., 1989. Crustal Evolution in the Seiland Region, North Norway: A Nd, Sr and Pb Isotopic Study (Doctoral dissertation, University College Dublin).

Aleinikoff, J.N., Wintsch, R.P., Fanning, C.M. and Dorais, M.J., 2002. U–Pb geochronology of zircon and polygenetic titanite from the Glastonbury Complex, Connecticut, USA: an integrated SEM, EMPA, TIMS, and SHRIMP study. *Chemical Geology*, 188(1-2), pp.125-147.

Andresen, A., Rehnström, E.F. and Holte, M., 2007. Evidence for simultaneous contraction and extension at different crustal levels during the Caledonian orogeny in NE Greenland. *Journal of the Geological Society*, 164(4), pp.869-880.

Baker, A.J., 1986. Eclogitic amphibolites from the Grampian Moines. *Mineralogical Magazine*, 50(356), pp.217-221.

Balašov, J.A., Teben'kov, A.M., Ohta, Y., Larionov, A.N., Sirotkin, A.N., Gannibal, L.F. and Ryungenen, G.I., 1995. Grenvillian U-Pb zircon ages of quartz porphyry and rhyolite clasts in a metaconglomerate at Vimsodden, southwestern Spitsbergen. *Polar Research*, 14(3), pp.291-302.

Balašov, Y.A., Peucat, J.J., Teben'kov, A.M., Ohta, Y., Larionov, A.N., Sirotkin, A.N. and Bjornerud, M., 1996. Rb-Sr whole rock and U-Pb zircon datings of the granitic-gabbroic rocks from the Skalfjellet Sub-Group, Southwest Spitsbergen. *Polar Research*, 15(2), pp.167-181.

Banks, C.J. and Winchester, J.A., 2007. Sedimentology and stratigraphic affinities of Neoproterozoic coarse clastic successions, Glenshirra Group, Inverness-shire, Scotland. *Scottish Journal of Geology*, 40(2), pp.159-174.

Banks, C.J., Smith, M., Winchester, J.A., Horstwood, M.S.A., Noble, S.R. and Ottley, C.J., 2007. Provenance of intra-Rodinian basin-fills: the lower Dalradian supergroup, Scotland. *Precambrian Research*, 153(1-2), pp.46-64.

Bird, A.F., Thirlwall, M.F., Strachan, R.A. and Manning, C.J., 2013. Lu–Hf and Sm–Nd dating of metamorphic garnet: evidence for multiple accretion events during the Caledonian orogeny in Scotland. *Journal of the Geological Society*, 170(2), pp.301-317.

Bird, A., Cutts, K., Strachan, R., Thirlwall, M.F. and Hand, M., 2018. First evidence of Renlandian (c. 950–940 Ma) orogeny in mainland Scotland: Implications for the status of the Moine Supergroup and circum-North Atlantic correlations. *Precambrian Research*, 305, pp.283-294.

de Capitani, C. and Petrakakis, K., 2010. The computation of equilibrium assemblage diagrams with Theriak/Domino software. *American Mineralogist*, 95(7), pp.1006-1016.

Cawood, P.A., Nemchin, A.A., Smith, M. and Loewy, S., 2003. Source of the Dalradian Supergroup constrained by U–Pb dating of detrital zircon and implications for the East Laurentian margin. *Journal of the Geological Society*, 160(2), pp.231-246.

Cawood, P.A., Nemchin, A.A., Strachan, R.A., Kinny, P.D. and Loewy, S., 2004. Laurentian provenance and an intracratonic tectonic setting for the Moine Supergroup, Scotland, constrained by detrital zircons from the Loch Eil and Glen Urquhart successions. *Journal of the Geological Society*, 161(5), pp.861-874.

Cawood, P.A., Strachan, R., Cutts, K., Kinny, P.D., Hand, M. and Pisarevsky, S., 2010. Neoproterozoic orogeny along the margin of Rodinia: Valhalla orogen, North Atlantic. *Geology*, 38(2), pp.99-102.

Cawood, P.A., Strachan, R.A., Merle, R.E., Millar, I.L., Loewy, S.L., Dalziel, I.W., Kinny, P.D., Jourdan, F., Nemchin, A.A. and Connelly, J.N., 2015. Neoproterozoic to early Paleozoic extensional and compressional history of East Laurentian margin sequences: The Moine Supergroup, Scottish Caledonides. *Bulletin*, 127(3-4), pp.349-371.

Cawood, P.A., Strachan, R.A., Pisarevsky, S.A., Gladkochub, D.P. and Murphy, J.B., 2016. Linking collisional and accretionary orogens during Rodinia assembly and breakup: Implications for models of supercontinent cycles. *Earth and Planetary Science Letters*, 449, pp.118-126.

Chew, D.M., Holland, C.H. and Sanders, I.S., 2009. Grampian orogeny. *The Geology of Ireland, 2nd edn. Dunedin Academic Press, Edinburgh*, pp.69-93.

Chew, D.M. and Strachan, R.A., 2014. The Laurentian Caledonides of Scotland and Ireland. *Geological Society, London, Special Publications*, 390(1), pp.45-91.

Cherniak, D.J., Watson, E.B., Grove, M. and Harrison, T.M., 2004. Pb diffusion in monazite: a combined RBS/SIMS study. *Geochimica et Cosmochimica Acta*, 68(4), pp.829-840.

Cutts, K.A., Hand, M., Kelsey, D.E. and Strachan, R.A., 2009. Orogenic versus extensional settings for regional metamorphism: Knoydartian events in the Moine Supergroup revisited. *Journal of the Geological Society*, 166(2), pp.201-204.

Cutts, K.A., Hand, M., Kelsey, D.E., Wade, B., Strachan, R.A., Clark, C. and Netting, A., 2009. Evidence for 930 Ma metamorphism in the Shetland Islands, Scottish Caledonides: implications for Neoproterozoic tectonics in the Laurentia–Baltica sector of Rodinia. *Journal of the Geological Society*, 166(6), pp.1033-1047.

Cutts, K.A., Kinny, P.D., Strachan, R.A., Hand, M., Kelsey, D.E., Emery, M., Friend, C.R.L. and Leslie, A.G., 2010. Three metamorphic events recorded in a single garnet: Integrated phase modelling, in situ LA-ICPMS and SIMS geochronology from the Moine Supergroup, NW Scotland. *Journal of Metamorphic Geology*, 28(3), pp.249-267.

Deer, W.A., Howie, R.A., Zussman J 2013 An Introduction to the Rock Forming Minerals 3rd Edition. London: The Mineralogical Society

Dempster, T.J., Rogers, G., Tanner, P.W.G., Bluck, B.J., Muir, R.J., Redwood, S.D., Ireland, T.R. and Paterson, B.A., 2002. Timing of deposition, orogenesis and glaciation within the Dalradian rocks of Scotland: constraints from U–Pb zircon ages. *Journal of the Geological Society*, 159(1), pp.83-94.

Essex, R.M. and Gromet, L.P., 2000. U-Pb dating of prograde and retrograde titanite growth during the Scandian orogeny. *Geology*, 28(5), pp.419-422.

Friend, C.R.L., Kinny, P.D., Rogers, G., Strachan, R.A. and Paterson, B.A., 1997. U-Pb zircon geochronological evidence for Neoproterozoic events in the Glenfinnan Group (Moine Supergroup): the formation of the Ardgour granite gneiss, north-west Scotland. *Contributions to Mineralogy and Petrology*, 128(2), pp.101-113.

Friend, C.R.L., Strachan, R.A., Kinny, P., and Watt, G.R., 2003, Provenance of the Moine Supergroup of NW Scotland: evidence from geochronology of detrital and inherited zircons from (meta)sedimentary rocks granites and migmatites: *Journal of the Geological Society*, London, v. 160, p. 247-257.

Ganguly, J. and Tirone, M., 1999. Diffusion closure temperature and age of a mineral with arbitrary extent of diffusion: theoretical formulation and applications. *Earth and Planetary Science Letters*, 170(1-2), pp.131-140.

Gasser, D., 2014. The Caledonides of Greenland, Svalbard and other Arctic areas: status of research and open questions. *Geological Society, London, Special Publications*, 390(1), pp.93-129

Gee, D.G., Johansson, Å., Ohta, Y., Tebenkov, A.M., Balashov, Y.A., Larionov, A.N., Gannibal, L.F. and Ryungenen, G.I., 1995. Grenvillian basement and a major unconformity within the Caledonides of Nordaustlandet, Svalbard. *Precambrian Research*, 70(3-4), pp.215-234.

Grand'Homme, A., Janots, E., Seydoux-Guillaume, A.M., Guillaume, D., Bosse, V. and Magnin, V., 2016. Partial resetting of the U-Th-Pb systems in experimentally altered monazite: Nanoscale evidence of incomplete replacement. *Geology*, 44(6), pp.431-434.

Gonçalves, G.O., Lana, C., Scholz, R., Buick, I.S., Gerdes, A., Kamo, S.L., Corfu, F., Marinho, M.M., Chaves, A.O., Valeriano, C. and Nalini Jr, H.A., 2016. An assessment of monazite from the Itambé pegmatite district for use as U–Pb isotope reference material for microanalysis and implications for the origin of the “Moacyr” monazite. *Chemical Geology*, 424, pp.30-50.

Halliday, A.N., Graham, C.M., Aftalion, M. and Dymoke, P., 1989. Short paper: the depositional age of the Dalradian Supergroup: U-Pb and Sm-Nd isotopic studies of the Tayvallich Volcanics, Scotland. *Journal of the Geological Society*, 146(1), pp.3-6.

Harlov, D.E. and Wirth, R., 2000. K-feldspar–quartz and K-feldspar–plagioclase phase boundary interactions in garnet–orthopyroxene gneiss's from the Val Strona di Omegna, Ivrea–Verbano Zone, northern Italy. *Contributions to Mineralogy and Petrology*, 140(2), pp.148-162.

Highton, A.J., 1992. The tectonostratigraphical significance of pre-750 Ma metagabbros within the northern Central Highlands, Inverness-shire. *Scottish Journal of Geology*, 28(1), pp.71-76.

Highton, A.J., Hyslop, E.K. and Noble, S.R., 1999. U-Pb zircon geochronology of migmatization in the northern Central Highlands: evidence for pre-Caledonian (Neoproterozoic) tectonometamorphism in the Grampian block, Scotland. *Journal of the Geological Society*, 156(6), pp.1195-1204.

Holland, T. and Powell, R., 2003. Activity–composition relations for phases in petrological calculations: an asymmetric multicomponent formulation. *Contributions to Mineralogy and Petrology*, 145(4), pp.492-501.

Holland, T.J.B. and Powell, R., 2011. An improved and extended internally consistent thermodynamic dataset for phases of petrological interest, involving a new equation of state for solids. *Journal of Metamorphic Geology*, 29(3), pp.333-383.

Horstwood, M.S., Košler, J., Gehrels, G., Jackson, S.E., McLean, N.M., Paton, C., Pearson, N.J., Sircombe, K., Sylvester, P., Vermeesch, P. and Bowring, J.F., 2016. Community-derived

standards for LA-ICP-MS U-(Th-) Pb geochronology—Uncertainty propagation, age interpretation and data reporting. *Geostandards and Geoanalytical Research*, 40(3), pp.311-332.

Hutton, D.H.W. and Alsop, G.I., 2004. Evidence for a major Neoproterozoic orogenic unconformity within the Dalradian Supergroup of NW Ireland. *Journal of the Geological Society*, 161(4), pp.629-640.

Hynes, A. and Rivers, T., 2010. Protracted continental collision—Evidence from the Grenville orogen. *Canadian Journal of Earth Sciences*, 47(5), pp.591-620.

Hyslop, E.K., 1992. Strain-Induced Metamorphism and Pegmatite Development in the Moine Rocks of Scotland [Ph. D. thesis]. Hull, UK, University of Hull.

Hyslop, E.K. and Piasecki, M.A.J., 1999. Mineralogy, geochemistry and the development of ductile shear zones in the Grampian Slide zone of the Scottish Central Highlands. *Journal of the Geological Society*, 156(3), pp.577-589.

Jahn, I., Strachan, R.A., Fowler, M., Bruand, E., Kinny, P.D., Clark, C. and Taylor, R.J., 2017. Evidence from U–Pb zircon geochronology for early Neoproterozoic (Tonian) reworking of an Archaean inlier in northeastern Shetland, Scottish Caledonides. *Journal of the Geological Society*, 174(2), pp.217-232.

Jensen, S.M., 1993. Lead isotopes studies on mineral showings and ore deposits in East Greenland.

Johansson, Å., Larionov, A.N., Tebenkov, A.M., Gee, D.G., Whitehouse, M.J. and Vestin, J., 1999. Grenvillian magmatism of western and central Nordaustlandet, northeastern Svalbard. *Earth and Environmental Science Transactions of The Royal Society of Edinburgh*, 90(3), pp.221-254.

Johansson, A., Larionov, A.N., Gee, D.G., Ohta, Y., Tebenkov, A.M., and Sandelin, S., 2004, Grenville and Caledonian tectono-magnetic activity in northeasternmost Svalbard. In: Gee, D.G., Pease, V.L., (Eds.), *The Neoproterozoic Timanide Orogen of Eastern Baltica*: London, Geological Society, London, Memoirs, 30, 207–232.

Kalsbeek, F., Thrane, K., Nutman, A.P. and Jepsen, H.F., 2000. Late Mesoproterozoic to early Neoproterozoic history of the East Greenland Caledonides: evidence for Grenvillian orogenesis?. *Journal of the Geological Society*, 157(6), pp.1215-1225.

Kinny, P.D., Strachan, R.A., Kocks, H. and Friend, C.R.L., 2003. U–Pb geochronology of late Neoproterozoic augen granites in the Moine Supergroup, NW Scotland: dating of rift-related, felsic magmatism during supercontinent break-up?. *Journal of the Geological Society*, 160(6), pp.925-934.

Kirkland, C.L., Daly, J.S. and Whitehouse, M.J., 2006. Granitic magmatism of Grenvillian and late Neoproterozoic age in Finnmark, Arctic Norway—constraining pre-Scandian deformation in the Kalak Nappe Complex. *Precambrian Research*, 145(1-2), pp.24-52.

Kirkland, C.L., Stephen Daly, J. and Whitehouse, M.J., 2007. Provenance and terrane evolution of the Kalak Nappe Complex, Norwegian Caledonides: implications for Neoproterozoic paleogeography and tectonics. *The Journal of Geology*, 115(1), pp.21-41.

Kirkland, C.L., Strachan, R.A. and Prave, A.R., 2008. Detrital zircon signature of the Moine Supergroup, Scotland: Contrasts and comparisons with other Neoproterozoic successions within the circum-North Atlantic region. *Precambrian Research*, 163(3-4), pp.332-350.

Kirkland, C.L., Hollis, J., Danišík, M., Petersen, J., Evans, N.J. and McDonald, B.J., 2017. Apatite and titanite from the Karrat Group, Greenland; implications for charting the thermal evolution of crust from the U-Pb geochronology of common Pb bearing phases. *Precambrian Research*, 300, pp.107-120.

Knoll, A.H., 1982. Microfossils from the late precambrian draken conglomerate, ny friesland, svalbard. *Journal of Paleontology*, pp.755-790.

Leslie, A.G. and Nutman, A.P., 2003. Evidence for Neoproterozoic orogenesis and early high temperature Scandian deformation events in the southern East Greenland Caledonides. *Geological Magazine*, 140(3), pp.309-333.

Leslie, A.G., Krabbendam, M. and Smith, R.A., 2006. The Gaick Fold Complex: large-scale recumbent folds and their implications for Caledonian structural architecture in the Central Grampian Highlands. *Scottish Journal of Geology*, 42(2), pp.149-159.

Leslie, A.G., Robertson, S., Smith, M., Banks, C.J., Mendum, J.R. and Stephenson, D., 2013. The Dalradian rocks of the northern Grampian Highlands of Scotland. *Proceedings of the Geologists' Association*, 124(1-2), pp.263-317.

Majka, J., Mazur, S., Manecki, M., Czerny, J. and Holm, D.K., 2008. Late Neoproterozoic amphibolite-facies metamorphism of a pre-Caledonian basement block in southwest Wedel Jarlsberg Land, Spitsbergen: New evidence from U–Th–Pb dating of monazite. *Geological Magazine*, 145(6), pp.822-830.

Majka, J., Kościńska, K., Bazarnik, J. and McClelland, W.C., 2021. The Ordovician Thores volcanic island arc of the Pearya Terrane from northern Ellesmere Island formed on Precambrian continental crust. *Lithos*, p.105999.

Mako, C.A., Law, R.D., Caddick, M.J., Thigpen, J.R., Ashley, K.T., Cottle, J. and Kylander-Clark, A., 2019. Thermal evolution of the Scandian hinterland, Naver nappe, northern Scotland. *Journal of the Geological Society*, 176(4), pp.669-688.

Mako, C.A., Law, R.D., Caddick, M.J., Kylander-Clark, A., Thigpen, J.R., Ashley, K.T., Mazza, S.E. and Cottle, J., 2021. Growth and fluid-assisted alteration of accessory phases before, during and after Rodinia breakup: U-Pb geochronology from the Moine Supergroup rocks of northern Scotland. *Precambrian Research*, 355, p.106089.

Malone, S.J., McClelland, W.C., von Gosen, W. and Piepjohn, K., 2017. The earliest Neoproterozoic magmatic record of the Pearya terrane, Canadian high Arctic: implications for Caledonian terrane reconstructions. *Precambrian Research*, 292, pp.323-349.

McClelland, W.C., Malone, S.J., von Gosen, W., Piepjohn, K. and Läufer, A., 2012. The timing of sinistral displacement of the Pearya Terrane along the Canadian Arctic Margin. *Zeitschrift der deutschen Gesellschaft fuer Geowissenschaften*, pp.251-259.

McKerrow, W.S., Mac Niocaill, C. and Dewey, J.F., 2000. The Caledonian orogeny redefined. *Journal of the Geological society*, 157(6), pp.1149-1154.

Millar, I.L., 1999. Neoproterozoic extensional basic magmatism associated with the West Highland granite gneiss in the Moine Supergroup of NW Scotland. *Journal of the Geological Society*, 156(6), pp.1153-1162.

Mazza, S.E., Mako, C., Law, R.D., Caddick, M.J., Krabbendam, M. and Cottle, J., 2018. Thermobarometry of the Moine and Sgurr Beag thrust sheets, northern Scotland. *Journal of Structural Geology*, 113, pp.10-32.

Noble, S.R., Hyslop, E.K. and Highton, A.J., 1996. High-precision U–Pb monazite geochronology of the c. 806 Ma Grampian Shear Zone and the implications for the evolution of the Central Highlands of Scotland. *Journal of the Geological Society*, 153(4), pp.511-514.

Oliver, G.J., Wilde, S.A. and Wan, Y., 2008. Geochronology and geodynamics of Scottish granitoids from the late Neoproterozoic break-up of Rodinia to Palaeozoic collision. *Journal of the Geological Society*, 165(3), pp.661-674.

Palin, R.M., Searle, M.P., Waters, D.J., Parrish, R.R., Roberts, N.M.W., Horstwood, M.S.A., Yeh, M.W., Chung, S.L. and Anh, T.T., 2013. A geochronological and petrological study of anatexitic paragneiss and associated granite dykes from the D ay N ui C on V oi metamorphic core complex, N orth V ietnam: constraints on the timing of metamorphism within the R ed R iver shear zone. *Journal of Metamorphic Geology*, 31(4), pp.359-387.

Parrish, R.R., 1990. U–Pb dating of monazite and its application to geological problems. *Canadian Journal of Earth Sciences*, 27(11), pp.1431-1450.

Paton, C., Woodhead, J.D., Hellstrom, J.C., Hergt, J.M., Greig, A. and Maas, R., 2010. Improved laser ablation U-Pb zircon geochronology through robust downhole fractionation correction. *Geochemistry, Geophysics, Geosystems*, 11(3).

Paton, C., Hellstrom, J., Paul, B., Woodhead, J. and Hergt, J., 2011. Lolite: Freeware for the visualisation and processing of mass spectrometric data. *Journal of Analytical Atomic Spectrometry*, 26(12), pp.2508-2518.

Pedersen, R.B., Dunning, G.R. and Robins, B., 1989. U-Pb ages of nepheline syenite pegmatites from the Seiland Magmatic Province, N. Norway. In *The Caledonides geology of Scandinavia. Conference dedicated to the Memory of Dr Sven Foyn* (pp. 3-8).

Peters, D. 2001. A geochemical and geochronological assessment of the Great Glen Fault as a terrane boundary. PhD thesis, University of Keele, UK.

Pettersson, C.H., Tebenkov, A.M., Larionov, A.N., Andresen, A. and Pease, V., 2009. Timing of migmatization and granite genesis in the Northwestern Terrane of Svalbard, Norway: implications for regional correlations in the Arctic Caledonides. *Journal of the Geological Society*, 166(1), pp.147-158.

Piasecki, M.A.J. and Van Breemen, O., 1979. The 'Central Highland Granulites': cover-basement tectonics in the Moine. *Geological Society, London, Special Publications*, 8(1), pp.139-144.

Piasecki, M.A.J., 1980. New light on the Moine rocks of the Central Highlands of Scotland. *Journal of the Geological Society*, 137(1), pp.41-59.

Piasecki, M.A.J. and Van Breemen, O., 1983. Field and isotopic evidence for a c. 750 Ma tectonothermal event in Moine rocks in the Central Highland region of the Scottish Caledonides. *Earth and Environmental Science Transactions of The Royal Society of Edinburgh*, 73(3), pp.119-134.

Piasecki, M.A.J. and Temperley, S., 1988. The Central Highland Division. In *Later Proterozoic stratigraphy of the Northern Atlantic regions* (pp. 46-53). Springer, Boston, MA.

Phillips, E.R., Highton, A.J., Hyslop, E.K. and Smith, M., 1999. The timing and P–T conditions of regional metamorphism in the Central Highlands, Scotland. *Journal of the Geological Society*, 156(6), pp.1183-1193.

Powell, R., White, R.W., Green, E.C.R., Holland, T.J.B. and Diener, J.F.A., 2014. On parameterizing thermodynamic descriptions of minerals for petrological calculations. *Journal of Metamorphic Geology*, 32(3), pp.245-260.

Putnis, A., 2009. Mineral replacement reactions. *Reviews in mineralogy and geochemistry*, 70(1), pp.87-124.

Prave, A.R., Fallick, A.E., Thomas, C.W. and Graham, C.M., 2009. A composite C-isotope profile for the Neoproterozoic Dalradian Supergroup of Scotland and Ireland. *Journal of the Geological Society*, 166(5), pp.845-857.

Roberts, R.J., Corfu, F., Torsvik, T.H., Ashwal, L.D. and Ramsay, D.M., 2006. Short-lived mafic magmatism at 560–570 Ma in the northern Norwegian Caledonides: U–Pb zircon ages from the Seiland Igneous Province. *Geological Magazine*, 143(6), pp.887-903.

Robertson, S. and Smith, M., 1999. The significance of the Geal Charn-Ossian steep belt in basin development in the central Scottish Highlands. *Journal of the Geological Society*, 156(6), pp.1175-1182.

Rogers, G., Hyslop, E.K., Strachan, R.A., Paterson, B.A. and Holdsworth, R.E., 1998. The structural setting and U–Pb geochronology of Knoydartian pegmatites in W Inverness-shire: evidence for Neoproterozoic tectonothermal events in the Moine of NW Scotland. *Journal of the Geological Society*, 155(4), pp.685-696.

Rogers, G., Kinny, P.D., Strachan, R.A., Friend, C.R.L. and Paterson, B.A., 2001. U–Pb geochronology of the Fort Augustus granite gneiss: constraints on the timing of Neoproterozoic and Palaeozoic tectonothermal events in the NW Highlands of Scotland. *Journal of the Geological Society*, 158(1), pp.7-14.

Rubatto, D., Williams, I.S. and Buick, I.S., 2001. Zircon and monazite response to prograde metamorphism in the Reynolds Range, central Australia. *Contributions to Mineralogy and Petrology*, 140(4), pp.458-468.

Salje, E.K., Taylor, R.D., Safarik, D.J., Lashley, J.C., Groat, L.A., Bismayer, U., Evans, R.J. and Friedman, R., 2011. Evidence for direct impact damage in metamict titanite CaTiSiO₅. *Journal of Physics: Condensed Matter*, 24(5), p.052202.

Smith, M., Robertson, S. and Rollin, K.E., 1999. Rift basin architecture and stratigraphical implications for basement-cover relationships in the Neoproterozoic Grampian Group of the Scottish Caledonides. *Journal of the Geological Society*, 156(6), pp.1163-1173.

Seydoux-Guillaume, A.M., Montel, J.M., Bingen, B., Bosse, V., de Parseval, P., Paquette, J.L., Janots, E. and Wirth, R., 2012. Low-temperature alteration of monazite: Fluid mediated coupled dissolution–precipitation, irradiation damage, and disturbance of the U–Pb and Th–Pb chronometers. *Chemical Geology*, 330, pp.140-158.

- Smye, A.J., Greenwood, L.V. and Holland, T.J.B., 2010. Garnet–chloritoid–kyanite assemblages: eclogite facies indicators of subduction constraints in orogenic belts. *Journal of Metamorphic Geology*, 28(7), pp.753-768.
- Spandler, C., Hammerli, J., Sha, P., Hilbert-Wolf, H., Hu, Y., Roberts, E. and Schmitz, M., 2016. MKED1: a new titanite standard for in situ analysis of Sm–Nd isotopes and U–Pb geochronology. *Chemical Geology*, 425, pp.110-126.
- Spencer, K.J., Hacker, B.R., Kylander-Clark, A.R.C., Andersen, T.B., Cottle, J.M., Stearns, M.A., Poletti, J.E. and Seward, G.G.E., 2013. Campaign-style titanite U–Pb dating by laser-ablation ICP: Implications for crustal flow, phase transformations and titanite closure. *Chemical Geology*, 341, pp.84-101.
- Spencer, C.J., Kirkland, C.L., Prave, A.R., Strachan, R.A. and Pease, V., 2019. Crustal reworking and orogenic styles inferred from zircon Hf isotopes: Proterozoic examples from the North Atlantic region. *Geoscience Frontiers*, 10(2), pp.417-424.
- Spencer, B.M., Thigpen, J.R., Law, R.D., Mako, C.A., McDonald, C.S., Hodges, K.V. and Ashley, K.T., 2020. Rapid cooling during late-stage orogenesis and implications for the collapse of the Scandian retrowedge, northern Scotland. *Journal of the Geological Society*, 178(1).
- Stephenson, D., Mendum, J.R., Fettes, D.J. and Leslie, A.G., 2013. The Dalradian rocks of Scotland: an introduction. *Proceedings of the Geologists' Association*, 124(1-2), pp.3-82.
- Stipp, M., StuÈnitz, H., Heilbronner, R. and Schmid, S.M., 2002. The eastern Tonale fault zone: a 'natural laboratory' for crystal plastic deformation of quartz over a temperature range from 250 to 700 C. *Journal of structural geology*, 24(12), pp.1861-1884.
- Storey, C.D., Brewer, T.S. and Parrish, R.R., 2004. Late-Proterozoic tectonics in northwest Scotland: one contractional orogeny or several?. *Precambrian Research*, 134(3-4), pp.227-247.
- Storey, Craig D., Teresa E. Jeffries, and Martin Smith. "Common lead-corrected laser ablation ICP–MS U–Pb systematics and geochronology of titanite." *Chemical Geology* 227, no. 1-2 (2006): 37-52.

Storey, C., 2008. The Glenelg-Attadale Inlier, NW Scotland, with emphasis on the Precambrian high-pressure metamorphic history and subsequent retrogression: an introduction and review. *Scottish Journal of Geology*, 44(1), pp.1-16.

Strachan, R.A., Nutman, A.P. and Friderichsen, J.D., 1995. SHRIMP U-Pb geochronology and metamorphic history of the Smalfejord sequence, NE Greenland Caledonides. *Journal of the Geological Society*, 152(5), pp.779-784.

Tanner, P.W.G. and Evans, J.A., 2003. Late Precambrian U–Pb titanite age for peak regional metamorphism and deformation (Knoydartian orogeny) in the western Moine, Scotland. *Journal of the Geological Society*, 160(4), pp.555-564.

Tanner, P.W.G., 2014. A kinematic model for the Grampian Orogeny, Scotland. *Geological Society, London, Special Publications*, 390(1), pp.467-511.

Taylor, R.J., Clark, C., Fitzsimons, I.C., Santosh, M., Hand, M., Evans, N. and McDonald, B., 2014. Post-peak, fluid-mediated modification of granulite facies zircon and monazite in the Trivandrum Block, southern India. *Contributions to Mineralogy and Petrology*, 168(2), p.1044.

Trettin, H.P., Loveridge, W.D. and Sullivan, R.W., 1982. U-Pb ages on zircons from the M'Clintock West massif and the Markham Fiord pluton, northernmost Ellesmere Island. *Current Research, Pt. C. Geol. Surv. Can. Pap*, pp.161-166.

Van Breemen, O., Pidgeon, R.T. and Johnson, M.R.W., 1974. Precambrian and Palaeozoic pegmatites in the Moines of northern Scotland. *Journal of the Geological Society*, 130(6), pp.493-504.

Vance, D., Strachan, R.A. & Jones, K.A., 1998. Extensional versus compressional settings for metamorphism: Garnet chronometry and pressure-temperature-time histories in the Moine Supergroup, northwest Scotland. *Geology*, 26(10), pp.927–930.

Vermeesch, P., 2018. IsoplotR: A free and open toolbox for geochronology. *Geoscience Frontiers*, 9(5), pp.1479-1493.

Walker, S., Bird, A.F., Thirlwall, M.F. and Strachan, R.A., 2021. Caledonian and Pre-Caledonian orogenic events in Shetland, Scotland: evidence from garnet Lu–Hf and Sm–Nd geochronology. *Geological Society, London, Special Publications*, 503(1), pp.305-331.

Walker, S., Thirlwall, M., Strachan, R. and Bird, A., 2017, April. Constraining the timing of orogenesis in Shetland using garnet and mica geochronology. In *EGU General Assembly Conference Abstracts* (p. 417).

Watt, G.R., Kinny, P.D. and Friderichsen, J.D., 2000. U–Pb geochronology of Neoproterozoic and Caledonian tectonothermal events in the East Greenland Caledonides. *Journal of the Geological Society*, 157(5), pp.1031-1048.

Williams, M.L., Jercinovic, M.J., Harlov, D.E., Budzyń, B. and Hetherington, C.J., 2011. Resetting monazite ages during fluid-related alteration. *Chemical Geology*, 283(3-4), pp.218-225.

White, R.W., Powell, R. and Holland, T.J.B., 2001. Calculation of partial melting equilibria in the system Na₂O–CaO–K₂O–FeO–MgO–Al₂O₃–SiO₂–H₂O (NCKFMASH). *Journal of metamorphic Geology*, 19(2), pp.139-153.

White, R.W., Powell, R., Holland, T.J.B. and Worley, B.A., 2000. The effect of TiO₂ and Fe₂O₃ on metapelitic assemblages at greenschist and amphibolite facies conditions: mineral equilibria calculations in the system K₂O–FeO–MgO–Al₂O₃–SiO₂–H₂O–TiO₂–Fe₂O₃. *Journal of Metamorphic Geology*, 18(5), pp.497-511.

White, R.W., Powell, R.O.G.E.R., Holland, T.J.B., Johnson, T.E. and Green, E.C.R., 2014. New mineral activity–composition relations for thermodynamic calculations in metapelitic systems. *Journal of Metamorphic Geology*, 32(3), pp.261-286.

White, R.W., Powell, R. and Johnson, T.E., 2014. The effect of Mn on mineral stability in metapelites revisited: New a–x relations for manganese-bearing minerals. *Journal of Metamorphic Geology*, 32(8), pp.809-828.

Whitney, D.L. and Evans, B.W., 2010. Abbreviations for names of rock-forming minerals. *American mineralogist*, 95(1), pp.185-187.

Appendix

METHODS APPENDIX

APPENDIX 1 CONCEPTS AND APPROACH

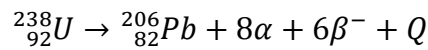
U/Pb GEOCHRONOLOGY

| Parent Isotope | λ_p |
|-------------------|---------------------------|
| ^{238}U | 1.55125×10^{-10} |
| ^{235}U | 9.8485×10^{-10} |
| ^{232}Th | 4.9475×10^{-11} |

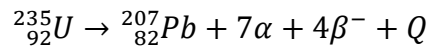
Table 1 Decay constants of relevant isotopes

Uranium lead geochronology relies on the decay chains of ^{238}U to ^{206}Pb and ^{235}U to ^{207}Pb .

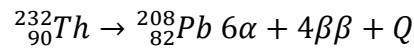
Equation 1.1 Decay of ^{238}U



Equation 1.2 Decay of ^{235}U



Equation 1.3 Decay of ^{232}Th



Equation 2.1 Decay equation for ^{238}U

$$\left(\frac{^{206}_{82}\text{Pb}}{^{204}_{82}\text{Pb}}\right) = \left(\frac{^{206}_{82}\text{Pb}}{^{204}_{82}\text{Pb}}\right)_0 + \left(\frac{^{238}_{92}\text{U}}{^{204}_{82}\text{Pb}}\right) (e^{\lambda_{238}t} - 1)$$

Equation 2.2 Decay equation for ^{235}U

$$\left(\frac{^{207}_{82}\text{Pb}}{^{204}_{82}\text{Pb}}\right) = \left(\frac{^{207}_{82}\text{Pb}}{^{204}_{82}\text{Pb}}\right)_0 + \left(\frac{^{235}_{92}\text{U}}{^{204}_{82}\text{Pb}}\right) (e^{\lambda_{235}t} - 1)$$

$$t = \left(\frac{1}{\lambda_p}\right) \ln \left[\left(\frac{n_d - n_{d0}}{n_p}\right) + 1 \right]$$

- Titanite has a closure temperature of 750°C. Therefore, titanite ages are accurate unless the lithology reached a peak temperature greater than 750°C. After which Pb loss would occur and ages would be reset (Spencer et al., 2013).
- Monazite has an experimentally determined closure temperature of 900 °C in dry conditions (Cherniak et al., 2004). However, fluid alteration and therefore potential for Pb loss can occur at temperatures in excess of 450 °C and 450MPa (Williams et al., 2011).

APPENDIX 2 METHODS AND TECHNIQUE

SAMPLE PREPARATION

- Sample slides were mounted to sample mounts on a cling film covered desk in the lab by hand while wearing clean plastic gloves.
- 1” epoxy pucks containing reference materials were mounted by hand while wearing clean plastic gloves to the sample mount.
- The sample mount was canned using a high resolution EPSON perfection V550 photocopier and then cleaned using high pressure nitrogen.
- Sample mount was then loaded into the reaction cell using a detachable handle with two tugs from within the cell indicating the sample was properly loaded.

DATA REDUCTION

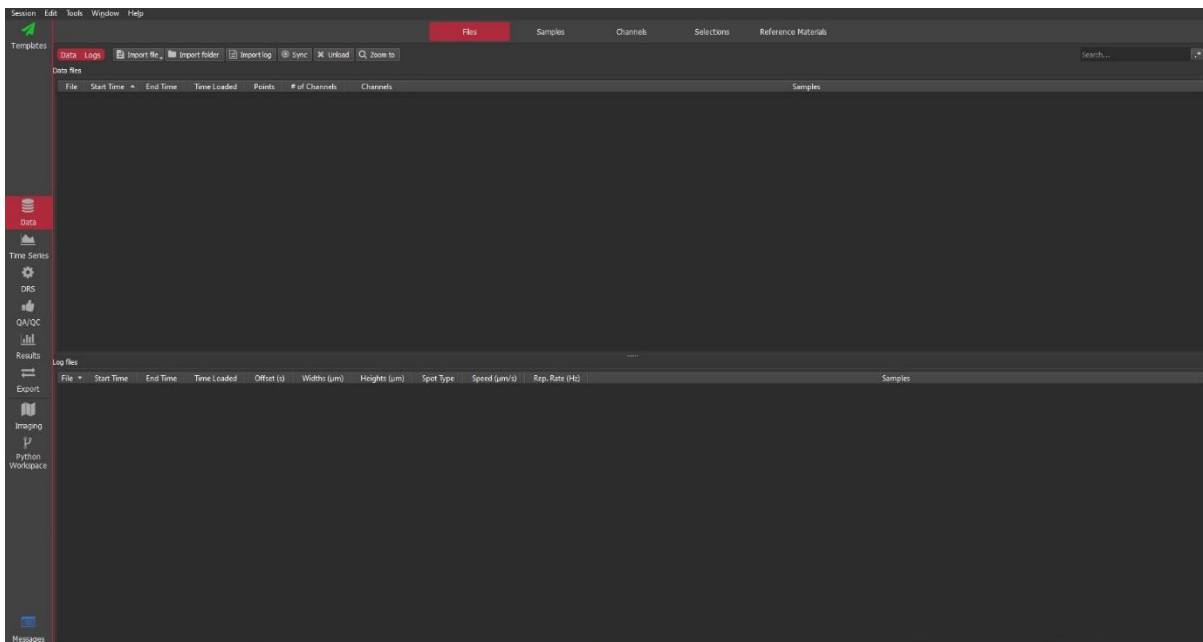


Figure 0-1 Iolite UI

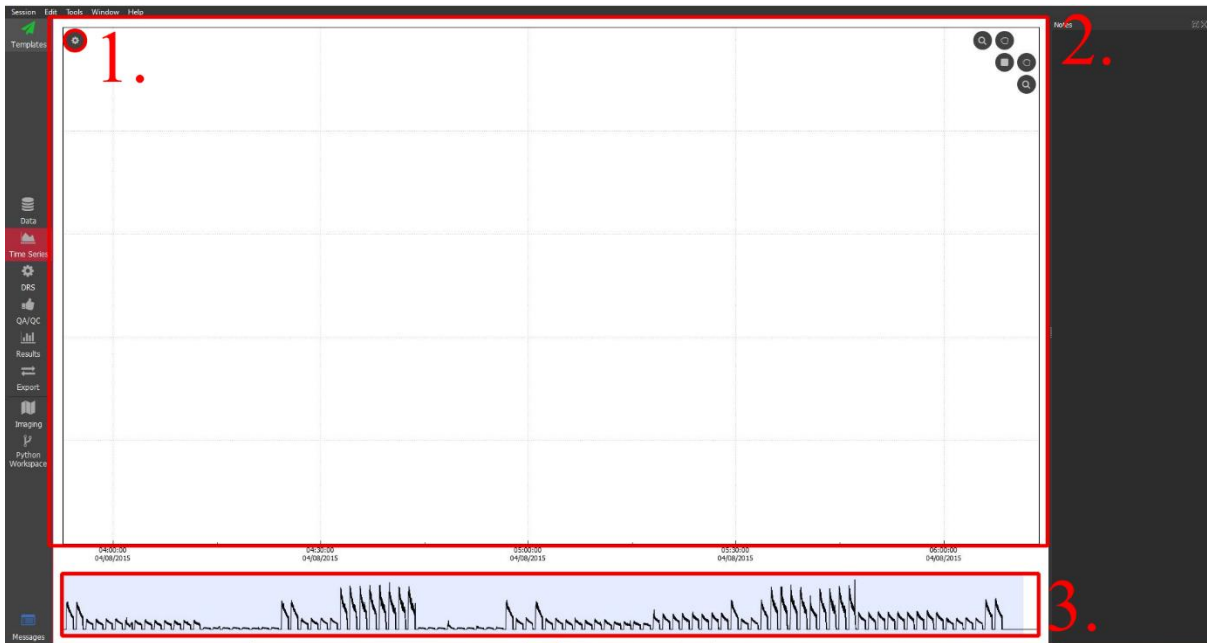


Figure 0-2 Iolite time series view. 1 is the button to access the plot settings and channels . 2 is the window that allows you to navigate a run. 3 is a screenshot of the run that allows for zooming in on parts of the run

- Iolite4 saves open sessions as io4. This file contains the raw data, selections and file data, which is stored as a HDF5 file format.
- The basic data reduction process of an iolite4 session is as follows
 1. Import data
 2. Create sections for baselines, reference materials and samples
 3. Selecting a data reduction scheme and running it
 4. Viewing results and or figure production
 5. Exporting of results and figures
- A selection is a period of time that related to the laser and the collection of data within the mass spectrometer. Selections are used to report the mean, median and uncertainty within data associated to that selection or time period.
- Selections are collated into groups to let Iolite4 know what is happening at what time i.e. RG1718a selections would be grouped into the RG1718a group. Groups can be anything however, groups will refer to the measurement of isotope counts from the ablation of a mineral or group of minerals within a sample.
- All data within Iolite4 is processed from time-point by time-point. This means that there is a calculated result for every time point in the experiment, allows for down hole corrections, detailed interpolation, spinning and smoothing of results.
- Channels are an array of data values with an associated measurement time. This can be the raw data from the mass spectrometer, calculated channels, such as intermediate and output channels.
- Splines are the calculated result for a given sample type within any time point within a given experiment. For example, a Baseline spline for a given isotope within a given sample that may be calculated.

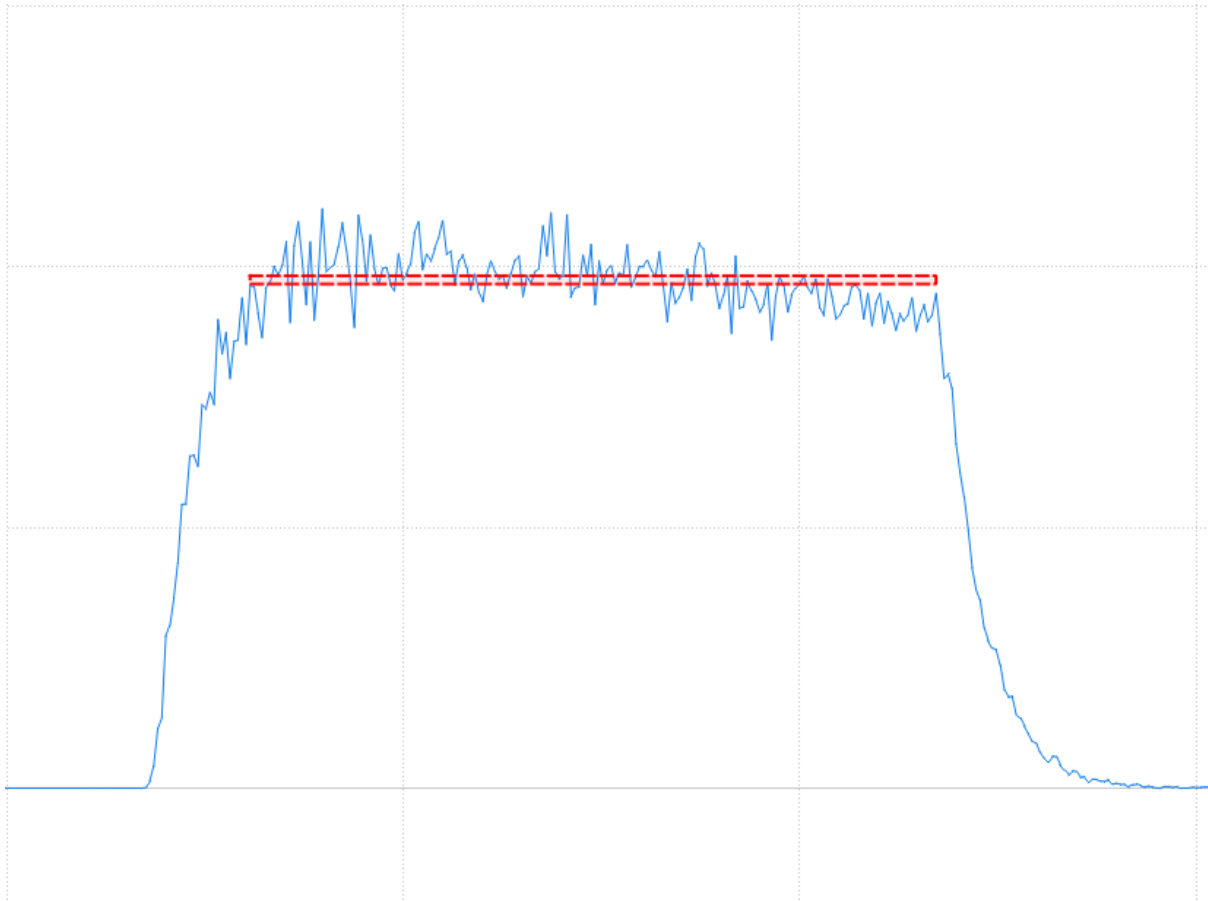


Figure 0-3 Ideal spike from the laser.

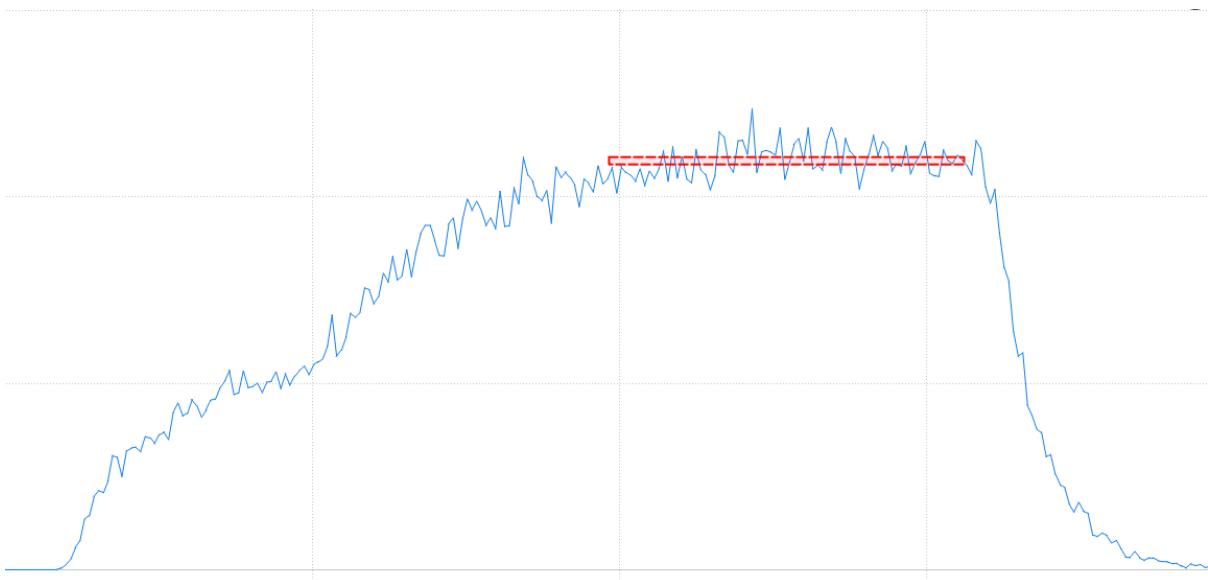


Figure 0-4 Spike with poor data. This spike shows low initial values. The red selection box represents a possible reduction of the spike data to achieve data that would represent a single age rather than a mixed age or data from 2 mineral domains

To quantify trace element concentrations Iolite4 used the concentration of analyte element equation from Longrich et al 1996.

Equation 3.1

$$C_{AN_{SAM}} = \frac{R_{AN_{SAM}}}{S}$$

- Where $C_{AN_{SAM}}$ is the concentration of the analyte element within the sample. $R_{AN_{SAM}}$ is the count rate of the analyte within the sample and S is the normalised sensitivity. The equation for normalised sensitivity is calculated using an analyte from a sample with known concentrations (a standard i.e Moacyr). S is calculated using equation 3.2 provided below.

Equation 3.2

$$S = \frac{R_{AN_{CAL}}}{C_{AN_{CAL}}} \left(\frac{R_{IS_{SAM}}}{R_{IS_{CAL}}} \frac{C_{IS_{CAL}}}{C_{IS_{SAM}}} \right)$$

- Where $R_{AN_{CAL}}$ is the count rate of the analyte within the calibration material. $C_{AN_{CAL}}$ is the concentration of the analyte within the calibration material. $R_{IS_{SAM}}$ is the count rate of the internal standard within the sample. $R_{IS_{CAL}}$ is the count rate of the internal standard within the calibration material. $C_{IS_{CAL}}$ is the concentration of the internal standard within the calibration material. $C_{IS_{SAM}}$ is the concentration of the internal standard within the sample.

SAMPLE DESCRIPTIONS APPENDIX

RG1703

| Mineral | Notes | Major Mineral % |
|-------------|--------------------------------------------------------------------------------------------------------------------------|-----------------|
| Hornblende | Dominant mineral in lithology. Deep green and strongly pleochroic indicates higher Fe content of the mineral. | 45% |
| Garnet | Large garnets up to 700µm across. 3 zones within the garnets have been identified based upon inclusions. | 7% |
| Biotite | Uncommon. Locally replaced by chlorite. | 12% |
| Plagioclase | Form porphyroblasts with quartz inclusions/mrmeketic. Mantled by quartz wings. Found locally in one part of the section. | 20% |
| Quartz | Found locally, predominantly associated with plagioclase. | 10% |

| | | |
|----------|----------------------------------------------------------------------------------------------------------------------------------------------------------------------------------------------------------|-----|
| Chlorite | Locally replacing biotite within a biotite band. | 2% |
| Titanite | 2 morphologies seen within section, droplet shaped titanites found within the outer layers of garnets as inclusions and angular rugged inclusions within garnet cores associated with acicular ilmenite. | N/A |
| Ilmenite | Associated with rugged titanite inclusions within garnet cores. | |
| Monazite | Found as rounded grains. Rare within section. | N/A |
| Rutile* | Not sure. Staining around grain boundaries. | N/a |

Sample RG1716

| Mineral | Notes | Major Mineral % |
|------------------|---------------------------------------------------------------------------------------------------------------------------------|-----------------|
| Quartz | | 29 |
| Microcline | Sericitized, Variable size with grains greater than 1cm. The only feldspar seen in section that forms the large porphyroblasts. | 26 |
| Anorthite | Sericitized blocky grains. Degree of sericitation is variable, with some grains having been almost completely replaced. | 22 |
| Biotite | Often replaced by chlorite. | 10 |
| Muscovite | Forms both large >200µm books and smaller mica grains. | 5 |
| Chlorite | Replacing biotite. | 5 |
| Monazite | Present as large, fractured grains. | |
| Xenotime | Present as small grains associated with the larger monazites. | |
| Haematite/Rutile | Formed by late fluid movement. Stains nearby grain boundaries. | |

Sample RG1718

| Mineral Present | Notes | Major Mineral % |
|-----------------|--------------------------------------------------------------------------|-----------------|
| Quartz | | 26 |
| Plagioclase | | 24 |
| Muscovite | Breaks down into zones clay sized minerals | 14 |
| Biotite | Breaks down into zones clay sized minerals | 22 |
| Garnet | | 10 |
| Chlorite | Replacing Garnet and biotite as part of a retrograde hydration reaction. | 4 |
| Fluorapatite | Rounded Grains. | |
| Monazite | Rare. Associated with fluorapatite and biotite. | |
| Ilmenite | Elongate opaque phase. | |
| Zircon | Found within biotites. | |

Sample RG1710

| Mineral | Notes | Major Mineral % |
|-------------|---------------------------------------------------------------------------------------------------------------------------------------|-----------------|
| Hornblende | Large, rounded clasts with quartz inclusions | 23 |
| Amphibole 2 | Same as above | 20 |
| Quartz | Some in the form of myrmekite with feldspar. Some replacing/overprinted by amphibole. Observed as a vermicular growth within biotite. | 27 |

| | | |
|---------------------------------|-----------------------------------------------------------------------------------------------------------------------|----|
| Microcline | Present as large amorphous grains. Grain fringes may be myrmeketic. | 18 |
| Biotite | Present. | 7 |
| Isotropic unidentified mineral. | Replacing amphibole. | |
| Titanite. | Droplet shaped titanites of varying size, up to 800µm, though only one titanite above 340µm in length has been found. | 4 |
| Opaque phase. | Forms rounded squares associated with the amphiboles. | |
| Acicular opaque phase. | Inclusion within biotite within cleavage. Ilmenite? | |
| Haematite | Rare | |

RESULTS APPENDIX

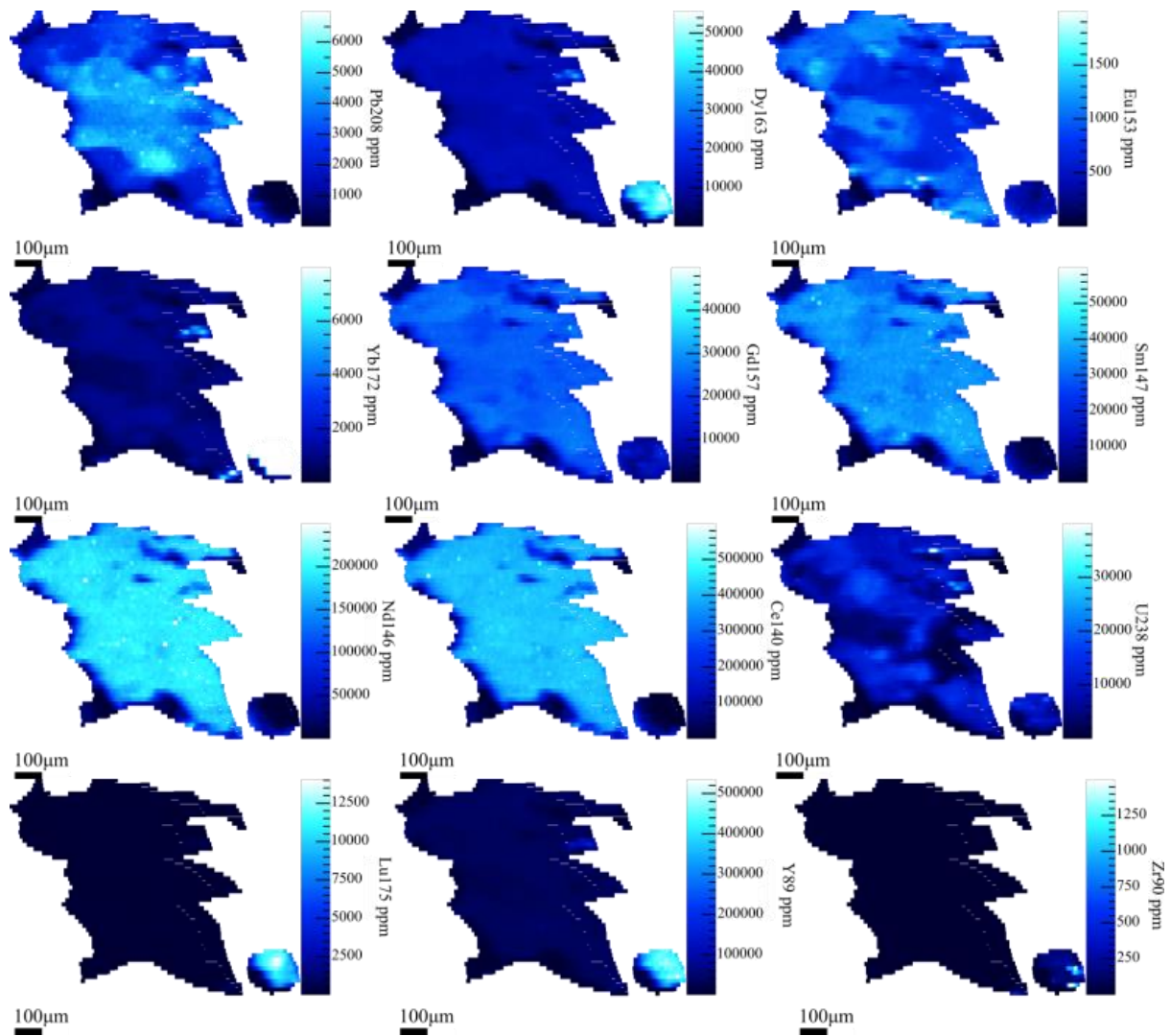


Figure 0-1 Maps Produced from sample RG1716

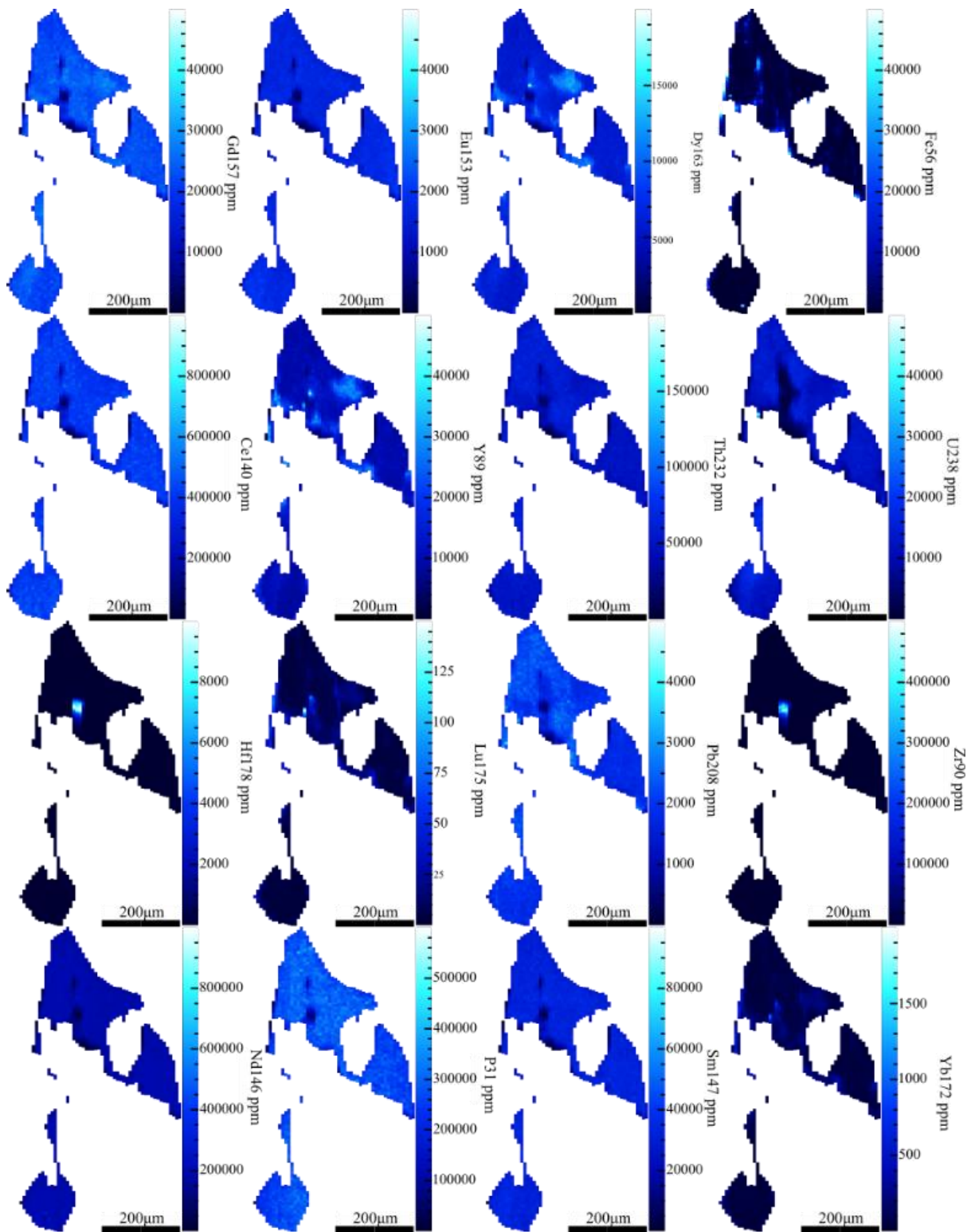


Figure 0-2 Maps produced from RG1718 monazite

METAMORPHIC MODELLING APPENDIX

Hyslop assemblage label numbers

1 = PL WM BI CHL ILM1 H2O q ru

- 2 = PL WM BI ST ILM1 H2O q
- 3 = PL GRT WM BI ST ILM1 H2O and q
- 4 = PL GRT WM BI ILM1 H2O and q
- 5 = (2)PL WM BI ILM1 H2O and q
- 6 = (2)PL BI ILM1 H2O and q
- 7 = (2)PL BI CORD ILM1 H2O and q
- 8 = (2)PL BI CORD ILM1 H2O q
- 9 = LIQt6 (2)PL BI CORD ILM1 H2O q
- 10 = LIQt6 PL BI CORD ILM1 H2O q
- 11 = LIQt6 (2)PL BI CORD ILM1 H2O q
- 12 = LIQt6 PL BI CORD ILM1 H2O q
- 13 = LIQt6 PL GRT BI CORD MTlow ILM1 H2O
- 14 = LIQt6 PL GRT BI CORD MTlow ILM1
- 15 = LIQt6 PL GRT BI CORD ILM1 q
- 16 = LIQt6 PL BI CORD ILM1 q
- 17 = LIQt6 PL BI CORD ILM1 sill q
- 18 = LIQt6 PL GRT CORD ILM1 q
- 19 = LIQt6 PL GRT BI CORD ILM1 sill q
- 20 = LIQt6 PL GRT BI CORD ILM1 H2O q
- 21 = LIQt6 PL GRT BI ILM1 H2O sill q
- 22 = LIQt6 PL BI ILM1 H2O sill q
- 23 = LIQt6 (2)PL BI ILM1 H2O sill q
- 24 = LIQt6 PL WM BI ILM1 H2O sill q

25 = LIQtc6 PL GRT WM BI ILM1 H2O sill q ru

26 = LIQtc6 PL GRT WM BI ILM1 sill q ru

27 = LIQtc6 PL GRT WM BI sill q ru

28 = LIQtc6 PL GRT WM BI H2O q ru

29 = LIQtc6 PL GRT WM BI ILM1 H2O q

30 = LIQtc6 GRT WM q ru

31 = PL GRT WM BI ST ILM1 H2O sill q

32 = PL EPI GRT WM BI ILM1 H2O q

33 = PL EPI GRT WM BI ILM1 H2O q ru

34 = PL EPI GRT WM BI H2O q ru

35 = PL GRT (2)WM BI H2O sph q ru

36 = PL GRT (2)WM BI H2O sph q

37 = GRT (2)WM BI H2O sph q

38 = EPI GRT (2)WM BI CHL H2O sph q ru

39 = PL EPI GRT WM BI CHL ILM1 H2O q

40 = PL EPI WM BI CHL ILM1 H2O q

41 = PL EPI WM BI CHL ILM1 H2O q ru

42 = PL EPI WM BI CHL H2O sph q =

43 PL EPI GRT WM BI CHL H2O sph q

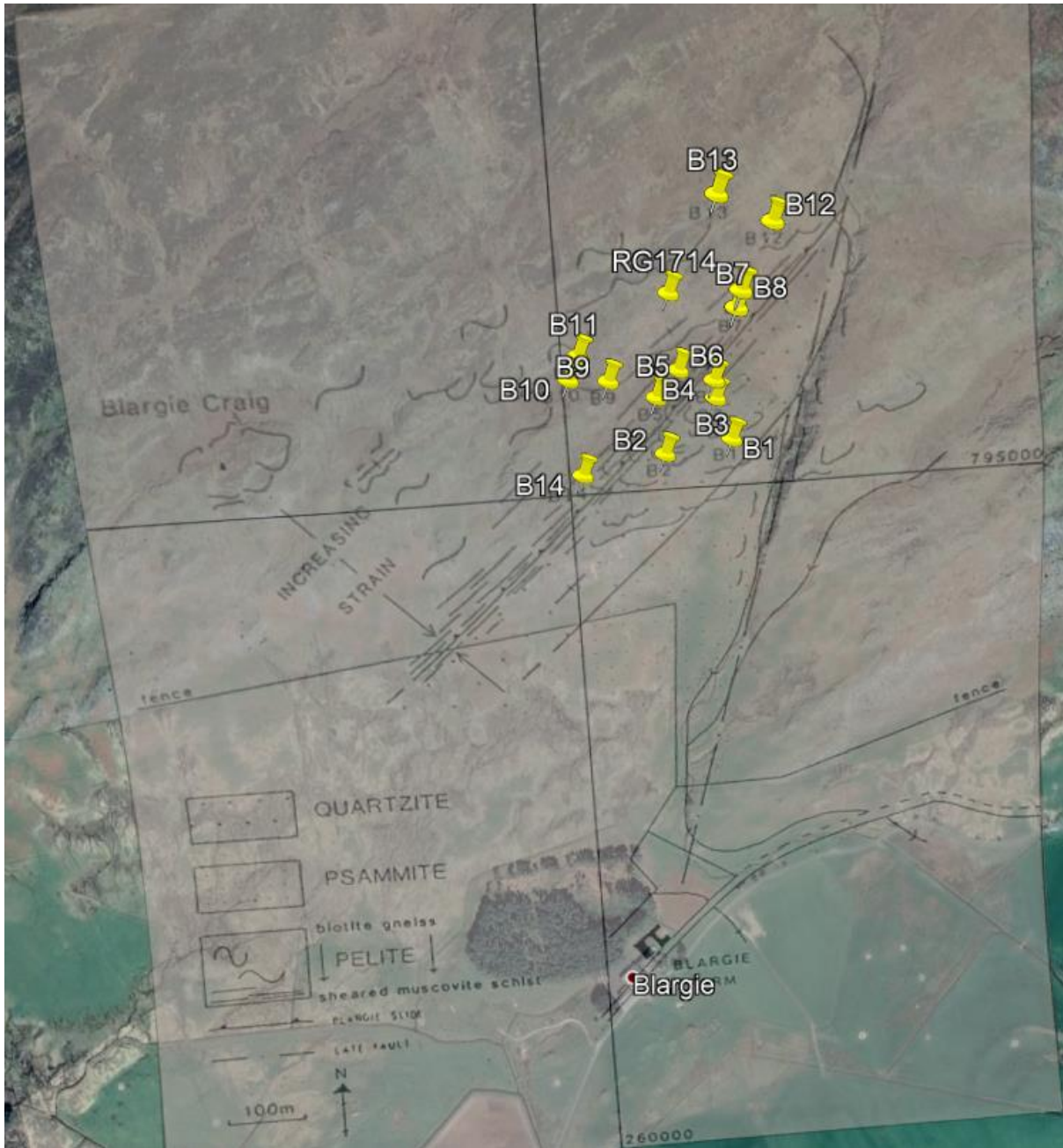


Figure 0-1 Blargie farm shear zone map from Hyslop (1992). Maps from thesis put into google earth to extract grid references from each sample location marker. This shows the methodology of using Hyslop (1992) Thesis maps to produce spatial data grid reference data for all of his plotted points

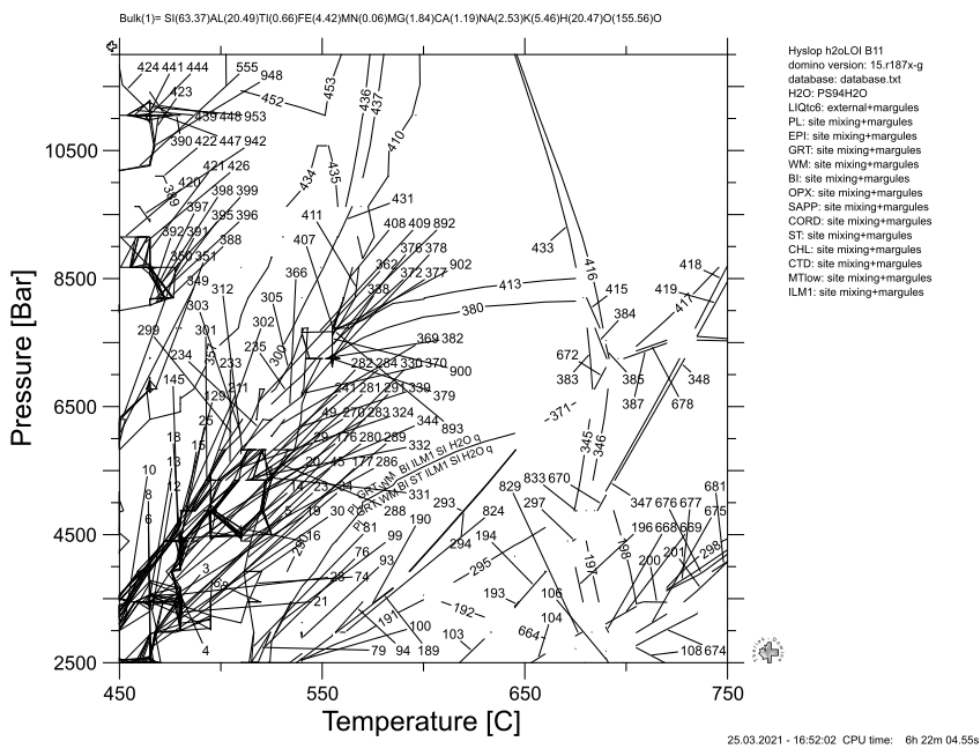


Figure 0-2 Raw output from Theriak Domino for sample B11 using LOI as the moles of H₂O. Muddled reaction lines had to be defined post generation. Using the reaction label information below and the strongest line plotted on the raw plot.

A. Bird 2013 Leven Schist label numbers

- 1 = PL WM BI CHL ILM1 H₂O q r u
- 2 = PL WM BI ST ILM1 H₂O q
- 3 = PL GRT WM BI ST ILM1 H₂O and q
- 4 = PL GRT WM BI ST ILM1 H₂O sill q
- 5 = (2)PL BI ILM1 H₂O and q
- 6 = (2)PL BI ILM1 H₂O sill q
- 7 = (2)PL BI CORD ILM1 H₂O sill q
- 8 = (2)PL BI CORD ILM1 H₂O and q
- 9 = (2)PL BI CORD ILM1 H₂O q
- 10 = LIQtC6 (2)PL BI CORD ILM1 H₂O q

- 11 = LIQtC6 PL BI CORD ILM1 H2O q
- 12 = LIQtC6 (2)PL BI CORD ILM1 H2O sill q
- 13 = LIQtC6 PL GRT BI CORD ILM1 H2O q
- 14 = LIQtC6 PL GRT BI CORD MTlow ILM1 H2O q
- 15 = LIQtC6 PL GRT BI CORD MTlow ILM1 H2O
- 16 = LIQtC6 PL GRT BI CORD ILM1 H2O
- 17 = LIQtC6 PL GRT BI CORD ILM1
- 18 = LIQtC6 PL GRT BI CORD ILM1 q
- 19 = LIQtC6 PL BI CORD ILM1 H2O sill q
- 20 = LIQtC6 PL BI ILM1 H2O sill q
- 21 = LIQtC6 (2)PL BI ILM1 H2O sill q
- 22 = LIQtC6 PL GRT BI CORD ILM1 H2O sill q
- 23 = LIQtC6 PL GRT BI CORD ILM1 sill q
- 24 = LIQtC6 PL WM BI ILM1 H2O sill q
- 25 = LIQtC6 PL GRT WM BI ILM1 H2O sill q
- 26 = LIQtC6 PL GRT WM BI ILM1 sill q
- 27 = LIQtC6 PL GRT WM BI ILM1 H2O q
- 28 = LIQtC6 PL GRT WM BI ILM1 q ru
- 29 = LIQtC6 PL GRT WM BI ILM1 ky q ru
- 30 = LIQtC6 PL GRT BI ILM1 sill q ru
- 31 = LIQtC6 PL GRT BI ILM1 ky q ru
- 32 = LIQtC6 PL GRT WM BI ky q ru
- 33 = LIQtC6 PL GRT WM BI ILM1 H2O q ru

34 = LIQt6 PL GRT WM BI H2O q ru

35 = PL GRT (2)WM BI H2O sph q ru

36 = PL GRT (2)WM BI H2O sph q

37 = PL GRT (2)WM BI ILM1 H2O q ru

38 = PL EPI GRT (2)WM BI ILM1 H2O q ru

39 = PL EPI GRT (2)WM BI H2O sph q ru

40 = PL GRT (2)WM BI CHL ILM1 H2O q

41 = PL EPI GRT (2)WM BI CHL ILM1 H2O q

42 = PL EPI WM BI CHL ILM1 H2O q

43 = PL EPI GRT (2)WM BI CHL H2O sph q

44 = PL EPI (2)WM BI CHL H2O sph q

45 = PL EPI WM BI CHL H2O sph q

OUTPUT DATA FROM IOLITE4.1

RG1716 U-Pb Run Data

| Final U238/Pb206_mean | Final U238/Pb206_2SE(int) | Final Pb207/Pb206_mean | Final Pb207/Pb206_2SE(int) | rho 207Pb/206Pb v 238U/206Pb |
|--------------------------|------------------------------|---------------------------|-------------------------------|------------------------------|
| 6.970453557 | 0.199443535 | 0.066849351 | 0.000740618 | 0.02290464 |
| 11.00103757 | 0.396523007 | 0.061412096 | 0.001569481 | 0.29009721 |
| 7.163181989 | 0.363281517 | 0.067618743 | 0.000864664 | 0.31791092 |
| 7.27714615 | 0.235909665 | 0.071022983 | 0.00286062 | 0.18665764 |
| 8.063357272 | 0.25095312 | 0.067026964 | 0.001434005 | 0.1027558 |
| 7.019358436 | 0.212417151 | 0.067155026 | 0.000894362 | -0.09472947 |
| 12.5864898 | 0.414368362 | 0.056567602 | 0.001009785 | -0.06663803 |
| 8.929818193 | 0.332097071 | 0.062644433 | 0.00171254 | 0.03926497 |
| 6.871267351 | 0.27693864 | 0.069190748 | 0.003406676 | -0.18620560 |
| 6.995412031 | 0.27305812 | 0.065376526 | 0.000766694 | 0.24457374 |
| 10.28180704 | 0.288264087 | 0.059703323 | 0.001180966 | 0.11671456 |
| 7.597271413 | 0.151712469 | 0.065595386 | 0.001032595 | -0.06787562 |
| 8.617976292 | 0.310628078 | 0.063363677 | 0.000992502 | 0.04149730 |
| 12.69328435 | 0.337136115 | 0.057460766 | 0.001015573 | 0.15645 |
| 6.279396121 | 0.242202797 | 0.066266324 | 0.000933713 | 0.22786149 |
| 13.18025265 | 0.873817621 | 0.05670612 | 0.000974841 | 0.27521100 |
| 12.36811394 | 0.443170791 | 0.05763337 | 0.001255106 | 0.22422457 |
| 7.2395892 | 0.270952208 | 0.064480811 | 0.001848776 | 0.09878632 |
| 9.247907024 | 0.468289567 | 0.062808715 | 0.00097024 | 0.17224111 |
| 7.081300707 | 0.283603989 | 0.064786016 | 0.001252825 | 0.19031295 |
| 8.316893548 | 0.30490675 | 0.068985793 | 0.002295731 | 0.4244926 |
| 8.20641312 | 0.242801506 | 0.071483479 | 0.003788338 | 0.28376453 |
| 7.866849791 | 0.242285541 | 0.065327971 | 0.001753816 | 0.17631204 |

| | | | | |
|-------------|-------------|-------------|-------------|-------------|
| 6.039074654 | 0.309300674 | 0.075333198 | 0.00527798 | 0.21521837 |
| 11.86595664 | 0.328440537 | 0.06388843 | 0.003434771 | 0.04618499 |
| 12.94176929 | 0.342841568 | 0.059205723 | 0.001647766 | 0.40720993 |
| 7.068219878 | 0.228965084 | 0.069530429 | 0.001441975 | 0.30360788 |
| 8.313939955 | 0.316102431 | 0.072542587 | 0.004269972 | 0.07048455 |
| 7.908791328 | 0.244548075 | 0.062324717 | 0.001418915 | 0.01439076 |
| 13.03580052 | 0.273245828 | 0.056803827 | 0.001081045 | -0.03360877 |
| 12.96535867 | 0.511500611 | 0.058741692 | 0.001468582 | 0.19098877 |
| 7.262001705 | 0.159644931 | 0.065531198 | 0.000709448 | 0.04044785 |
| 8.154165596 | 0.288216253 | 0.06429624 | 0.001238674 | 0.09114401 |
| 7.48834368 | 0.235852377 | 0.065841045 | 0.001242808 | 0.08626326 |
| 9.255176143 | 0.383882927 | 0.095198254 | 0.006263945 | -0.0545387 |
| 10.28381924 | 0.436428891 | 0.068269238 | 0.004760699 | 0.09498831 |
| 7.008163651 | 0.327977709 | 0.062924734 | 0.001429233 | 0.20720176 |
| 12.51638837 | 0.40105082 | 0.061240365 | 0.001831643 | 0.08663136 |
| 12.32825713 | 0.444555825 | 0.058982079 | 0.001328477 | 0.47783517 |

RG1718 U-Pb Run data

| Final U238/Pb206_mean | Final U238/Pb206_2SE(int) | Final Pb207/Pb206_mean | Final Pb207/Pb206_2SE(int) | rho 207Pb/206Pb v 238U/206Pb | Age (Ma) | +/- |
|-----------------------|---------------------------|------------------------|----------------------------|------------------------------|----------|------|
| 10.53082835 | 0.415536517 | 0.085721883 | 0.002472655 | 0.178337582 | 586.3 | 12.6 |
| 13.05238782 | 0.533285241 | 0.060141882 | 0.001081733 | 0.074414957 | 498.41 | 9 |
| 13.11427119 | 0.472958101 | 0.056538947 | 0.000894213 | 0.303690186 | 473.45 | 6.39 |
| 13.1902913 | 0.197137461 | 0.056384659 | 0.000861745 | 0.083615141 | 470.84 | 3.26 |
| 13.38542063 | 0.344822961 | 0.055945233 | 0.000907714 | -0.053654569 | 463.19 | 5.54 |
| 12.74991937 | 0.534570194 | 0.06125236 | 0.001288691 | 0.051223256 | 507.18 | 9.78 |
| 11.85922189 | 0.459571581 | 0.05893355 | 0.001265204 | 0.420888385 | 531.29 | 7.28 |

| | | | | | | |
|-------------|-------------|-------------|-------------|--------------|--------|------|
| 12.93693739 | 0.379317408 | 0.059984135 | 0.001043951 | 0.062920681 | 492.48 | 6.62 |
| 12.91615219 | 0.39407686 | 0.057429216 | 0.000943876 | 0.143390142 | 484.95 | 6.31 |
| 12.58069908 | 0.390704709 | 0.056942362 | 0.001023113 | 0.086582136 | 492.38 | 6.68 |
| 11.77045289 | 0.352593659 | 0.067149311 | 0.001189583 | -0.062706611 | 531.44 | 8.31 |
| 10.80712928 | 0.453150363 | 0.058957299 | 0.001091867 | 0.092318589 | 568.92 | 9.51 |
| 12.66204569 | 0.400881512 | 0.062239872 | 0.001242262 | -0.109692081 | 494.71 | 7.81 |
| 11.22027078 | 0.436699966 | 0.0751159 | 0.002342857 | 0.158222911 | 570.6 | 11 |
| 11.47221413 | 0.565769557 | 0.064550942 | 0.001557344 | 0.310679989 | 590.2 | 11.1 |
| 12.68451222 | 0.285623029 | 0.058215564 | 0.001025141 | 0.113265207 | 493.33 | 5.02 |
| 12.58562011 | 0.373264009 | 0.057036241 | 0.001023263 | 0.089789424 | 492.75 | 6.42 |
| 11.75404147 | 0.489087186 | 0.056826929 | 0.001002624 | -0.065500493 | 516.93 | 9.21 |
| 13.48937507 | 0.534905442 | 0.057241742 | 0.00094238 | 0.154429823 | 469.47 | 7.6 |
| 10.29124103 | 0.595709624 | 0.059200233 | 0.001211931 | -0.07940978 | 589.3 | 13.5 |
| 12.81579877 | 0.392123424 | 0.0562239 | 0.000884591 | 0.242556762 | 479.96 | 5.85 |
| 12.33569827 | 0.40152541 | 0.056925859 | 0.00114705 | 0.172905754 | 500.23 | 6.89 |
| 12.75579904 | 0.39840809 | 0.055963163 | 0.000833978 | -0.122969815 | 481.33 | 6.81 |
| 13.11409215 | 0.491146702 | 0.056131001 | 0.000934968 | 0.17975253 | 469.98 | 7.09 |
| 12.80785909 | 0.518342019 | 0.057150229 | 0.001042448 | -0.001745313 | 486.71 | 8.62 |
| 13.25071381 | 0.682280511 | 0.057405971 | 0.000989916 | 0.012407383 | 479 | 10.2 |
| 12.17692206 | 0.410743161 | 0.055732742 | 0.001101724 | -0.00224877 | 499.4 | 7.48 |
| 13.15308417 | 0.321681292 | 0.05594289 | 0.00091322 | 0.28767051 | 468.97 | 4.69 |
| 12.66296347 | 0.332402359 | 0.057445407 | 0.00103022 | 0.095933735 | 491.89 | 5.77 |
| 13.1929008 | 0.342273066 | 0.05690503 | 0.000950439 | -0.079634434 | 472.09 | 5.76 |
| 10.1163965 | 0.195595118 | 0.090644819 | 0.005035371 | -0.020307895 | 602.47 | 5.64 |
| 13.10766009 | 0.306610884 | 0.055890737 | 0.000940767 | 0.291606058 | 470.32 | 4.53 |
| 13.31298755 | 0.358453784 | 0.05624413 | 0.000938838 | 0.087687267 | 466.2 | 5.58 |
| 12.41337535 | 0.454818905 | 0.056321854 | 0.001022437 | 0.032254481 | 493.2 | 7.8 |
| 8.966871906 | 0.621373551 | 0.10559276 | 0.00659204 | 0.191795347 | 656.1 | 25.2 |
| 14.1808373 | 0.557743183 | 0.056858037 | 0.000961322 | 0.104200886 | 447.54 | 7.53 |

| | | | | | | |
|-------------|-------------|-------------|-------------|--------------|--------|------|
| 13.24584342 | 0.175803483 | 0.055120754 | 0.000861568 | 0.013663454 | 467.31 | 2.93 |
| 13.39291903 | 0.356814644 | 0.055451336 | 0.000924244 | 0.182029668 | 459.43 | 5.23 |
| 12.35106583 | 0.500999705 | 0.06453071 | 0.00138135 | 0.169949329 | 537.68 | 9.77 |
| 9.761077508 | 0.591037105 | 0.118933285 | 0.00271975 | -0.015267483 | 205.3 | 11.6 |
| 11.13606721 | 0.491204447 | 0.070869847 | 0.001530411 | 0.225743865 | 624.3 | 12.5 |
| 11.94484708 | 0.630524845 | 0.074955264 | 0.002344953 | 0.323603799 | 579.8 | 14.2 |
| 12.45068158 | 0.419875915 | 0.062640723 | 0.001228336 | 0.32067015 | 531.7 | 7.16 |
| 12.46552453 | 0.402257294 | 0.063487453 | 0.001040342 | 0.147016906 | 530.42 | 7.65 |
| 13.20391362 | 0.368069377 | 0.057083595 | 0.001078301 | 0.215026593 | 473.53 | 5.64 |
| 12.92413049 | 0.480041471 | 0.065166226 | 0.001555448 | 0.074132011 | 496.69 | 9 |
| 12.05331769 | 0.463662866 | 0.071979623 | 0.001529345 | 0.057382435 | 519 | 11.1 |
| 13.67440234 | 0.592649768 | 0.075399433 | 0.002402878 | -0.001476951 | 428.8 | 10.2 |
| 9.125867423 | 0.673224579 | 0.072481601 | 0.002270961 | -0.050168078 | 742.5 | 28.1 |
| 11.30694765 | 0.624982977 | 0.072963486 | 0.001742405 | 0.240216576 | 636.7 | 16.9 |
| 11.85903228 | 0.403353125 | 0.087228501 | 0.003027398 | 0.140346101 | 513.97 | 9.04 |
| 13.55828054 | 0.439029998 | 0.062784329 | 0.001360133 | 0.259326793 | 484.49 | 6.84 |

Monazite U-Pb Standards. Both samples (RG1716 and RG1718) were included within the same run. The standards apply to both samples.

| | Final U238/Pb206_mean | Final U238/Pb206_2SE(int) | Final Pb207/Pb206_mean | Final Pb207/Pb206_2SE(int) | rho 207Pb/206Pb v 238U/206Pb |
|-----------|----------------------------------|--------------------------------------|-----------------------------------|---------------------------------------|-----------------------------------------|
| Bananeira | 12.14371529 | 0.086819608 | 0.062008166 | 0.001751793 | 0.174590905 |
| | 12.08290695 | 0.091319519 | 0.058870988 | 0.001243477 | 0.135921461 |
| | 11.3723176 | 0.099169039 | 0.086111615 | 0.002180576 | -0.178935916 |
| | 11.82376609 | 0.119190487 | 0.057672685 | 0.001260225 | 0.138787983 |
| | 11.90137336 | 0.08849036 | 0.058347547 | 0.00127931 | 0.196527724 |
| | 12.09346795 | 0.087801777 | 0.057719531 | 0.001307916 | 0.135495704 |
| | 11.92543083 | 0.096565487 | 0.056520464 | 0.001183969 | 0.204259586 |

| | | | | | |
|------|-------------|-------------|-------------|-------------|--------------|
| | 11.85375585 | 0.091918088 | 0.061167396 | 0.001585565 | -0.093031848 |
| | 11.41996893 | 0.178775147 | 0.099999728 | 0.005863 | -0.235285251 |
| | 12.1144143 | 0.225009572 | 0.060604479 | 0.00342736 | 0.204003894 |
| | 11.94240431 | 0.091774433 | 0.056862023 | 0.001055051 | 0.271921157 |
| | 12.02318377 | 0.089901908 | 0.057453929 | 0.001136201 | 0.260636077 |
| | 11.45182183 | 0.076213772 | 0.089944294 | 0.001602084 | 0.147931429 |
| | 12.10505272 | 0.074686646 | 0.057423786 | 0.001253309 | 0.314425414 |
| | 12.33375395 | 0.105366232 | 0.056589134 | 0.001240375 | 0.157055434 |
| | 12.09648668 | 0.084647145 | 0.05670355 | 0.001099284 | 0.186705348 |
| Mean | 11.91773877 | 0.139960129 | 0.064624957 | 0.006969181 | |

| | | | | | |
|-------|-------------|-------------|-------------|-------------|-------------|
| Stern | 12.04863536 | 0.077600671 | 0.057539451 | 0.001188438 | 0.174523586 |
| | 11.9731341 | 0.084330617 | 0.056773678 | 0.001116013 | 0.158048918 |
| | 12.0886484 | 0.086697318 | 0.057582766 | 0.001140724 | 0.217872647 |
| | 12.08637272 | 0.087672312 | 0.0579053 | 0.001340277 | 0.168731655 |
| | 11.98139777 | 0.092194702 | 0.056643711 | 0.001165402 | 0.191379286 |
| | 11.99818133 | 0.078566568 | 0.057426514 | 0.001208023 | 0.312576764 |
| | 12.02489582 | 0.089772145 | 0.057705097 | 0.001181938 | 0.182980395 |
| | 12.08999086 | 0.086861859 | 0.05687633 | 0.001198639 | 0.101800655 |
| | 11.90103311 | 0.126351917 | 0.057728953 | 0.001617969 | 0.188322729 |
| | 12.13281488 | 0.099422595 | 0.057232179 | 0.001486646 | 0.324386424 |
| | 11.95807395 | 0.111732044 | 0.057175903 | 0.001450567 | 0.156684977 |
| | 12.06119287 | 0.153444142 | 0.056879848 | 0.002313657 | 0.251416434 |
| | 12.04873682 | 0.093484094 | 0.057544794 | 0.001305808 | 0.259967856 |
| | 12.06080823 | 0.10377484 | 0.057579971 | 0.001208601 | 0.130225982 |
| | 11.97302683 | 0.099830473 | 0.056801304 | 0.001239051 | 0.213551223 |
| | 12.08858222 | 0.09832487 | 0.057163713 | 0.001481604 | 0.369006569 |
| | 12.114216 | 0.100863954 | 0.057007779 | 0.001136011 | 0.133276676 |
| | 11.9975105 | 0.085564497 | 0.057210635 | 0.001291041 | 0.181792539 |

| | | | | | |
|------|-------------------|-------------------|--------------------|--------------------|-------------|
| | 11.76810454 | 0.086676975 | 0.057260511 | 0.001396758 | 0.163622626 |
| | 12.30366159 | 0.099186271 | 0.058144474 | 0.001342417 | 0.199699275 |
| Mean | <i>12.0349509</i> | <i>0.04697854</i> | <i>0.057309146</i> | <i>0.000182484</i> | |

| | | | | | |
|---------|-------------------|--------------------|--------------------|--------------------|-------------|
| NIST610 | 3.999711587 | 0.211041983 | 0.928032469 | 0.01745297 | -0.01675623 |
| | 4.183002526 | 0.227255295 | 0.928834756 | 0.018456819 | 0.462449909 |
| | 4.010950344 | 0.168694845 | 0.914681416 | 0.017657716 | 0.205210017 |
| | 4.120057885 | 0.170887715 | 0.90203112 | 0.018492263 | 0.196843686 |
| | 4.356005614 | 0.267041992 | 0.915171221 | 0.018939091 | 0.357335212 |
| | 4.023361752 | 0.181228564 | 0.918926418 | 0.020493679 | 0.139645451 |
| | 3.982251408 | 0.100973551 | 0.903958511 | 0.019508337 | 0.308140325 |
| | 4.13907351 | 0.200075739 | 0.894349335 | 0.020876294 | 0.205336342 |
| | 4.069645848 | 0.153415581 | 0.908150467 | 0.019296476 | 0.074310553 |
| | 4.146217328 | 0.206004144 | 0.911663975 | 0.017578362 | 0.042878421 |
| Mean | <i>4.10302778</i> | <i>0.071507219</i> | <i>0.912579969</i> | <i>0.006969232</i> | |

RG1703 U-Pb run lolite 4.1 output data including standards

| | Final U238/Pb206_mean | Final U238/Pb206_2SE(int) | Final Pb207/Pb206_mean | Final Pb207/Pb206_2SE(int) | rho 207Pb/206Pb v 238U/206Pb |
|--------|----------------------------------|--------------------------------------|-----------------------------------|---------------------------------------|-----------------------------------------|
| RG1703 | 8.493112482 | 0.292581711 | 0.384306707 | 0.02200781 | 0.508256162 |
| | 7.435193042 | 0.337422694 | 0.423185393 | 0.030475988 | 0.397436038 |
| | 6.675696546 | 0.228838855 | 0.440980839 | 0.024226338 | 0.616877833 |
| | 6.052531939 | 0.219499983 | 0.480068471 | 0.024035099 | 0.52195502 |
| | 8.511604241 | 0.415801687 | 0.351384004 | 0.027720141 | 0.366403602 |
| | 6.198308857 | 0.225221256 | 0.506825821 | 0.02330853 | 0.460430062 |
| | 7.323440477 | 0.432732117 | 0.464276296 | 0.039433463 | 0.610523085 |
| | 8.979169499 | 0.340369209 | 0.332393241 | 0.024230722 | 0.442795878 |

| | | | | |
|-------------|-------------|--------------|-------------|-------------|
| 7.287252098 | 0.24456868 | 0.441853789 | 0.02473259 | 0.469000344 |
| 8.422091858 | 0.371204989 | 0.373054957 | 0.028599415 | 0.260880224 |
| 6.377823019 | 0.293809183 | 0.484794101 | 0.03125536 | 0.555421316 |
| 8.58359668 | 0.424813186 | 0.322603361 | 0.023947247 | 0.49362808 |
| 7.218820646 | 0.238937413 | 0.445910895 | 0.023587191 | 0.400489262 |
| 9.138503661 | 0.342423883 | 0.358448802 | 0.026351587 | 0.500107141 |
| 5.217700231 | 0.292906871 | 0.54393099 | 0.048042495 | 0.447463893 |
| 6.502518285 | 0.233624525 | 0.487706974 | 0.025307661 | 0.463535386 |
| 0.085175402 | 0.114950728 | -0.007739514 | 0.414230086 | 0.137528503 |
| 8.616002663 | 0.26246508 | 0.367508847 | 0.018913971 | 0.537835781 |
| 9.557382013 | 0.290644179 | 0.296014988 | 0.01821427 | 0.318893159 |
| 13.55193942 | 0.923348683 | 0.154778444 | 0.022071296 | 0.4530933 |
| 10.39848404 | 0.364345998 | 0.227296699 | 0.013161977 | 0.463232718 |
| 8.201285225 | 0.256196956 | 0.357196422 | 0.017614907 | 0.504156527 |
| 0.070297444 | 0.023012258 | 0.935382831 | 0.079580542 | 0.420963058 |
| 0.1656786 | 0.042100798 | 0.863712882 | 0.089238311 | 0.222210963 |
| 0.199083588 | 0.050947232 | 0.613149588 | 0.06545062 | 0.303296176 |
| 0.156333372 | 0.036212617 | 0.876927237 | 0.079131944 | 0.070592948 |
| 0.318986344 | 0.033739991 | 0.799393749 | 0.057008549 | 0.262612659 |
| 1.588448093 | 0.185147623 | 0.756269298 | 0.050210541 | 0.06206197 |
| 9.067830225 | 0.263602202 | 0.332457542 | 0.018906816 | 0.620957871 |
| 3.439058853 | 0.243888579 | 0.648848209 | 0.042950447 | 0.149993702 |
| 8.072958184 | 0.278464191 | 0.391090835 | 0.023795221 | 0.403492237 |
| 4.169419246 | 0.211580301 | 0.62739012 | 0.041953527 | 0.617111086 |
| 5.124892835 | 0.172059317 | 0.523400246 | 0.027011546 | 0.333604513 |
| 2.955814565 | 0.231581611 | 0.626210698 | 0.054262586 | 0.584674052 |
| 7.040493561 | 0.37406026 | 0.452535632 | 0.03560588 | 0.535371154 |
| 7.002160545 | 0.273413707 | 0.451340073 | 0.023360497 | 0.174145304 |
| 6.019921244 | 0.278410525 | 0.522867097 | 0.030455248 | 0.502738941 |

| | | | | | |
|---------|-------------|-------------|-------------|-------------|-------------|
| | 6.074309157 | 0.266430158 | 0.516800758 | 0.024188034 | 0.348634546 |
| | 7.163975546 | 0.241378697 | 0.433664055 | 0.018634382 | 0.4911687 |
| | 8.59589424 | 0.273937201 | 0.313325692 | 0.013960708 | 0.320051849 |
| | 8.253729914 | 0.257060274 | 0.332835155 | 0.017297194 | 0.631821865 |
| | 0.21714876 | 0.116237794 | 0.515150492 | 0.22314605 | 0.344046394 |
| | 9.513069488 | 0.326528053 | 0.276598123 | 0.014882911 | 0.423650097 |
| | 7.283707185 | 0.232762246 | 0.343784385 | 0.018450591 | 0.553696162 |
| | 9.0751895 | 0.295233937 | 0.284753023 | 0.016058517 | 0.391269984 |
| | 8.494946445 | 0.338015223 | 0.357681596 | 0.018854936 | 0.61477969 |
| | 7.398973914 | 0.340534343 | 0.416445312 | 0.03117449 | 0.5811363 |
| | 4.088591345 | 0.278386265 | 0.604309052 | 0.044706126 | 0.211018608 |
| | 5.661509064 | 0.281602108 | 0.489270813 | 0.036553944 | 0.544635529 |
| | 8.358850304 | 0.232354259 | 0.366609854 | 0.01655817 | 0.501152815 |
| | 8.087845284 | 0.25018326 | 0.371874102 | 0.017245858 | 0.394780238 |
| | 7.925743172 | 0.215067128 | 0.377627824 | 0.019531942 | 0.302540898 |
| | 2.639580356 | 0.135685072 | 0.674804529 | 0.046539734 | 0.386980985 |
| | 6.960510685 | 0.220854252 | 0.470847241 | 0.023117463 | 0.56146699 |
| | 3.237573154 | 1.140877355 | 0.533410851 | 0.144085638 | 0.584582264 |
| | 7.808859577 | 0.210992054 | 0.415667605 | 0.02133849 | 0.439459747 |
| | 3.101187395 | 0.163959535 | 0.675203705 | 0.042659061 | 0.615944772 |
| | 3.978613337 | 0.222049629 | 0.573332549 | 0.035942882 | 0.457247559 |
| | 7.206662868 | 0.252847762 | 0.463164907 | 0.026140524 | 0.574983535 |
| | 8.080261089 | 0.241317919 | 0.391099138 | 0.01660536 | 0.288664259 |
| | 8.803593715 | 0.252858781 | 0.338026689 | 0.016540839 | 0.385052993 |
| | 11.15166647 | 0.234238438 | 0.185379878 | 0.010003253 | 0.359562482 |
| | 8.933971689 | 0.291977854 | 0.277739097 | 0.016185412 | 0.389336473 |
| Mean | 6.385951947 | 0.272353947 | 0.454875603 | 0.041282427 | |
| NIST610 | 4.002556025 | 0.041062866 | 0.925858974 | 0.007264583 | 0.300992641 |
| | 3.988927462 | 0.042926776 | 0.934446671 | 0.007457511 | 0.317508256 |

| | | | | | |
|---------|-------------|-------------|-------------|-------------|-------------|
| | 3.997331155 | 0.047506776 | 0.925046237 | 0.007355748 | 0.430990711 |
| | 4.014559913 | 0.040662474 | 0.908799692 | 0.007404919 | 0.201296935 |
| | 3.968371425 | 0.045150097 | 0.913590239 | 0.007682528 | 0.311403704 |
| | 3.964118293 | 0.040660062 | 0.91744882 | 0.008063917 | 0.479434817 |
| | 3.932833487 | 0.043759364 | 0.912091061 | 0.007129371 | 0.294540191 |
| | 3.947364773 | 0.041495129 | 0.919504938 | 0.007731344 | 0.376442728 |
| | 3.98782147 | 0.0393389 | 0.923281518 | 0.007138776 | 0.3721406 |
| | 3.965805564 | 0.046571569 | 0.913745179 | 0.007644527 | 0.418461036 |
| | 3.972598722 | 0.03876436 | 0.908017417 | 0.007388006 | 0.387811392 |
| | 3.98584649 | 0.043328078 | 0.914600672 | 0.008063393 | 0.31018222 |
| | 3.924249421 | 0.046128628 | 0.926213571 | 0.008257246 | 0.344587978 |
| | 3.965256684 | 0.043049009 | 0.928577661 | 0.006912195 | 0.354178343 |
| | 3.976365187 | 0.042164835 | 0.91468972 | 0.00740749 | 0.391998201 |
| | 4.006869937 | 0.042021719 | 0.912212556 | 0.006837508 | 0.342173074 |
| | 4.012450025 | 0.043954181 | 0.911708541 | 0.007732732 | 0.442603829 |
| Mean | 3.977254473 | 0.042855578 | 0.918225498 | 0.007498341 | |
| NIST612 | 3.653377749 | 0.078316333 | 0.959055755 | 0.024441 | 0.497183447 |
| | 3.52888516 | 0.079283963 | 0.930425934 | 0.02369819 | 0.606462068 |
| | 3.626813681 | 0.080500318 | 0.927315975 | 0.025861953 | 0.562016452 |
| | 3.594256735 | 0.078903191 | 0.910308055 | 0.022762108 | 0.536855475 |
| | 3.619948999 | 0.085966067 | 0.910389566 | 0.024813238 | 0.585284083 |
| | 3.59488659 | 0.076064025 | 0.911545961 | 0.024414408 | 0.554439576 |
| | 3.571288411 | 0.086922165 | 0.935683858 | 0.021846764 | 0.525274943 |
| | 3.617465865 | 0.081736052 | 0.941499389 | 0.022941022 | 0.549105585 |
| | 3.573256057 | 0.07909351 | 0.925836917 | 0.02167127 | 0.564808145 |
| | 3.600362918 | 0.076459996 | 0.913244206 | 0.021799344 | 0.515398085 |
| | 3.48649447 | 0.064698453 | 0.892638383 | 0.021297963 | 0.485536108 |
| | 3.567521049 | 0.073911396 | 0.894136412 | 0.021923649 | 0.530433675 |
| | 3.570444417 | 0.078060696 | 0.944462459 | 0.02254442 | 0.582374659 |

| | | | | | |
|-------|-------------|-------------|-------------|-------------|-------------|
| | 3.567966925 | 0.084832047 | 0.942768361 | 0.023647897 | 0.472494694 |
| | 3.605734868 | 0.079878691 | 0.929789456 | 0.020761151 | 0.519191263 |
| | 3.588446087 | 0.075829031 | 0.921269233 | 0.022287099 | 0.583578224 |
| | 3.622518023 | 0.073216903 | 0.90943088 | 0.019384187 | 0.492612826 |
| Mean | 3.58762753 | 0.078451343 | 0.923517694 | 0.02271151 | |
| Mked1 | 3.788527839 | 0.052751902 | 0.096188178 | 0.00259287 | 0.245925421 |
| | 3.795576026 | 0.044655403 | 0.095861844 | 0.002522081 | 0.277772999 |
| | 3.766670422 | 0.047200264 | 0.095331228 | 0.002546809 | 0.27687152 |
| | 3.802257139 | 0.044879311 | 0.096918155 | 0.002564025 | 0.233118534 |
| | 3.776123051 | 0.049110966 | 0.096041215 | 0.002595691 | 0.324505711 |
| | 3.799480746 | 0.05177483 | 0.09542935 | 0.00285877 | 0.394444661 |
| | 3.786944639 | 0.048547611 | 0.096074182 | 0.002557965 | 0.362086174 |
| | 3.794152141 | 0.050219112 | 0.096480769 | 0.00287896 | 0.266446716 |
| | 3.777087135 | 0.045323478 | 0.095461376 | 0.002726193 | 0.096536948 |
| | 3.816343947 | 0.043264593 | 0.095675842 | 0.002468814 | 0.194714533 |
| | 3.72602004 | 0.04345513 | 0.096799289 | 0.002711061 | 0.308743029 |
| | 3.827602956 | 0.043159157 | 0.096518783 | 0.002481332 | 0.13504285 |
| | 3.755261892 | 0.044931685 | 0.095171947 | 0.00230019 | 0.245332406 |
| | 3.812663802 | 0.043595957 | 0.095846709 | 0.002463199 | 0.263453234 |
| | 3.787698631 | 0.050724493 | 0.097013727 | 0.002901955 | 0.3599904 |
| | 3.778988859 | 0.048002969 | 0.09556925 | 0.002726711 | 0.319862696 |
| | 3.782721037 | 0.038900789 | 0.09605717 | 0.002597523 | 0.317815687 |
| Mean | 3.786712959 | 0.046499862 | 0.096025824 | 0.002617303 | |

RG1710 U-Pb run data. Includes all spots analysed. Some spots may not be titanite grains but misfires. The standard data for this run can be found within the following table.

| | Final U238/Pb206_mean | Final U238/Pb206_2SE(int) | Final Pb207/Pb206_mean | Final Pb207/Pb206_2SE(int) | rho 207Pb/206Pb v 238U/206Pb |
|--------|----------------------------------|--------------------------------------|-----------------------------------|---------------------------------------|-----------------------------------------|
| RG1710 | 12.2728485 | 0.24050699 | 0.140458723 | 0.00693877 | 0.160275725 |
| | 8.072593273 | 0.352558106 | 0.364906998 | 0.032819445 | 0.540276232 |
| | 8.76446891 | 0.482500896 | 0.376622955 | 0.038432441 | 0.313421187 |
| | 8.721540143 | 0.43064804 | 0.306566928 | 0.027684943 | 0.401467046 |
| | 9.33102043 | 0.476561952 | 0.340815809 | 0.02590858 | 0.498355114 |
| | 11.90375073 | 0.196737648 | 0.156118605 | 0.007373237 | 0.086073024 |
| | 11.65504928 | 0.28538146 | 0.128995055 | 0.007921629 | 0.325776168 |
| | 7.632438382 | 0.468225402 | 0.377935822 | 0.031156967 | -0.001609223 |
| | 10.02453538 | 0.286803616 | 0.236863969 | 0.015368306 | 0.436947435 |
| | 9.947820674 | 0.243527693 | 0.23274754 | 0.013179623 | 0.368683065 |
| | 8.843315171 | 0.495319458 | 0.351488546 | 0.027175017 | 0.495443504 |
| | 8.717770124 | 0.322524147 | 0.202182225 | 0.019030444 | 0.586213484 |
| | 2.51603572 | 0.299437463 | 0.392793224 | 0.022804623 | -0.702359535 |
| | 11.17212253 | 0.135991531 | 0.146623642 | 0.005034574 | 0.159087757 |
| | 5.932943922 | 0.222839431 | 0.314207407 | 0.021383441 | 0.420359913 |
| | 10.43180614 | 0.152042332 | 0.178327212 | 0.004940608 | 0.081920539 |
| | 3.314108397 | 0.160451524 | 0.49770408 | 0.018824176 | 0.07460997 |
| | 10.61736461 | 0.309175643 | 0.257524987 | 0.013324204 | 0.167959416 |
| | 10.25410246 | 0.307345509 | 0.25545568 | 0.016674194 | 0.246746793 |
| | 10.56181928 | 0.254621378 | 0.222150601 | 0.013619067 | 0.37312815 |
| | 10.63041067 | 0.445707416 | 0.213622176 | 0.020513608 | 0.341144737 |
| | 2.887754927 | 0.143807643 | 0.747857149 | 0.042407241 | 0.472087895 |
| | 11.81620903 | 0.302073326 | 0.182566926 | 0.012142872 | 0.425395556 |
| | 12.00032102 | 0.266374941 | 0.126115141 | 0.009345771 | 0.125322741 |
| | -0.008497793 | 0.000721423 | 0.843625486 | 0.038357454 | -0.070937087 |

| | | | | |
|-------------|-------------|-------------|-------------|--------------|
| 0.000249999 | 7.04465E-05 | 0.884364426 | 0.041981021 | 0.118442388 |
| 6.252973961 | 0.420527369 | 0.473542611 | 0.060667171 | 0.153195728 |
| 5.826752518 | 0.194489507 | 0.457522131 | 0.024297296 | 0.412876051 |
| 7.257649049 | 0.239042746 | 0.422056396 | 0.022852249 | 0.545507847 |
| 11.65839602 | 0.27566247 | 0.165319604 | 0.009371001 | 0.188261752 |
| 7.329853267 | 0.217855393 | 0.33747941 | 0.018471123 | 0.493850621 |
| 12.13871694 | 0.26966923 | 0.119541264 | 0.009680196 | 0.045876559 |
| 8.400676143 | 0.251998497 | 0.217744465 | 0.0124043 | 0.460235649 |
| 12.13957957 | 0.208546936 | 0.119294267 | 0.006285877 | 0.385386903 |
| 3.295238116 | 0.096786955 | 0.518114162 | 0.017844145 | 0.437154529 |
| 10.27215805 | 0.357409355 | 0.208337869 | 0.011159576 | 0.534140048 |
| 13.07665405 | 0.180058704 | 0.084810019 | 0.003991707 | 0.327815869 |
| 11.86137641 | 0.224897406 | 0.113670567 | 0.005986433 | 0.129679497 |
| 11.62986237 | 0.352471825 | 0.142563883 | 0.007546967 | 0.351864965 |
| 10.47805026 | 0.315517354 | 0.214158116 | 0.016543347 | 0.584310493 |
| 11.1226812 | 0.193363801 | 0.186906861 | 0.008049744 | 0.275775074 |
| 7.889514617 | 0.248552677 | 0.391165699 | 0.018600478 | 0.58757391 |
| 10.95260997 | 0.312680137 | 0.150621844 | 0.008992729 | 0.380665816 |
| 8.258810319 | 0.374234559 | 0.368301024 | 0.030154791 | 0.565619371 |
| 10.61783646 | 0.263338366 | 0.172147652 | 0.009703399 | 0.254065419 |
| 1.714810484 | 0.068371308 | 0.551257339 | 0.023086868 | 0.385082087 |
| 5.87475986 | 0.152161831 | 0.378701503 | 0.012111847 | 0.012647454 |
| 7.678499215 | 0.271876362 | 0.292286013 | 0.020609328 | 0.092628814 |
| 3.603214857 | 0.222851389 | 0.553667573 | 0.02837131 | 0.098078796 |
| 4.15507564 | 0.217694353 | 0.626712816 | 0.035373724 | 0.302856179 |
| 5.540892988 | 0.307078837 | 0.52319805 | 0.031943136 | -0.10982108 |
| 0.081898459 | 0.082572919 | 0.434012687 | 0.948116299 | 0.741164407 |
| 0.354485255 | 0.131903011 | 1.359876773 | 0.462764945 | -0.254474415 |
| 11.91932824 | 0.318643004 | 0.1357027 | 0.00899746 | 0.372996878 |

| | | | | |
|-------------|-------------|-------------|-------------|--------------|
| 9.393185637 | 0.185627992 | 0.243112009 | 0.01049788 | 0.338265144 |
| 8.526844008 | 0.238853008 | 0.365192119 | 0.016840083 | 0.363444643 |
| 10.91189144 | 0.270528652 | 0.208447231 | 0.013668674 | 0.124644114 |
| 11.16117543 | 0.283152859 | 0.198518352 | 0.011352572 | 0.350764271 |
| 10.6951493 | 0.291674968 | 0.21727252 | 0.011628239 | 0.296946824 |
| 10.42176239 | 0.313053323 | 0.240930182 | 0.012536505 | 0.461156645 |
| 11.15721453 | 0.267094202 | 0.176437977 | 0.010407593 | 0.378123198 |
| 12.0332022 | 0.245836418 | 0.151879482 | 0.010763592 | -0.397079117 |
| 12.15526721 | 0.252965396 | 0.147225548 | 0.007399194 | 0.296668454 |
| 9.445805311 | 0.319967042 | 0.206689859 | 0.01215681 | 0.05294752 |
| 6.629444703 | 0.197559096 | 0.327923675 | 0.012186717 | -0.029703831 |
| 5.620571491 | 0.294957872 | 0.427350356 | 0.029702168 | 0.318480295 |
| 6.979515176 | 0.265903325 | 0.213370427 | 0.015435118 | 0.424313882 |
| 2.733059308 | 0.131329738 | 0.701760967 | 0.042949257 | 0.542023163 |
| 9.061148132 | 0.478917142 | 0.211010247 | 0.021481061 | 0.007009261 |
| 5.71547585 | 0.267690193 | 0.495545212 | 0.029750577 | 0.28683225 |
| 11.06330039 | 0.355518496 | 0.198369589 | 0.014024696 | 0.431831704 |
| 10.11276029 | 0.296466013 | 0.208032008 | 0.01157758 | 0.043003873 |
| 5.877598178 | 0.175730805 | 0.313270607 | 0.016998038 | 0.429320672 |
| 8.992741277 | 0.178273841 | 0.249175702 | 0.009301919 | 0.330629397 |
| 9.11456581 | 0.162456622 | 0.174834526 | 0.008606216 | 0.15885446 |
| 9.181981939 | 0.208090455 | 0.232450073 | 0.009804865 | -0.102006581 |
| 11.38217348 | 0.234466838 | 0.150819561 | 0.006496217 | 0.252419321 |
| 11.32847679 | 0.311214353 | 0.181493874 | 0.010107943 | 0.464117292 |
| 11.17639961 | 0.312362428 | 0.209914878 | 0.014434871 | 0.322261177 |
| 6.555718505 | 0.250915258 | 0.433784477 | 0.025529993 | 0.325410253 |
| 2.92366138 | 0.199463382 | 0.683926334 | 0.034797677 | 0.081420123 |
| 11.33513663 | 0.337803451 | 0.207829463 | 0.015394838 | 0.387638541 |
| 12.0067725 | 0.241486252 | 0.148911079 | 0.006650745 | 0.278370724 |

| | | | | |
|-------------|-------------|-------------|-------------|--------------|
| 8.562489453 | 0.259422565 | 0.327667117 | 0.018360259 | 0.388742102 |
| 5.277182287 | 0.205650278 | 0.314466852 | 0.020290695 | 0.181605137 |
| 11.37418479 | 0.256420099 | 0.16714617 | 0.009853492 | 0.382848901 |
| 6.843685978 | 0.178910152 | 0.117728789 | 0.007922912 | 0.027883296 |
| 10.46682472 | 0.279769231 | 0.236753624 | 0.014432634 | 0.374410883 |
| 11.10051152 | 0.288731458 | 0.179359092 | 0.011562386 | 0.275016901 |
| 7.795749239 | 0.211439453 | 0.292194218 | 0.013655488 | -0.056088188 |
| 10.85975689 | 0.349703263 | 0.224422977 | 0.015817754 | 0.322961661 |
| 9.579704819 | 0.266400604 | 0.249702715 | 0.010456642 | -0.071650369 |
| 11.62115686 | 0.323083234 | 0.141863047 | 0.010580494 | 0.315184831 |
| 12.17965472 | 0.179908567 | 0.129656094 | 0.006493992 | 0.158082018 |
| 10.32103776 | 0.42385375 | 0.235217523 | 0.017215778 | 0.140848413 |
| 4.02018328 | 0.354063263 | 0.420850184 | 0.014446621 | -0.342498735 |
| 11.35151726 | 0.353220176 | 0.194040929 | 0.011653641 | 0.188535649 |
| 9.048427007 | 0.227521353 | 0.259456246 | 0.012433053 | 0.321604065 |
| 10.81038376 | 0.238083124 | 0.192448427 | 0.011675886 | 0.231865143 |
| 8.050992748 | 0.261358312 | 0.318166957 | 0.022188816 | 0.444623291 |
| 10.03919832 | 0.28050436 | 0.22450426 | 0.012665768 | 0.407644788 |
| 8.737729501 | 0.272212457 | 0.287808571 | 0.015559834 | 0.259094418 |
| 8.274294096 | 0.168600596 | 0.128465856 | 0.007052217 | 0.31990404 |
| 11.96399279 | 0.243100412 | 0.134202832 | 0.006509675 | 0.281792917 |
| 11.70319847 | 0.414798195 | 0.17411766 | 0.011044103 | 0.201022929 |
| 11.89622116 | 0.290305372 | 0.147314076 | 0.008763984 | -0.095796001 |
| 12.25904024 | 0.317247325 | 0.135860391 | 0.009255058 | 0.300802524 |
| 10.86071054 | 0.207258633 | 0.213191292 | 0.00987893 | 0.45626414 |
| 9.901371527 | 0.16834419 | 0.210127083 | 0.006530883 | 0.246107619 |
| 1.513156437 | 0.061869315 | 0.600585845 | 0.027631238 | 0.387704118 |
| 12.48569558 | 0.193638157 | 0.102647093 | 0.004896331 | -0.085457617 |
| 9.189535817 | 0.35123176 | 0.34167658 | 0.021174128 | 0.448088255 |

| | | | | | |
|------|-------------|-------------|-------------|-------------|-------------|
| | 10.35764056 | 0.122586275 | 0.084479729 | 0.003003069 | 0.152510151 |
| | 8.694887257 | 0.117969146 | 0.091326386 | 0.003401033 | 0.257061293 |
| | 7.412058457 | 0.119133003 | 0.08469304 | 0.002948305 | 0.403162484 |
| | 11.43069759 | 0.205579762 | 0.120665815 | 0.005427059 | 0.323400083 |
| | 10.95451379 | 0.277928506 | 0.157027145 | 0.007947011 | 0.45929884 |
| | 11.69555009 | 0.284868597 | 0.162551268 | 0.009843283 | 0.313413094 |
| | 8.893039338 | 0.377132328 | 0.293786645 | 0.022666465 | 0.483767295 |
| | 11.05110307 | 0.411689887 | 0.166427508 | 0.013769574 | 0.048048733 |
| | 12.04939129 | 0.27399812 | 0.126068206 | 0.007701683 | 0.271101326 |
| Mean | 8.873675406 | 0.259827326 | 0.281913233 | 0.027334806 | 0.26066335 |

MKED1

| Final U238/Pb206_mean | Final U238/Pb206_2SE(int) | Final Pb207/Pb206_mean | Final Pb207/Pb206_2SE(int) | Age | Notes |
|-----------------------|---------------------------|------------------------|----------------------------|------|--------------------|
| 3.780532512 | 0.033273354 | 0.095812818 | 0 | 1515 | |
| 3.78419327 | 0.038214989 | 0.097412167 | 0 | 1515 | |
| 3.776857384 | 0.033792511 | 0.095259535 | 0 | 1515 | |
| 3.779575226 | 0.034939553 | 0.095970016 | 0 | 1515 | |
| 3.773677072 | 0.033788952 | 0.095381575 | 0 | 1517 | |
| 3.782904216 | 0.03499677 | 0.097695551 | 0 | 1517 | Plots to the right |
| 3.770543745 | 0.033753641 | 0.095263737 | 0 | 1517 | |
| 3.784395039 | 0.035125758 | 0.094318197 | 0 | 1512 | |
| 3.780773351 | 0.03695052 | 0.097751677 | 0 | 1517 | Plots to the right |
| 3.793585904 | 0.031419641 | 0.09635619 | 0 | 1511 | |

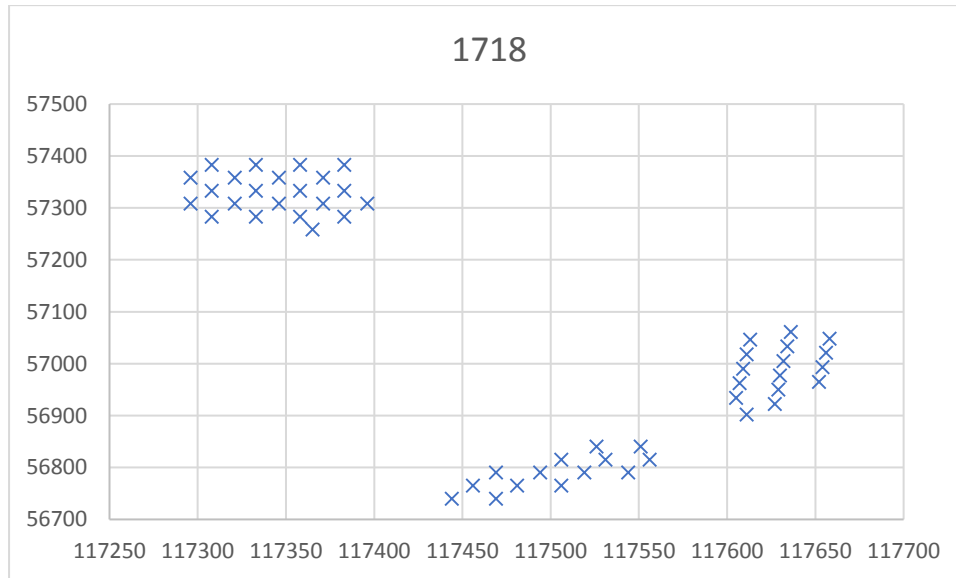
| | | | | | |
|-------------|-------------|-------------|---|------|--------------------------|
| 3.753753446 | 0.030819858 | 0.096374684 | 0 | 1524 | |
| 3.788857212 | 0.033150999 | 0.094756009 | 0 | 1511 | |
| 3.798306786 | 0.035794501 | 0.09644078 | 0 | 1510 | |
| 3.762158716 | 0.031047262 | 0.096046146 | 0 | 1521 | |
| 3.788360542 | 0.036861549 | 0.095057207 | 0 | 1511 | |
| 3.782049424 | 0.03203897 | 0.098346124 | 0 | 1517 | Plots to the right |
| 3.756592755 | 0.03231466 | 0.095396612 | 0 | 1522 | |
| 3.804853078 | 0.033274348 | 0.092705809 | 0 | 1503 | |
| 3.758466374 | 0.032163668 | 0.097678333 | 0 | 1525 | Plots to the right |
| 3.78176267 | 0.032701823 | 0.09649005 | 0 | 1516 | |

Spot Order and Spatial data for Monazite RG1718

| Order | X | Y |
|-------|--------|-------|
| 1 | 117611 | 56902 |
| 2 | 117605 | 56934 |
| 3 | 117627 | 56922 |
| 4 | 117607 | 56962 |
| 5 | 117629 | 56950 |
| 6 | 117609 | 56990 |
| 7 | 117630 | 56977 |
| 8 | 117652 | 56965 |
| 9 | 117611 | 57018 |
| 10 | 117632 | 57005 |

| | | |
|----|--------|-------|
| 11 | 117654 | 56993 |
| 12 | 117613 | 57046 |
| 13 | 117634 | 57033 |
| 14 | 117656 | 57021 |
| 15 | 117636 | 57061 |
| 16 | 117658 | 57048 |
| 17 | 117365 | 57258 |
| 18 | 117308 | 57283 |
| 19 | 117333 | 57283 |
| 20 | 117358 | 57283 |
| 21 | 117383 | 57283 |
| 22 | 117296 | 57308 |
| 23 | 117321 | 57308 |
| 24 | 117346 | 57308 |
| 25 | 117371 | 57308 |
| 26 | 117396 | 57308 |
| 27 | 117308 | 57333 |
| 28 | 117333 | 57333 |
| 29 | 117358 | 57333 |
| 30 | 117383 | 57333 |
| 31 | 117296 | 57358 |
| 32 | 117321 | 57358 |
| 33 | 117346 | 57358 |
| 34 | 117371 | 57358 |
| 35 | 117308 | 57383 |
| 36 | 117333 | 57383 |
| 37 | 117358 | 57383 |
| 38 | 117383 | 57383 |
| 39 | 117444 | 56740 |
| 40 | 117469 | 56740 |

| | | |
|----|--------|-------|
| 41 | 117456 | 56765 |
| 42 | 117481 | 56765 |
| 43 | 117506 | 56765 |
| 44 | 117469 | 56790 |
| 45 | 117494 | 56790 |
| 46 | 117519 | 56790 |
| 47 | 117544 | 56790 |
| 48 | 117506 | 56815 |
| 49 | 117531 | 56815 |
| 50 | 117556 | 56815 |
| 51 | 117526 | 56840 |
| 52 | 117551 | 56840 |

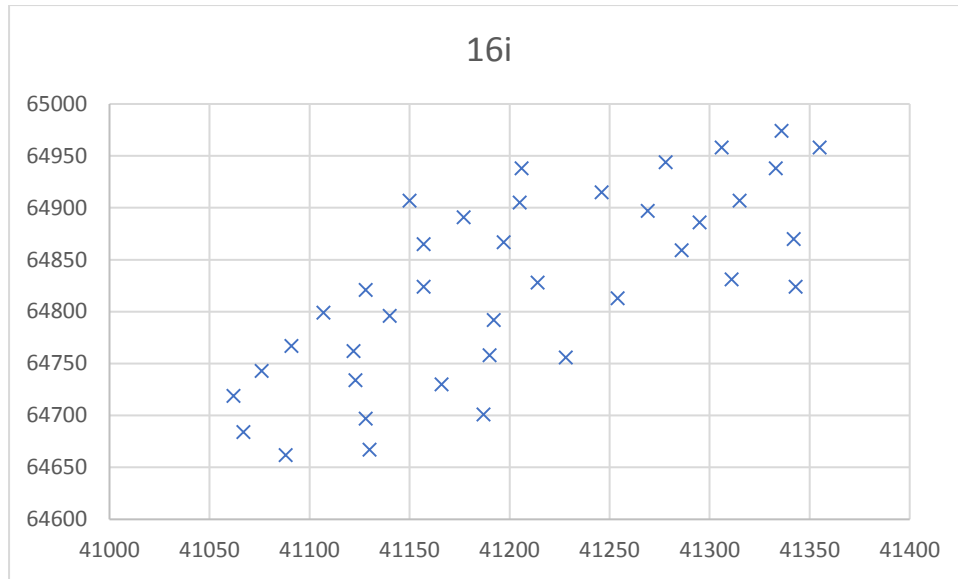


RG1718 monazite Spot spatial data plot. This figure was used to determine the spot order on the grain and tie the spot to the lolite4.1 output data. This data is spot spatial data taken from the laser. If the X and Y of this graph represent the axis, the laser would come either in or out of this plane produced by the X and Y axis.

RG1716 Spatial Data

| Order | X | Y |
|-------|-------|-------|
| 1 | 41190 | 64758 |
| 2 | 41067 | 64684 |
| 3 | 41228 | 64756 |
| 4 | 41246 | 64915 |
| 5 | 41157 | 64865 |
| 6 | 41157 | 64824 |
| 7 | 41214 | 64828 |
| 8 | 41166 | 64730 |
| 9 | 41130 | 64667 |
| 10 | 41062 | 64719 |
| 11 | 41128 | 64821 |
| 12 | 41286 | 64859 |
| 13 | 41311 | 64831 |
| 14 | 41343 | 64824 |
| 15 | 41254 | 64813 |
| 16 | 41122 | 64762 |
| 17 | 41107 | 64799 |
| 18 | 41295 | 64886 |
| 19 | 41205 | 64905 |
| 20 | 41192 | 64792 |

| | | |
|----|-------|-------|
| 21 | 41140 | 64796 |
| 22 | 41150 | 64907 |
| 23 | 41128 | 64697 |
| 24 | 41088 | 64662 |
| 25 | 41123 | 64734 |
| 26 | 41333 | 64938 |
| 27 | 41355 | 64958 |
| 28 | 41269 | 64897 |
| 29 | 41206 | 64938 |
| 30 | 41177 | 64891 |
| 31 | 41197 | 64867 |
| 32 | 41187 | 64701 |
| 33 | 41076 | 64743 |
| 34 | 41091 | 64767 |
| 35 | 41278 | 64944 |
| 36 | 41315 | 64907 |
| 37 | 41342 | 64870 |
| 38 | 41306 | 64958 |
| 39 | 41336 | 64974 |



RG1716 monazite Spot spatial data plot